



VCU

Virginia Commonwealth University
VCU Scholars Compass

Theses and Dissertations


Graduate School

2017

SALVIANOLIC ACID B FOR PULMONARY DELIVERY TOWARDS REVERSAL OF EMPHYSEMA

Sneha Dhapare

Follow this and additional works at: <https://scholarscompass.vcu.edu/etd>

 Part of the [Cell Biology Commons](#), [Medicinal Chemistry and Pharmaceutics Commons](#), and the [Pharmacology Commons](#)

© The Author

Downloaded from

<https://scholarscompass.vcu.edu/etd/4812>

This Dissertation is brought to you for free and open access by the Graduate School at VCU Scholars Compass. It has been accepted for inclusion in Theses and Dissertations by an authorized administrator of VCU Scholars Compass. For more information, please contact libcompass@vcu.edu.

**SALVIANOLIC ACID B FOR PULMONARY DELIVERY TOWARDS
REVERSAL OF EMPHYSEMA**

A dissertation submitted in partial fulfillment of the requirements for the degree of
Doctor of Philosophy at Virginia Commonwealth University

by

SNEHA DHAPARE, B. Pharm., M.S.
Mumbai University, India, 2011
Creighton University, Omaha, NE, 2013

Director: MASAHIRO SAKAGAMI, Ph.D.
Associate Professor
Department of Pharmaceutics, School of Pharmacy

Virginia Commonwealth University
Richmond, Virginia
May 2017

ACKNOWLEDGEMENTS

First and foremost, I would like to express my sincere gratitude to my advisor, Dr. Masahiro Sakagami for the opportunity to pursue this Ph.D. endeavor under his guidance and mentorship. His ability to inspire me to pursue the highest standards has made this research possible. Thank you for the insightful discussions, critical feedback and words of encouragement, which has helped me become an independent and articulate scientist. I would like to thank my graduate advisory committee members: Dr. Byron, Dr. Sweet, Dr. Heise and Dr. McRae, for their significant contributions and valuable advice throughout my graduate studies. I would especially like to thank Dr. Byron and Dr. Hindle for the inspiring discussions that have helped me develop professionally and personally. I am very grateful to Hua Li for her patience in training me in animal handling and Western blot techniques, and for her friendship.

I would like to thank Dr. McRae, Dr. Gerk, Dr. Sweet and their lab members for the unrestricted access to their laboratories that has provided valuable resources for my research. I would like to acknowledge Aerosol Research Group members: Dr. Peter Byron, Dr. Masahiro Sakagami, Dr. Joanne Peart, Dr. Michael Hindle, Dr. Sandro da Rocha, Dr. Bhawana Saluja, Dr. Ruba Darweesh, Dr. Min Li, Dr. Laleh Golshahi, Dr. Anubhav Kaviratna, Dr. Xiangyin Wei, Dr. Tien Truong, Mandana Azimi, Susan Boc and Anuja Raut. I am truly thankful for the inspiring and stimulating discussions that have been instrumental in developing my research.

I appreciate the financial support towards this research project and my graduate education. Virginia Commonwealth University (VCU) School of Pharmacy and the Graduate School Dissertation Assistantship award have provided the financial support throughout my graduate studies. Thank you to the wonderful Pharmaceutics department staff: Shakim Jackson, Keyetta Tate, and Laura Georgiadis, for providing the much needed administrative support.

I have been so fortunate to have phenomenal professors and mentors through my graduate studies: Dean Joseph Dipiro, Dr. Aron Lichtman, Dr. Jurgen Venitz, Dr. Susana Wu-Pong, Dr. Douglas Sweet, Dr. Tyler Stevens, Dr. Umesh Desai, Dr. Tom Karnes, Dr. Matthew Halquist and Dr. Phillip Gerk. I am truly grateful for your guidance, advice and support. As I reflect on my time here as a graduate student, I am thankful for the friendships I have made through these 4 years. Thank you Neha, Anuja, Mandana, Deblina, Bishoy, Ray, Susan and Chris for making the graduate student life so gratifying. I would especially like to thank my friends in Richmond, I will always cherish the memories of the time we spent together.

I fall short of words in expressing my gratitude towards my family back in India for their unconditional love and support throughout my studies in the US and my husband for his unwavering support and encouragement to pursue my dreams. Thank you for everything.

TABLE OF CONTENTS

ACKNOWLEDGEMENTS	ii
LIST OF TABLES	viii
LIST OF FIGURES	ix
ABBREVIATIONS AND SYMBOLS	xiv
ABSTRACT	xviii
CHAPTER	
1. BACKGROUND AND SIGNIFICANCE	
1.1 COPD and Emphysema.....	2
1.2 Current Treatment of COPD/Emphysema.....	3
1.3 Pathogenesis of COPD/Emphysema.....	6
1.4 JAK2-STAT3-VEGF Signaling Pathway.....	9
1.5 Salvianolic acid B (SalB).....	11
1.6 Towards Reversal of Emphysema.....	15
2. HYPOTHESIS AND SPECIFIC AIMS	18
3. SALVIANOLIC ACID B (SalB): ANTI-OXIDATIVE, ANTI-ELASTASE AND STAT3 AND VEGF ELEVATING ACTIVITIES	
3.1 Introduction.....	20
3.2 Materials and Methods	
3.2.1 Anti-oxidative activity assessment.....	21
3.2.2 Anti-elastase activity assessment.....	22
3.2.3 In vivo pSTAT3 and VEGF activation in the lung tissues.....	23
3.2.4 Data description and statistical analyses.....	24

3.3 Results and Discussion	
3.3.1 In vitro ABTS radical scavenging activity of SalB.....	25
3.3.2 In vitro anti-elastase activity of SalB.....	27
3.3.3 Elevated pSTAT3 and VEGF expression in the lungs following SalB treatment.....	28
3.4 Conclusions.....	31
4. IN VITRO CHARACTERIZATION OF ANTI-CELL DEATH, CELL PROLIFERATION, MIGRATION AND RECRUITMENT STIMULATORY ACTIVITIES OF SALVIANOLIC ACID B (SalB)	
4.1 Introduction.....	32
4.2 Materials and Methods	
4.2.1 SalB and inhibitors.....	34
4.2.2 Lung alveolar epithelial, endothelial and mesenchymal stem cell culture.....	34
4.2.3 Anti-cell death activity assessments.....	35
4.2.4 Cell proliferation activity assessment.....	37
4.2.5 Cell migration activity assessment.....	38
4.2.6 Trans-endothelial migratory stem cell recruitment activity assessment.....	38
4.2.7 Data description and statistical analyses.....	42
4.3 Results	
4.3.1 Anti-lung cell death activities of SalB.....	43
4.3.2 Lung cell proliferation stimulatory activities of SalB.....	50

4.3.3	Lung cell migration promoting activities of SalB.....	55
4.3.4	Stem cell recruitment promoting activities of SalB.....	64
4.4	Discussion	
4.4.1	SalB protects lung epithelial and endothelial cells from oxidative stress and VEGF-receptor blockade	68
4.4.2	SalB stimulates proliferation and migration of lung epithelial and endothelial cells.....	70
4.4.3	SalB restores the impaired recruitment of stem cells.....	74
4.5	Conclusion.....	76

5. SALVIANOLIC ACID B (SalB): IN VIVO REVERSAL OF EMPHYSEMA IN RATS FOLLOWING LUNG DELIVERY

5.1	Introduction.....	76
5.2	Materials and Methods	
5.2.1	Animals	77
5.2.2	Protocols with PPE- and CSE -induced rat models of established emphysema.....	77
5.2.3	Treadmill exercise endurance	82
5.2.4	Alveolar airspace size by mean linear intercept (MLI).....	82
5.2.5	Alveolar structural destruction by destructive index (DI).....	83
5.2.6	Protein extraction and western blot analysis.....	84
5.2.7	Lung Myeloperoxidase (MPO) activity.....	85

5.2.8	Data description and statistical analyses.....	85
5.3 Results		
5.3.1	SalB reversed impaired exercise endurance in <i>established</i> emphysema.....	86
5.3.2	SalB reversed airspace enlargement and alveolar destruction in <i>established</i> emphysema	90
5.3.3	Lung tissue expression of protein markers.....	96
5.3.4	Lung MPO activity	102
5.4 Discussion		
5.4.1	SalB recovers functional impairment in PPE and CSE –induced <i>established</i> emphysema	104
5.4.2	SalB reverses morphological impairment in PPE and CSE– induced <i>established</i> emphysema	105
5.4.3	SalB normalizes the lung tissue expression of cleaved caspase-3 and VEGF but has no effect on the MPO activity.....	106
5.5	Conclusion.....	108
6. SUMMARY AND GENERAL CONCLUSIONS.....		109
APPENDICES		
1.	Western blot analysis.....	113
2.	Treadmill exercise endurance training and testing.....	116
3.	Counting of migrated DILC12-labeled MSCs using ImageJ.....	118
REFERENCES.....		121
VITA.....		131
DATA SHEETS.....		132

LIST OF TABLES

Table 1.1	FDA approved drugs for COPD/emphysema treatment.....	5
Table 4.1	Effects of AG490 and S31-201 on SU5416 –induced A549 cell death.....	49
Table 5.1	Six experimental groups to examine the reversal activities of SalB in the PPE- and CSE-induced rat models of <i>established</i> emphysema.....	77

LIST OF FIGURES

Figure 1.1	Normal and emphysematous alveoli in the lung	8
Figure 1.2	Intracellular JAK2-STAT3-VEGF activation pathway.....	10
Figure 1.3	(A) <i>Salvia miltiorrhiza</i> ; and (B) the structure and physicochemical properties of its major active component, salvianolic acid B (SalB)	13
Figure 1.4	Proposed mechanism of emphysema reversal by SalB.....	14
Figure 3.1	Absorbance increase in 5 min (Δ Abs) at 750 nm as a function of concentration of SalB in the chemical antioxidant assay.....	26
Figure 3.2	Fraction of HSE activity remaining as a function of concentration of SalB in the chromogenic substrate hydrolysis assay.....	28
Figure 3.3	Lung tissue expression of cytoplasmic pSTAT3 (A) and VEGF (B) in healthy rats dosed with saline or SalB at 0.2 mg/kg.....	30
Figure 4.1	Figure 4.1: (A) Fluoroblock transwell insert (B) Florescence microscope image (100X) of DiIC12-labelled HMVEC-L monolayer grown on the fibronectin-coated fluoroblock transwell filter (C) Schematic representation of the trans-endothelial migration assay showing cross section of the fluoroblock insert transwell.....	41
Figure 4.2	In vitro anti-cell death activities of SalB at 1, 10 and 25 μ M against H ₂ O ₂ -induced cell death in the A549 cells, determined by the trypan blue exclusion assay.....	45
Figure 4.3	In vitro anti-cell death activities of SalB at 25 μ M against H ₂ O ₂ -induced cell death in the A549 cells, determined by PI –based fluorescence flow cytometry.....	46
Figure 4.4	(A) In vitro cytoprotective activities of SalB at 25 μ M against cell death induced by SU5416 at 10 or 20 μ M in the A549 cells with or without AG490 (25 μ M) or S31-	

	201 (100 μM), determined by the trypan blue exclusion assay; (B) Effect of AG490 or S31-201 addition on SalB's anti-cell death activity.....47
Figure 4.5	In vitro cytoprotective activities of SalB at 25 μM against cell death induced with SU5416 at 20 μM in the HMVEC-L cells with or without AG490 (25 μM) or S31-201 (50 μM), determined by the trypan blue exclusion assay (A) SU5416 induced cell death and its inhibition with SalB; (B) Effect of AG490 or S31-201 addition on SalB's anti-cell death activity.....48
Figure 4.6	In vitro cell proliferation activities in the A549 cells following various treatments determined with the 570 nm absorbance (Abs_{570}) by the MTT assay.....52
Figure 4.7	In vitro cell proliferation activities in the HMVEC-L cells following various treatments determined with the 570 nm absorbance (Abs_{570}) by the MTT assay (A) following 0, 24 and 48 h incubation.....53
Figure 4.8	In vitro cell proliferation activities in HMVEC-L following 24 h treatment with SalB at 10 or 25 μM or the vehicle, determined with the 450 nm absorbance (Abs_{450}) by the BrdU assay.....54
Figure 4.9	Representative images of linear scratch wounds made at 0 h and their closures at 24 and 48 h in the A549 cells in three different wells, treated with the vehicle or SalB at 25 μM57
Figure 4.10	(A) Representative images of linear scratch wound at 0 and 48 h of the treatment with the vehicle or SalB at 25 μM in the A549 cells; (B) % wound closure in the A549 cells following 48 h treatment with the vehicle or SalB at 10 and 25 μM58
Figure 4.11	In vitro % wound closure at 48 h in the A549 cells with or without SalB at 25 μM and/or inhibitors: (A) Effect of AG490 (25 μM) or S31-201 (100 μM); and (B)

	Effect of SU5416 (5 μ M).....	59
Figure 4.12	Representative images of linear scratch wounds made at 0 h and their closures at 12 h in the HMVEC-L cells in three different wells, treated with the vehicle or SalB at 25 μ M.....	60
Figure 4.13	(A) Representative images of the linear scratch at 0 and 12 h of the treatment with the vehicle or SalB at 25 μ M in the HMVEC-L cells; (B) Time course changes of the % wound closure over 18 h during the treatment with the vehicle or SalB at 10 μ M in the HMVEC-L cells.....	61
Figure 4.14	In vitro % wound closure in the HMVEC-L cells following 12 h treatment with SalB at 2.5 – 25 μ M or the vehicle.....	62
Figure 4.15	In vitro % wound closure in the HMVEC-L cells treated with or without SalB at 25 μ M and/or inhibitors.....	63
Figure 4.16	% of MSCs migrated through the fluoroblock filters to the basolateral side with or without the HMVEC-L monolayers at 24 h.....	65
Figure 4.17	Trans HMVEC-L cell monolayer migration of MSCs in 24 h with or without 30 % FBS.....	65
Figure 4.18	(A) Representative images of MSCs migrated to the basolateral side of the Fluoroblock transwell insert under fluorescence microscope and fluorescent cells counted by ImageJ in each of the microscopic image (B) Trans-HMVEC-L cell monolayer migration of MSCs in 24 h with or without SalB at 25 μ M and/or SU5416 (5 μ M) pretreatment.....	66, 67
Figure 4.19	HMVEC-L cell (cytoplasmic) expression of pSTAT3 (A) and pVEGFR2 (B) after 24 h treatment with S31-201 at 50 μ M or SU5416 at 5 μ M, respectively.....	73

Figure 5.1	Experimental protocol used to assess the reversal activities of SalB in the PPE-induced rat model of <i>established</i> emphysema. (OT, orotracheal instillation).....	80
Figure 5.2	Experimental protocol used to assess the reversal activities of SalB in the CSE-induced rat model of <i>established</i> emphysema. (IP, intraperitoneal injection).....	81
Figure 5.3	Treadmill exercise endurance of each rat measured on day 21-22 and 43-44, respectively, before (Pre) and after (Post) three weeks of pulmonary administration of saline or SalB at 0.1 or 0.2 mg/kg (three times per week) in rat models of <i>established</i> emphysema induced with PPC and CSE, compared to that in healthy rats with or without two weeks pulmonary administration of SalB at 0.2 mg/kg (fives times/week).....	88
Figure 5.4	Difference in the exercise endurance (Δ Endurance) measured on day 20,21 and day 41,42 i.e. before (Pre) and after (Post) three weeks of pulmonary administration of saline or SalB at 0.1 or 0.2 mg/kg (three times per week) in rat models of <i>established</i> emphysema induced with PPE and CSE.....	89
Figure 5.5	The representative H&E stained micrographs of the alveolar airspaces in the left lung lobes in rat models of <i>established</i> emphysema induced with PPE or CSE following three weeks pulmonary administration of saline or SalB (0.2 mg/kg, three times/week), compared to those in healthy rats with or without two weeks pulmonary administration of SalB (0.2 mg/kg, five times/week).....	92
Figure 5.6	Mean linear intercept (MLI) values of the alveolar airspaces in the rat models of <i>established</i> emphysema induced with PPE or CSE following three weeks pulmonary administrations of saline or SalB at 0.2 mg/kg (three times/week), compared to those in healthy rats treated with saline or SalB (0.2 mg/kg, five times/week).....	93

Figure 5.7	Destructive index (DI) measurements obtained from the H&E stained 100X images of healthy or PPE –induced emphysema rats either treated with saline or SalB.....	94
Figure 5.8	Correlation between alveolar airspace enlargement (MLI) and destruction (DI) in healthy saline treated rats, PPE-induced SalB -treated rats and PPE- induced saline treated rats.....	95
Figure 5.9	Lung tissue (cytosolic) expression of cleaved caspase 3 in the rat model of <i>established</i> emphysema induced with PPE following three weeks pulmonary administration of saline or SalB (0.2 mg/kg, three times/week), relative to that in healthy rats.....	98
Figure 5.10	Lung tissue (cytosolic) expression of proliferating cell nuclear antigen (PCNA) in the rat model of <i>established</i> emphysema induced with PPE following three weeks pulmonary administration of saline or SalB (0.2 mg/kg, three times/week), relative to that in healthy rats.....	99
Figure 5.11	Lung tissue cytosolic and nuclear expression of pSTAT3 in the rat model of <i>established</i> emphysema induced with PPE following three weeks pulmonary administration of saline or SalB (0.2 mg/kg, three times/week), relative to that in healthy rats.....	100
Figure 5.12	Lung tissue (cytosolic) expression of VEGF in the rat model of <i>established</i> emphysema induced with PPE following three weeks pulmonary administration of saline or SalB (0.2 mg/kg, three times/week), relative to that in healthy rats.....	101
Figure 5.13	Lung MPO activity in the rat model of <i>established</i> emphysema induced with PPE following three weeks pulmonary administration of saline or SalB (0.2 mg/kg three times/week), compared to that in healthy rats.....	103

ABBREVIATIONS AND SYMBOLS

%	percentage
=	equal to
~	approximately
<	less than
>	greater than
±	plus or minus
°C	temperature in celsius scale
AAALAC	Association for Assessment and Accreditation of Laboratory Animal Care
ABTS•+	2,2-azinobis(3-ethyl-benzothiazoline-6-sulphonic acid)
ΔAbs	absorbance change
Abs ₄₅₀	absorbance at 450 nm
Abs ₅₇₀	absorbance at 570 nm
AG490	tyrphostin
ANOVA	analysis of variance
ATCC	American Type Culture Collection
ATI	alveolar type I cells
ATII	alveolar type II cells
BCA	bicinchoninic acid
BrdU	5-bromo-2-deoxyuridine
BSA	bovine serum albumin

C	concentration
CA	caffeic acid
CI	confidence interval
COPD	chronic obstructive pulmonary disease
CSE	cigarette smoke extract
D	destroyed alveolus
Da	dalton
DDW	distilled, deionized water
DI	destructive index
DMSO	dimethyl sulfoxide
DPPH	2,2-diphenyl-1-picrylhydrazyl
Δ Endurance	change in endurance
EGF	epidermal growth factor
EGFR	epidermal growth factor receptor
ELISA	enzyme linked immunosorbant assay
FBS	fetal bovine serum
FDA	Food and Drug Administration
GOLD	Global initiative for Chronic Obstructive Lung Disease
HDAC	histone deacetylase
H&E	hematoxylin-eosin
HIF-1 α	hypoxia-inducible factor-1 alpha
H ₂ O ₂	hydrogen peroxide
HRP	horse radish peroxidase

HSE	human sputum elastase
HS	Hill slope
IACUC	Institutional Animal Care and Use Committee
IC ₅₀	half-maximal inhibitory concentration
ICS	inhaled corticosteroid
IP	intraperitoneal
JAK2	janus kinase 2
kDa	kilo dalton
LogD _{7.5}	distribution coefficient at ph 7.5
LogP	partition coefficient
LVRS	lung volume reduction surgery
min	minutes
MLI	mean linear intercept
MeOSuc-AAPV-pNA	n-methoxysuccinyl ala-ala-pro-val p-nitroanilide
MPO	myeloperoxidase
MSC	mesenchymal stem cells
MTT	3-[4,5-dimethylthiazol-2-yl]-2,5-diphenyltetrazolium bromide
N	normal alveolus
NIH	National Institute of Health
NS	Not significant
OT	orotracheal
PCNA	proliferating cell nuclear antigen
PI	propidium iodide

pSTAT3	phosphorylated STAT3-tyr705
pSTAT3	phosphorylated STAT3-tyr705
pVEGFR2	phosphorylated VEGF-receptor 2
ROS	reactive oxygen species
SD	standard deviation
SE	standard error
T	temperature
TBS	tris buffered saline
TEER	transendothelial electrical resistance
U	unit
US	United States
VCU	Virginia Commonwealth University
WA _{pre}	pre-incubation scratch wound area
WA _{post}	post-incubation scratch wound area
WHO	World Health Organization

ABSTRACT

SALVIANOLIC ACID B FOR PULMONARY DELIVERY TOWARDS REVERSAL OF EMPHYSEMA

by Sneha Dhapare, M.S., B.Pharm.

A dissertation submitted in partial fulfillment of the requirements for the degree of Doctor
of Philosophy at Virginia Commonwealth University

Virginia Commonwealth University, 2017

Major Director: Masahiro Sakagami, Ph.D.
Associate Professor
Department of Pharmaceutics, School of Pharmacy

A new pathobiologic hypothesis has recently emerged that the alveolar structural destruction and loss in emphysema are caused by the deficiency of vascular endothelial growth factor (VEGF). Therefore, this project hypothesized that such pathobiologic VEGF deficiency of emphysematous lungs can be recovered with a natural caffeic acid tetramer, salvianolic acid B (SalB), through activation of signal transducer and activator of transcription 3 (STAT3), so that emphysema can be reversed as a result of inhibition of induced cell death, stimulation of cell proliferation and migration, and promotion of stem cell recruitment to the lungs.

SalB was first shown to be potently anti-oxidative ($IC_{50} = 3.7 \mu M$), but devoid of anti-elastase activity. SalB was then administered to the lungs of healthy rats at 0.2 mg/kg for two weeks, verifying ~1.7-fold increased lung tissue expressions of phosphorylated STAT3 (pSTAT3; an activated form of STAT3) and VEGF. Subsequently, SalB was examined in the anti-cell death assay, cell proliferation and migration assays, and trans-

endothelial stem cell recruitment assay in the in vitro lung epithelial (A549) and endothelial (HMVEC-L) cell systems. SalB at 25 μ M exerted significant 48-88 % inhibitory activities against cell death induced with oxidative stress and VEGF receptor blockade (with SU5416) in both cell systems, measured by the trypan blue exclusion and propidium iodide-based flow cytometry assays. SalB at 25 μ M also stimulated A549 and HMVEC-L cell proliferation by \sim 1.4-fold and promoted cell migration by \sim 1.6-fold, while recovering stem cell recruitment impaired with SU5416 by 60 %. The anti-cell death, and proliferation and migration stimulatory activities of SalB were significantly opposed by pharmacological inhibitors of JAK2 (Janus kinase 2; an upper signal of STAT3), STAT3 and VEGF.

SalB was then examined for its in vivo reversal activities in emphysema induced with porcine pancreatic elastase (PPE) and cigarette smoke extract (CSE) in rats. Upon establishment of emphysema on day 21, SalB was administered to the lungs three times weekly over three weeks. SalB at 0.2 mg/kg significantly recovered \sim 85 %-impaired treadmill exercise endurance by 57-82 %; and reduced abnormal airspace enlargement by 59-75 %. In the PPE-induced emphysematous rats, SalB also reduced the 4-fold greater alveolar destruction index by 61 %. The lung tissue protein expression by Western blot analysis found that cleaved caspase 3 (cell apoptotic marker) was induced by 13-fold, and VEGF was reduced by 60 % in the PPE -induced emphysematous rats. However, pulmonary treatment with SalB at 0.2 mg/kg normalized these proteins, and also significantly increased the expression of a cell proliferation marker, proliferative cell nuclear antigen (PCNA) by 2.6-fold. Note however that SalB treatment did not reduce the neutrophilic myeloperoxidase activity in the lungs induced in the PPE-induced rats. Taken

all together, this study has demonstrated that SalB potently inhibited lung cell death, stimulates lung cell proliferation and migration, and restores stem cell migration with its mechanism of STAT3 activation and VEGF elevation and reversed *established* emphysema in rat models.

CHAPTER 1

BACKGROUND AND SIGNIFICANCE

1.1. COPD and Emphysema

Chronic obstructive pulmonary disease (COPD) is comprised of two lung diseases, chronic bronchitis and emphysema (Rabe et al. 2007). Hence, emphysema is a manifestation of COPD, and pathobiologically causes a loss of lung's elastic recoil and destruction of the alveolar septa, resulting in airspace enlargement and airflow obstruction (Snider et al. 1985). This alveolar structural destruction and loss are progressive and believed to be irreversible, thereby eventually leading to death (Snider et al. 1985). Epidemiological studies indicate that COPD affects 24 million Americans, but a half of them remain undiagnosed (Akinbami et al. 2013). It is currently the third-leading cause of death in the United States (US) with annual 120,000 deaths, and is predicted to be the third-leading cause of death worldwide by 2020 (Punturieri et al. 2008). In the US, its increasing socioeconomic burden reaches \$50 billion in annual direct and indirect health care expenditures (Akinbami et al. 2013). Even so, the pharmacological treatment of COPD/emphysema remains palliative only to improve the disease status (Diette et al. 2015). While chronic cigarette smoking is the predominant risk factor, COPD/emphysema also occurs in non-smokers, 35 % of which are due to genetic factors like the α 1-antitrypsin deficiency or air pollution in low-to-middle income countries (WHO 2004).

1.2. Current Treatment of COPD/Emphysema

Approximately 85 % of COPD/emphysema deaths are associated with active or passive exposure to cigarette smoke (Marcelino et al. 2014). Hence, smoking cessation is a preventive therapy, yet it has shown a very low success rate of 7-10 % (Messer et al. 2008). This is in contrast to the nicotine replacement therapies using nicotine gum, patches, lozenges, nasal spray, and inhalers, reporting an increased success rate of smoking cessation by 60 % (Zhang et al. 2015). In fact, a Cochrane systematic review has attested that a combination of behavioral treatment and pharmacotherapy is the most effective in helping smokers with COPD quit smoking (van Eerd et al. 2016). Meanwhile, pulmonary rehabilitation programs like lung volume reduction surgery (LVRS) have resulted in improved performance in some patients with severe emphysema, however, they are cost-prohibitive and are associated with an increased risk of morbidity and mortality (van Agteren et al. 2006). The current inability in transforming COPD/emphysema treatment has been suggested to be associated with a number of factors including failure to diagnose early stages of the disease (Marchetti & Criner 2016).

To date, the pharmacological treatment options for COPD/emphysema are limited to inhaled corticosteroids (ICSs), bronchodilators (β_2 agonists and anticholinergic) and phosphodiesterase-4 inhibitors or a combination thereof (Stockley et al. 2008). Table 1 summarizes the commonly used medications in COPD/emphysema approved by the US Food and Drug Administration (FDA) (Schamberger et al. 2014). These are used to manage symptoms, reduce the frequency and severity of exacerbations and improve the overall health by treating the co-morbidities (Punturieri et al. 2008; Marchetti & Criner

2016). Nevertheless, none of these molecules have conclusively shown to modify the long-term lung function decline seen in COPD/emphysema patients (GOLD 2017; Barnes & Stockley 2005). Therefore, there is no pharmacological therapy to reverse or repair emphysematous lung damages (Marchetti & Criner 2016). New molecules for COPD that are currently being studied in clinical trials include anti-inflammatory agents: theophylline, phosphoinositide 3-kinase inhibitors and curcumin; and anti-oxidants: andrographolide, sulforaphane and chalcones (<https://clinicaltrials.gov>). However, again, these molecules are expected for management of the disease symptoms, so that reversal of the emphysematous lung damages would not be feasible.

Table 1.1: FDA approved drugs for COPD/emphysema treatment (Schamberger et al. 2014)

Medication	Classification	Drug
<i>Bronchodilators</i>	β 2-agonists (short-acting)	Fenoterol, Levalbuterol, Salbutamol, Terbutaline
	β 2-agonists (long-acting)	Formoterol, Arformoterol, Indacaterol, Salmeterol, Tulobuterol
	Anticholinergics (short-acting)	Ipratropium bromide, Oxitropium bromide
	Anticholinergics (long-acting)	Acclidinium bromide, Glycopyrronium bromide, Tiotropium bromide
	Methylxantines	Aminophylline, Theophylline
<i>Combination bronchodilator therapy</i>		Fenoterol/Ipratropium bromide, Salbutamol/Ipratropium bromide, Vilanterol/Umeclidium bromide
<i>Corticosteroids</i>	Inhaled corticosteroids	Beclomethasone, Budesonide, Fluticasone
	Systemic corticosteroids	Prednisone, Methyl-prednisolone
<i>Combination bronchodilator therapy/ inhaled corticosteroid</i>		Formoterol/Budesonide, Formoterol/Mometasone, Salmeterol/Fluticasone, Vilanterol/Fluticasone
<i>Phosphodiesterase-4 inhibitors</i>		Roflumilast

1.3. Pathogenesis of COPD/Emphysema

While chronic cigarette smoking has been shown to be the most important risk factor in COPD/emphysema, its pathogenesis still remains enigmatic even as of today (Taraseviciene-stewart & Voelkel 2008; Fletcher & Peto 1977). Cigarette smoke has protean detrimental effects on both the lung's epithelia and endothelia, causes damages and loss of the microvasculature, and eventually destroys alveolar structures (Figure 1.1) (Hueper et al. 2015). It has been a long-term belief that this is due to three predominant pathogenic factors, namely, oxidative stress, elastolysis and inflammation, collectively referred to as the "triple threat" (Snider 1981). Accordingly, potential applications of inhibitors of each of these pathways have been explored over the last three decades, but remain to prove beneficial in reversing emphysema in clinical studies (Fischer et al. 2011).

The alveolar septa in patients with COPD are thin and often almost avascular, which implies that reduced vascularization may be involved in this pathogenesis (Liebow 1959). Although the "triple threat" hypothesis is supported by the evidence of elevated lung inflammation, oxidative stress and proteolysis in emphysema, it does not explain how the progressive nature of the alveolar structural destruction and loss persists even after cessation of smoking (Fletcher & Peto 1977). As a part of the effort to clarify if alternate cellular mechanisms are responsible for the development and progression of emphysema, Kasahara et al. (2000) identified that endothelial cell apoptosis was induced in emphysema lungs, associated with reduced expression of vascular endothelial growth factor (VEGF) and one of its receptor, VEGF -receptor 2 (VEGFR2). Accordingly, Kasahara et al. (2001) then showed that the blockade of VEGF -receptor induced

endothelial cell death by apoptosis and emphysema in rats. Reduced VEGF expression in the sputum and lung tissues of emphysema patients were also identified, which supported the impaired VEGF signaling in emphysema (Kanazawa et al. 2003; Yasuo et al. 2011). Subsequently, this “VEGF deficiency” was linked to decreased expressions of VEGF’s upstream regulating molecules, hypoxia inducible factor 1 α (HIF-1 α) and histone deacetylase (HDAC), seen as a result of chronic cigarette smoking (Ito et al. 2005; Mizuno et al. 2011). These evidences were sufficient to propose VEGF as a critical “lung structure maintenance factor” and thus, its reduced expression and impaired signaling as an essential pathologic mechanism in emphysema lungs (Medford & Millar 2006). If so, pharmacological recovery of VEGF expression may be an approach for lung structural repair and reversal of emphysema.

VEGF and its signaling are however involved in many aspects of COPD, more than just emphysema, such as bronchial wall remodeling and pulmonary hypertension. Thus targeting VEGF in COPD may cause off-target effects on some of such other aspects, which are largely unknown or unpredictable (Bakakos et al. 2015). Even so, the loss of alveolar capillary structure in emphysema surely causes a vascular disease, which can be corrected by restoring and/or stimulating VEGF expression, given the vulnerability of the endothelial cells to VEGF paracrine and autocrine survival signals (Taraseviciene-stewart & Voelkel 2008). Apart from improving cell survival, VEGF is also proposed to promote repair of the adult lung tissues in emphysema, given its role as an important growth factor.

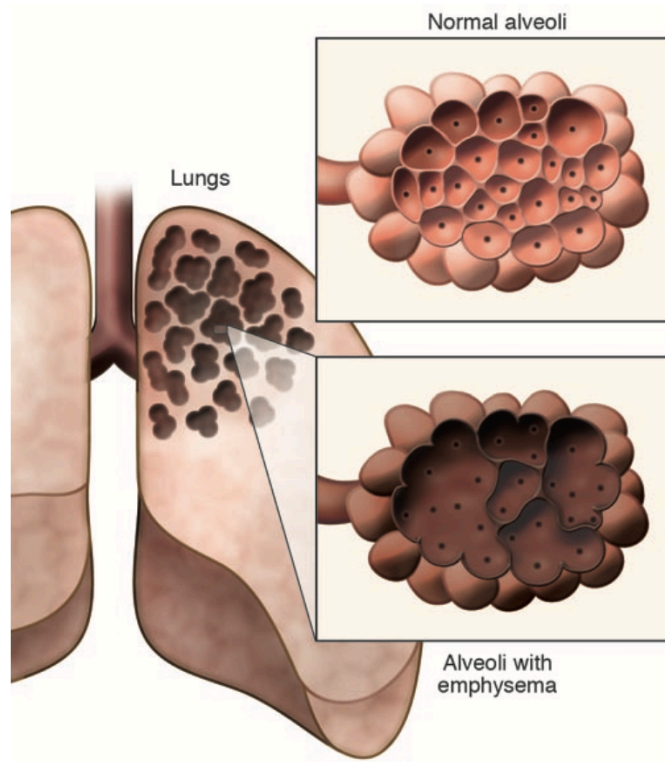


Figure 1.1: Normal and emphysematous alveoli in the lung (Taraseviciene-Stewart & Voelkel 2008)

1.4. JAK2-STAT3-VEGF Signaling Pathway

One of the upstream regulators for both VEGF and HIF-1 α is the signal transducer and activator of transcription 3, STAT3 (Xu et al. 2005). Upon activation of cytokine, erythropoietin or growth factor receptors bound to intracellular janus kinases 2 (JAK2), STAT3 is phosphorylated to its active form phosphorylated STAT3 (pSTAT3), which induces its dimerization and translocation into the nucleus for binding to the VEGF promoter region for VEGF transcription, as schematically described in Figure 1.2 (Chen & Zhong 2008; Dong et al. 2010). This pSTAT3 is also associated co-operatively with HIF-1 α on the VEGF promoter region to participate in VEGF regulation (Xu et al. 2005). Therefore, activation of the JAK2-STAT3 signaling can in theory elevate tissue expression of VEGF.

Apart from its critical role in VEGF regulation, STAT3 is also a key factor to promote cell proliferation, differentiation and angiogenesis (Chen & Zhong 2008). Cigarette smoke was shown to induce STAT3 activation, playing a protective role in maintaining normal lung homeostasis and function by regulating critical processes in inflammation, apoptosis, and protease expression (Geraghty et al. 2013). This study speculated that targeting STAT3 could be used as an approach to counter the injurious effects of cigarette smoke exposure. JAK2 has also been shown to play an important role in mediating proliferation and differentiation of alveolar cells (Wagner et al. 2004). Thus, targeting JAK2-STAT3 could correct pathologically reduced VEGF levels in emphysema to promote lung repair by increasing cell survival and proliferation.

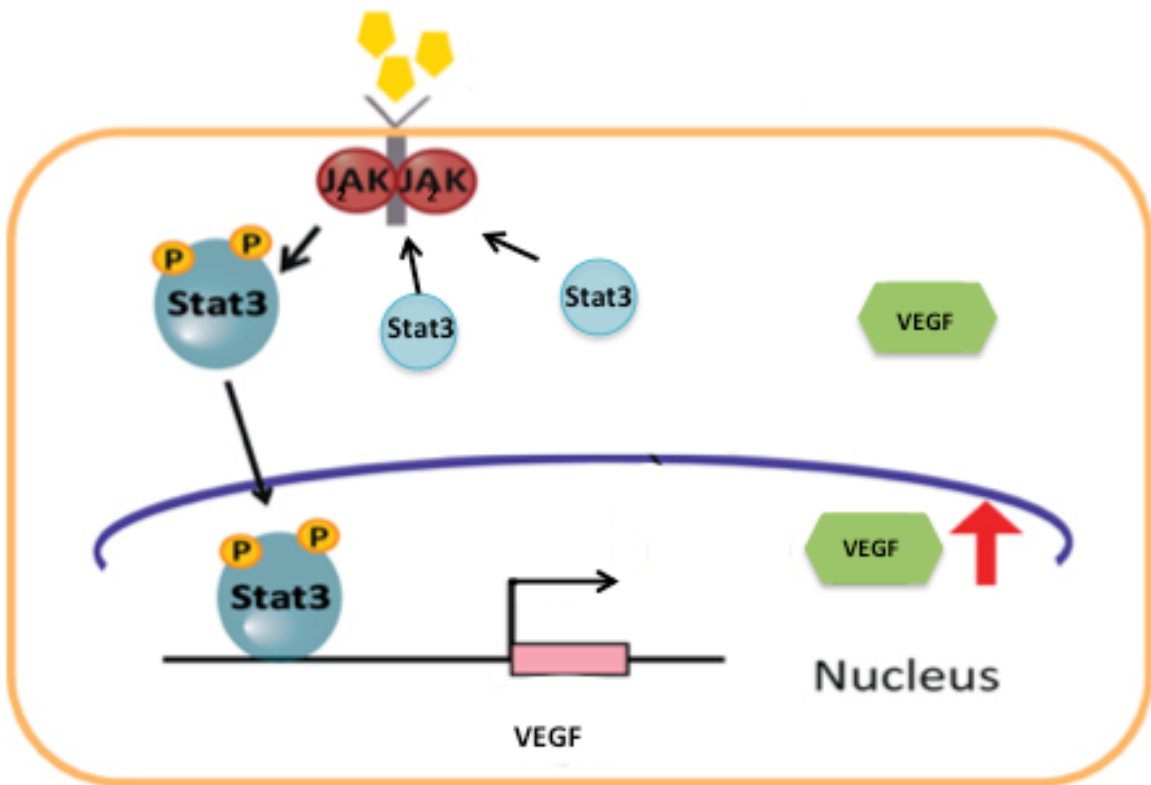


Figure 1.2: Intracellular JAK2-STAT3-VEGF activation pathway

1.5. Salvianolic acid B (SalB)

SalB is a polyphenol and a major water-soluble bioactive compound extracted from danshen, a dried root of *Salvia miltiorrhiza* (Figure 1.3). As a traditional Chinese medicine, danshen has long been used to improve blood circulation in the treatment of cardiovascular diseases. Hence, many danshen products are commercially available as oral tablets, capsules, liquids and dripping pills as well as for intravenous injection, creating a \$120 million market worldwide (Chen et al. 2014). However, danshen has not yet been approved by the FDA and is currently in Phase II clinical trials for cardiovascular disease treatments (<https://clinicaltrials.gov>).

SalB has been studied in animal models for anti-oxidation, anti-inflammation, anti-coagulant, anti-thrombotic, anti-cancer and angiogenic activities (Wang et al. 2013). These activities were aimed at treating diseases like myocardial infarction, ischemia-reperfusion injury, atherosclerosis, Alzheimer disease and head and neck cancer (Ho & Hong 2011; Zhao et al. 2011; Chen et al. 2014; Lay et al. 2003). The applications of SalB, however, have been limited due to its poor oral bioavailability of less than 3% (Wu et al. 2006). Moreover, despite such various activities, its cellular and molecular targets or downstream signal network has not been clarified (Feng et al. 2011).

SalB was shown to increase angiogenesis by enhancing the gene expression of VEGF and its receptor in murine endothelial cells (Lay et al. 2003). Another recent study reported an increased expression of pSTAT3 following SalB treatment in embryonic stem cells (Liu et al. 2014). Hence, these SalB's promotion of STAT3-VEGF signaling may be capable of pharmacologically reversing the reduced VEGF expression in emphysematous lungs. In addition, its anti-oxidative and anti-inflammatory properties may also suppress

the induced oxidative stress and inflammation. Given its low oral absorption, hydrophilicity and ionization potential, SalB when administered via inhalation, is expected to result in slower and lower absorption from the lung and thereby in turn enable longer retention. It was hypothesized therefore that pulmonary administration of SalB is capable of STAT3 activation and VEGF elevation, thereby reversing lung damages in emphysema, as shown in the Figure 1.4.

A)

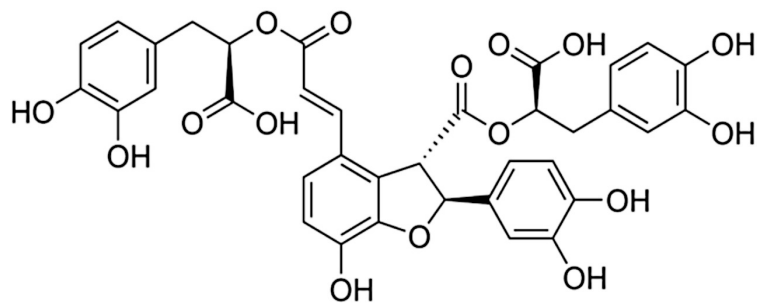


(a) Portion above ground



(b) Roots for pharmaceutical use

B)



Salvianolic acid B

Molecular formula: $C_{36}H_{30}O_{16}$

Molecular weight: 718.61

LogP = 2.14 (Huang et al. 2014)

LogD_{7.5} = -2.88 (Zhou et al. 2009)

pKa = 2.77 (Huang et al. 2014)

Figure 1.3: (A) *Salvia miltiorrhiza*; and (B) the structure and physicochemical properties of its major active component, salvianolic acid B (SalB) (Wang et al. 2013).

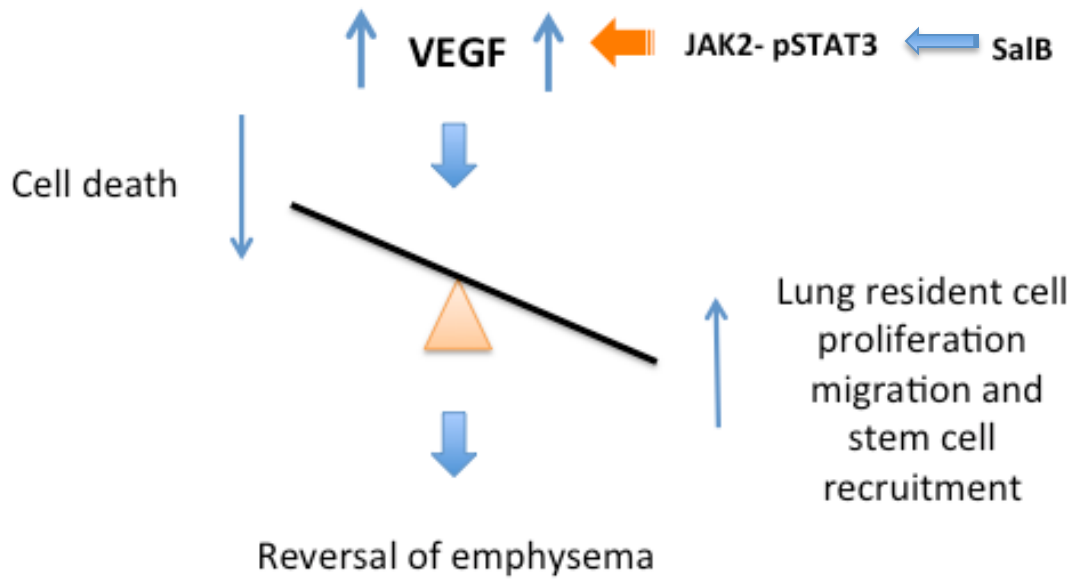


Figure 1.4: Proposed mechanism for emphysema reversal by SalB

1.6. Towards Reversal of Emphysema

Alveolar structural destruction and loss in emphysema are considered to be the result of a pathologic imbalance between cell death and cellular repair processes, and has been attributed, at least in part, to the VEGF deficiency (Lee et al. 2012; Morissette et al. 2009). VEGF receptor blockade in animals induced apoptosis of lung cells and caused emphysema that remained irreversible even by their natural repair mechanisms (Kasahara et al. 2001; Voelkel et al. 2006). Correcting this progressive cell loss would be critical in restoring the alveolar structures. While deficiency of growth factors like VEGF was linked to reduced cell proliferation, conflicting evidences exist as to cell proliferative activities in emphysematous lung (Yokohori et al. 2004; Imai et al. 2005). Regardless of the disease state, however, stimulating cell proliferation would be essential to restore the alveolar structure and function. Emphysema has also been characterized by dysregulated wound healing and cell migration processes, which is also somehow regulated by VEGF (Shaw & Martin 2016; Perotin et al. 2014). Thus restoring VEGF can be proposed not only to protect the lung cells from damages, but also to promote cell proliferation and migration towards reversal of emphysema.

A modern concept has emerged that both tissue resident and bone marrow-derived circulating stem cells participate in the (patho)physiologic maintenance of the adult lung structures (Taraseviciene-stewart & Voelkel 2008). Among such stem cell populations, mesenchymal stem cells (MSCs), progenitor cells of mesodermal origin, have shown the most promising results in many cases owing to their multi-lineage potential and ability to migrate to the sites of tissue injury and to exert anti-inflammatory activities (Siniscalco et al. 2008). However, homing to the lung in the recruitment of such

bone marrow-derived stem cells is considerably inefficient (Conese et al. 2014). Moreover, as VEGF regulates stem cell mobilization and recruitment, it has been speculated that these processes may be impaired in emphysema (Ishizawa et al. 2004; Taraseviciene-stewart & Voelkel 2008). If so, a molecule intended to repair damaged lungs in emphysema can also promote recruitment of circulating stem cells into the lung. The complementary processes of cell death and cell proliferation, migration and recruitment may therefore need to be balanced in emphysema, as shown in Figure 1.4.

While the VEGF hypothesis naturally concerns endothelial cell death (Kasahara et al. 2000), the proteases and oxidants imbalance hypotheses (Morissette et al. 2011) concern epithelial cell damages in emphysematous lung. However, studies have shown that there are significant interactions between the two cell types in the alveoli, such that a severe damage to one could lead to disruption of the other (Sirianni et al. 2003). Thus, both of these cell types are necessary to study, when emphysema reversal activities are sought. Moreover, damages to the alveolar type I (ATI) cells stimulate proliferation and migration, and even differentiation of surviving alveolar type II (ATII) cells at the wounded sites (Kim et al. 2010; Sugahara et al. 2006).

Taken all together, this dissertation project aimed to demonstrate the reversal activities of SalB as a novel natural chemical entity for pulmonary delivery in the treatment of emphysema and COPD. After confirming its anti-oxidative activity and lack of anti-elastase activity, a series of in vitro lung epithelial and endothelial cell systems were used to examine its inhibitory activities in cell death; and promoting activities of cell proliferation, migration and trans-endothelial migratory recruitment of MSCs. Their JAK2-STAT3-VEGF dependence was also examined with respective pharmacologic

inhibitors. SalB was examined with pulmonary delivery in the rat models of *established* emphysema induced with porcine pancreatic elastase (PPE) and cigarette smoke extract (CSE). The lung functional and morphological recoveries as well as changes of key protein and biochemical markers in the lungs were determined.

CHAPTER 2

HYPOTHESES AND SPECIFIC AIMS

This dissertation project aimed to demonstrate the therapeutic activity of salvianolic acid B (SalB) as a novel drug molecule for pulmonary delivery in the treatment of emphysema. It was hypothesized that SalB reverses *established* emphysema by pharmacologically recovering and/or stimulating VEGF expression in the lungs through STAT3 activation. Specifically, this project was designed and structured 1) to confirm the anti-oxidative activity, absence of anti-elastase activity, and lung's STAT3 and VEGF elevating activity of SalB 2) to examine JAK2-STAT3-VEGF dependent anti-cell death, cell proliferation, migration and MSC recruitment promoting activities of SalB in a series of in vitro cell systems; and 3) to assess the reversal activities of SalB in the in vivo rat models of *established* emphysema. This project pursued the following 5 hypotheses:

1. SalB is potently anti-oxidative but not anti-elastase, while elevating the lung tissue expression of STAT3 and VEGF following pulmonary administration
2. SalB exerts potent JAK2-STAT3-dependent anti-cell death activities against lung epithelial and endothelial cell death induced with oxidative stress and by VEGF receptor blockade
3. SalB exerts potent JAK2-STAT3-VEGF-dependent lung epithelial and endothelial cell proliferation and migration stimulatory activities

4. SalB promotes the trans-endothelial migratory recruitment of stem cells
5. Pulmonary administration of SalB enables functional and morphological reversal of emphysema induced with porcine pancreatic elastase (PPE) and cigarette smoke extract (CSE) in rats by normalizing VEGF expression

In Chapter 3, SalB will be examined in the *in vitro* systems to confirm its anti-oxidative potency and lack of anti-elastase activity. Additionally, SalB's *in vivo* potencies for STAT3 activation and VEGF elevation will be identified in healthy rats following pulmonary administration. In Chapter 4, SalB's inhibitory activities against induced emphysematous cell death and stimulatory activities in cell proliferation and migration will be assessed in the lung epithelial and endothelial cell systems. The effects of JAK2, STAT3 and VEGF inhibitors on each of these activities will also be assessed to explore its mechanism of action. Subsequently, the *in vitro* trans-endothelial migration assay for MSCs will be developed and used to assess SalB's promoting activities of MSC migratory recruitment with or without VEGF receptor blockade. In Chapter 5, emphysema will be induced and established with PPE and CSE and then, SalB will be administered to the lungs over 3 weeks. Changes in the lung functionality and morphology as well as key protein and biochemical markers in the lungs will be determined. Finally, Chapter 6 will summarize all the findings in this dissertation project and provide overall conclusions.

CHAPTER 3

SALVIANOLIC ACID B (SalB): ANTI-OXIDATIVE, ANTI-ELASTASE AND STAT3 AND VEGF ELEVATING ACTIVITIES

3.1. Introduction

As described in Chapter 1, anti-oxidative and anti-elastase activities continue to be sought to treat damaged lungs of emphysema and COPD, given their “triple threat” pathogenesis of induced oxidative stress, elastolysis and inflammation (Snider 1981). By contrast, “VEGF deficiency” has also been implicated in the emphysematous lungs as a result of impaired epigenetic regulations (Yasuo et al. 2011; Wagner 2003). In this context, a natural polyphenolic caffeic acid tetramer, salvianolic acid B (SalB), has become of our interest as a molecule that may be capable of treating damaged lungs in emphysema by virtue of its catechol-based anti-oxidative activity as well as its potency of stimulating VEGF signaling via activation of an upstream transcription factor STAT3 (Zhao et al. 2008; Liu et al. 2014). However, whether SalB possesses anti-elastase activity in addition to the anti-oxidative activity, activates STAT3 and elevates VEGF in lung tissues remain unknown. Hence, in this chapter, SalB was examined in the *in vitro* chromogenic radical scavenging and elastase inhibitory activity assays. SalB was also assessed *in vivo* in rat lungs to examine its potency and effective dose to activate STAT3 (i.e., STAT3 phosphorylation) and elevate VEGF as a molecular proof of concept for the assessments of *in vitro* and *in vivo* therapeutic activities in emphysema in Chapter 4 and 5.

3.2. Materials and Methods

3.2.1. Anti-oxidative activity assessment

SalB was purchased from Ivy Fine Chemicals (98 % purity, Cherry Hill, NJ) as a pale yellow-to-off white powder and stored at room temperature in a desiccator with silica gel prior to experiments. The in vitro chemical anti-oxidation assay kit obtained from Cayman Chemical Company (Ann Arbor, MI) was used in a 96-well plate format, according to Cayman's protocol. The assay employed formation of a stable chromogenic radical cation, $ABTS^{\bullet+}$ from 2,2'-azinobis(3-ethyl-benzothiazoline-6-sulphonic acid) (ABTS) during incubation with metmyoglobin and hydrogen peroxide (H_2O_2) at room temperature. This produced a blue-green color that could be measured at 750 nm. SalB was added at 0.01-100 μM in this assay kit, and the absorbance change (ΔAbs) in the first 5 min was monitored using a plate reader (SynergyTM 2, BioTek Instruments, Inc., Winooski, VT) as the initial rate of $ABTS^{\bullet+}$ production. The ΔAbs (Y) was then plotted as a function of logarithmic concentrations (C) of SalB. The half-maximal (50 %) inhibitory concentration (IC_{50}) and Hill slope (HS) values were derived from the concentration-response curves fitted to the following 4-parameter logistic function equation:

$$Y = Y_{\min} + (Y_0 - Y_{\min}) / [1 + (C/IC_{50})^{HS}]$$

Where, Y_0 is the ΔAbs value in the absence of SalB and Y_{\min} is the lowest asymptotic ΔAbs value seen at the highest test concentration (i.e., 100 μM). The non-linear curve fitting was performed using Prism[®] 7 (GraphPad Software, San Diego, CA). The

“goodness-of-fit” of the curve fitting was ensured with >0.99 of the Prism-derived R² values, in addition to visual inspection of residuals.

3.2.2. Anti-elastase activity assessment

The in vitro anti-elastase activities of SalB were determined using human sputum elastase (HSE) hydrolysis of a chromogenic substrate N-methoxysuccinyl Ala-Ala-Pro-Val p-nitroanilide (MeOSuc-AAPV-pNA, Sigma-Aldrich) in a 96-well format, according to the method described by Saluja et al. (2013). MeOSuc-AAPV-pNA was prepared as a 8.75 mM stock solution in dimethyl sulfoxide (DMSO; Sigma-Aldrich, St. Louis, MO). HSE (8750 U/mg) purchased from Elastin Products and Co. (Owensville, MO) was prepared as a 50 U/ml stock solution in acetate buffer (pH 5.5). A 0.18 ml solution of SalB at 0.1 – 200 μM was incubated with 0.02 ml of HSE stock solution and 0.06 ml of the 0.87 mM MeOSuc-AAPV-pNA solution to initiate the hydrolysis reaction. The initial rate of absorbance change (ΔAbs) due to p-nitroaniline generation was measured in the first 10 min at 405 nm using the microplate reader (SynergyTM2). The fraction of HSE activity remaining (Y) was determined from the following equation and plotted as a function of logarithmic concentration (C) of SalB:

$$\text{Fraction of HSE activity remaining} = \frac{\Delta Abs \text{ with SalB}}{\Delta Abs \text{ without SalB}}$$

The IC₅₀ and HS values were derived from the concentration-response curves fitted to the 4-parameter logistic function equation, as described above (3.2.1. Anti-oxidative activity assessment).

3.2.3. In vivo pSTAT3 and VEGF activation in the lung tissues

Adult male Sprague-Dawley rats (250–275 g; Hilltop Lab Animals, Scottsdale, PA) were used, according to the animal experimental protocols approved by the VCU's Institutional Animal Care and Use Committee (IACUC). Saline or SalB at 0.2 mg/kg (0.1 ml) was orotracheally spray-instilled to the lung with PennCentury's Microsprayer under short anesthesia with isoflurane once daily for 5 days per week over two weeks, as described previously (Saluja 2014). Animals were then sacrificed via exsanguination under surgical anesthesia with an intraperitoneal urethane at 1 g/kg. While the left lung lobes were inflated with warm agarose solution (0.5 %) for the assessment of the airspace enlargement (as described in Chapter 5), the right lung tissues were immediately minced for Western blot analysis to determine the lung tissue levels of pSTAT3 and VEGF, as described below.

Western blot analysis is fully described in the Appendix 1. The minced lung tissues (300 mg) were homogenized on ice using hand homogenizer (Pro 200; Pro Scientific, Inc., Oxford, CT) with the NP-40 lysis buffer. The lysis buffer was 1 % Nonidet P40 (NP-40; Thermo Fisher Scientific, Waltham, MA), 50 mM Tris (pH 8; Sigma-Aldrich) and 150 mM NaCl (Thermo Fisher Scientific), which dissolved a cOmplete™ protease inhibitor cocktail tablet (Roche Diagnostics, Indianapolis, IN), according to the supplier's recommendation. For detection of pSTAT3, a PhosSTOP™ phosphatase inhibitor tablet (Roche) was also dissolved in the lysis buffer, according to Roche's recommendation. Supernatant was collected after centrifugation at 16,000 g in 4°C (Aventi JE Centrifuge; Beckman Coulter).

After protein content determination by the BCA assay (Thermo, Grand Island,

NY), 40 µg of protein was denatured at 100 °C for 10 min, electrophoresed on a 10 % Mini-PROTEAN TGX polyacrylamide gel (Bio-Rad; Hercules, CA), and transferred to the nitrocellulose membranes (0.2 mm; Bio-Rad). After 1 h blocking at room temperature in the blocking buffer recommended for each antibody by its supplier, the membrane was probed via overnight incubation at 4 °C with each of the mouse or rabbit antibodies raised against: pSTAT3 (1:1000, phosphorylated STAT3-Tyr705, rabbit polyclonal, #9131, Cell Signaling Technology, Danvers, MA), VEGF (1:100, mouse monoclonal, sc-7269, Santa Cruz, Dallas, TX) and β-actin (1:5,000, mouse monoclonal, Sigma-Aldrich). The membranes were then incubated in horseradish peroxidase-conjugated goat anti-mouse or anti-rabbit antibody (Bio-Rad Laboratories) for 80 min at room temperature. The probed protein was detected with the SuperSignal West Pico enhanced chemiluminescent substrate kit (Pierce, Rockford, IL) in the film processor (X-Omat 2000A; Eastman Kodak, Rochester, NY). Their band signals were quantified with the ImageJ software (NIH, Bethesda, MD). Each protein signal was normalized with the corresponding β-actin signal within the same membranes, and expressed as the value relative to that for the untreated healthy rat lungs.

3.2.5. Data description and statistical analyses

The results of the in vitro anti-oxidative and anti-elastase assessments were expressed as mean ± standard deviation (SD) from triplicate experiments (n=3). The in vivo protein expression results were expressed as treatment group mean ± standard error (SE) from n = 3 or 4. Statistical analyses for group comparison were performed with JMP-Pro[®] 12 (SAS Institute, Inc., Cary, NC) using two-tailed *t*-test with p<0.05 as significant.

3.3. Results and Discussion

3.3.1. In vitro ABTS radical scavenging activity of SalB

Figure 3.1 shows the ΔAbs in the first 5 min due to $\text{ABTS}\cdot^+$ generation at various concentrations of SalB. SalB exhibited potent concentration-dependent radical scavenging activities, as indicated by ΔAbs suppression with increasing concentration. The IC_{50} value was $3.67\pm 0.09\ \mu\text{M}$ (95% CI: 3.48-3.88 μM). This ABTS scavenging activity was more potent than the same radical scavenging activity of Trolox ($\text{IC}_{50} = 9.4\ \mu\text{M}$) as well as caffeic acid (CA) $16.82\pm 1.16\ \mu\text{M}$ (Saluja et al. 2013). Due to its polyphenolic nature, SalB has been thought to possess antioxidant activity. In fact, the reactive oxygen species (ROS) scavenging activity of SalB against $\text{HO}\cdot$, $\text{O}_2\cdot^-$, DPPH (2,2-diphenyl-1-picryl-hydrazyl-hydrate) radicals was found to be more potent than that of Vitamin C (Zhao et al. 2008). Since SalB is structurally a CA tetramer, the 4 -fold more potent activity of SalB is likely related to this oligomer structure. The catechol moiety in the structure of SalB and CA has also been shown to exert the anti-oxidant property (Rice-Evans, 1996). The anti-oxidative effects of SalB and CA may therefore be attributed to this catechol moiety that has also been found in other CA oligomers (Saluja et al. 2013). The Hill-slope value for SalB was 3.7 ± 0.3 , which suggested apparent cooperativity. By the virtue of this anti-oxidative activity, SalB was further examined in Chapter 4 to assess its cytoprotective activity against oxidative stress-induced cell death.

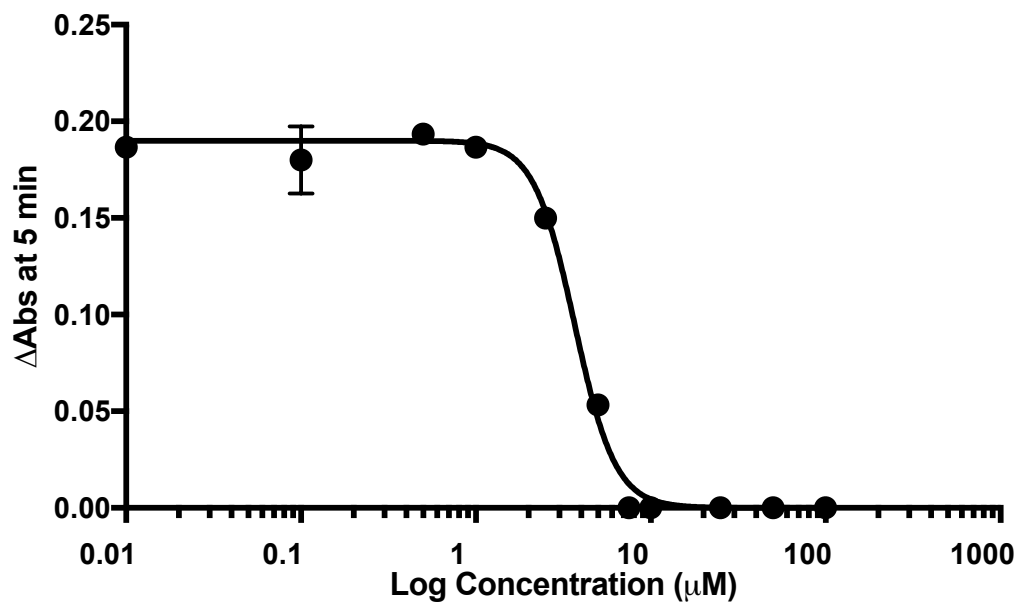


Figure 3.1: The absorbance increase in 5 min (ΔAbs) at 750 nm as a function of concentration of SalB in the chemical antioxidant assay. Data: mean \pm SD (n=3). The solid lines are the result of curve-fitting.

3.3.2. In vitro anti-elastase activity of SalB

The in vitro elastase inhibitory activity of SalB was assessed using the substrate hydrolysis assay that utilized a chromogenic HSE substrate to release p-nitroaniline, detected at 450 nm (Bieth & Wermuth 1973). Figure 3.2 shows the fraction of HSE activity remaining in the presence of different concentrations of SalB. SalB was devoid of HSE inhibitory activity at least upto 0.2 mM. This lack of HSE inhibitory activity of SalB implied a lack of elastolytic inhibition in the rat model of emphysema used to examine the reversal activity of SalB described in Chapter 5.

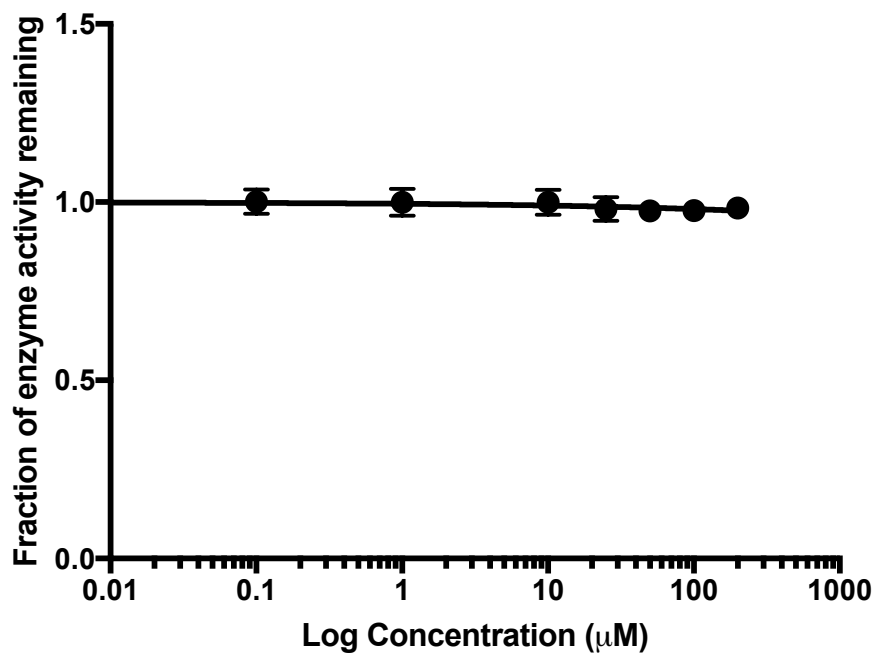


Figure 3.2: The fraction of HSE activity remaining as a function of concentration of SalB in the chromogenic substrate hydrolysis assay. Data: mean \pm SD (n=3).

3.3.3. Elevated pSTAT3 and VEGF expression in the lungs following SalB treatment

Figure 3.3 (A) shows the representative Western blot for pSTAT3 expression in the lungs of saline and SalB-dosed rats and the treatment group comparison by densitometry analysis. The two weeks pulmonary administration of SalB at 0.2 mg/kg elevated the lung tissue expression of pSTAT3 by 1.8-fold, compared to the saline-dosed control ($p < 0.05$). Likewise, as shown in Figure 3.5 (B), SalB administration also showed an increased VEGF expression by 1.6 -fold. However this increase did not reach significance, presumably due to their high variability. It appears, however, that SalB at 0.2 mg/kg was likely sufficient to activate STAT3 and stimulate VEGF in the lung tissues with pulmonary administration. It should be noted that this SalB treatment did not impair treadmill exercise endurance or cause abnormality of the airspace, as described in Chapter 5. Therefore, SalB at 0.2 mg/kg has been chosen for the therapeutic reversal activity assessments in the in vivo rat models of *established* emphysema in Chapter 5.

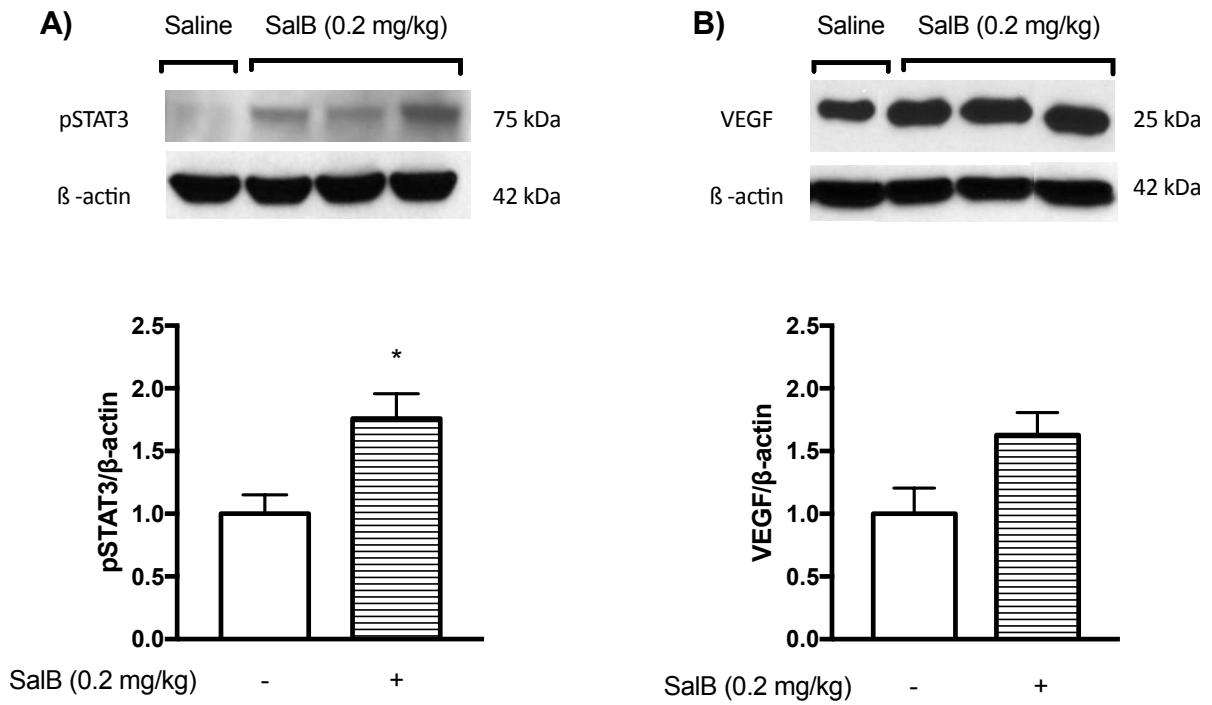


Figure 3.3: Lung tissue expression of cytoplasmic pSTAT3 (A) and VEGF (B) in healthy rats dosed with saline or SalB at 0.2 mg/kg, as indicated by representative bands at 75 and 25 kDa. Data: mean \pm SE (n=3 or 5) (+) present; (-) absent. * $p < 0.05$, compared to the saline control by two-tailed t -test.

3.4. Conclusions

SalB showed the potent free radical scavenging activity with IC_{50} of 3.67 μ M, but was devoid of the anti-elastase activity. In rats, pulmonary administration of SalB at 0.2 mg/kg appeared to elevate the lung expression of pSTAT3 and VEGF. Therefore, unlike the “triple-threat” inhibitors, SalB would fall under a different mechanistic class of compounds targeting VEGF stimulation to treat emphysematous lung damage. This VEGF stimulation appeared to arise from STAT3 activation, as reported previously elsewhere (Liu et al. 2014).

CHAPTER 4

IN VITRO CHARACTERIZATION OF ANTI-CELL DEATH, CELL PROLIFERATION, MIGRATION AND RECRUITMENT STIMULATORY ACTIVITIES OF SALVIANOLIC ACID B (SalB)

4.1 Introduction

As described in Chapter 1, progressive destruction and loss of alveolar septal structures in emphysema is thought to be a result of an imbalance between induced cell death and suppressed cell proliferation, migration and recruitment in the lung. In this context, VEGF has received considerable attention by the virtue of its regulatory activities in the alveolar epithelial and endothelial cell survival, proliferation, migration as well as trans-endothelial recruitment of circulating stem cells to the lungs (Takahashi et al. 2005; Caiado & Dias 2012). In fact, the lung tissue level of VEGF was reduced in patients with emphysema/COPD; and VEGF receptor blockade caused lung cell death and emphysematous structural damages in animals (Yasuo et al. 2011; Kasahara et al. 2000). Therefore, pharmacological recovery of VEGF may enable reversal of this lung cellular pathobiologic imbalance, and thereby repair of the alveolar structural destruction in emphysema.

Salvianolic acid B (SalB) has been reported to stimulate VEGF as a result of activation of Janus kinase 2 (JAK2) and signal transducer and activator of transcription 3 (STAT3) in vitro (Liu et al. 2014). In Chapter 3, SalB at a dose of 0.2 mg/kg was shown to increase the lung tissue expression of pSTAT3 and VEGF in vivo, in addition to its potent anti-oxidation activity. Accordingly, in this chapter, SalB was assessed in the lung

alveolar epithelial (A549) and endothelial (HMVEC-L) cell systems to examine its activities in 1) protecting cells against oxidative stress and VEGF receptor blockade – induced cell death; 2) stimulating cell proliferation and migration; and 3) promoting trans-endothelial stem cell recruitment. Pharmacologic inhibitors of JAK2, STAT3 and VEGF were then used to assess the JAK2, STAT3 and VEGF -dependent mechanisms.

4.2. Materials and Methods

4.2.1. SalB and inhibitors

SalB (Ivy Fine Chemicals) was stored at room temperature in a desiccator with silica gel and freshly prepared as a 1 mM (0.718 mg/ml) aqueous solution before each experiment. SU5416, a VEGF receptor antagonist, was a gift from Dr. Voelkel (VCU Pulmonary Medicine) and stored at -20°C prior to use. SU5416 stock solution (20 mM) was prepared in dimethylsulfoxide (DMSO; Sigma-Aldrich) that had been degassed by purging N₂ gas for 5 min. AG490 (Tyrphostin; Sigma-Aldrich) was used as a tyrosine kinase inhibitor of JAK2, while S31-201 (Sigma-Aldrich) as an inhibitor of STAT3 phosphorylation and dimerization (Hermann et al. 2009; Park et al. 2014). These inhibitors were prepared as 50 mM and 68 mM stock solutions in degassed DMSO and stored as 50 µl aliquots at -20 °C and -80 °C, respectively.

4.2.2 Lung alveolar epithelial, endothelial and mesenchymal stem cell culture

Human alveolar epithelial A549 cells (American Type Culture Collection; ATCC, Manassas, VA) were cultured in the Dulbecco's Modified Eagle's medium/F-12 (ATCC) supplemented with 10 % fetal bovine serum (FBS; Gibco-Australia) and 1 % Penicillin-streptomycin (ATCC); propagated in the 25 or 75 cm² culture flasks (Corning Costar; Cambridge, MA) according to the ATCC's protocol [Product Information Sheet, ATCC]; and used between 20-30 of the passages. Human pulmonary microvascular endothelial cells (HMVEC-L) cells (Lonza, Walkersville, MD) were cultured in the endothelial cell growth medium (Lonza) with growth factors, cytokines and supplements (Lonza); grown in the 75 cm² culture flasks, according to the Lonza's protocol; and used between 5-9 of

the passages. Bone marrow derived human mesenchymal stem cells (MSCs; Roosterbio, Frederick, MD) were cultured in DMEM/F12, GlutaMAX (Thermo) supplemented with 10 % FBS; propagated in the 75 cm² culture flasks, according to the Roosterbio's protocol; and used between 3-6 of the passages. These cell cultures were maintained in a humidified atmosphere of 5 % CO₂/95 % air at 37 °C in the incubator (CO2 cell standard, BMT USA, LLC, Monroe, WA). The culture media were replaced three times in a week and the cells were passaged upon reaching 90 % confluence, monitored under the microscope (Nikon-TMS phase contrast microscope, Image Systems Inc., Columbia, MD).

4.2.3 Anti-cell death activity assessments

The in vitro protective activities of SalB and their JAK2 and STAT3 dependence were assessed in the A549 and HMVEC-L cells against cell death induced by oxidative stress and/or VEGF-receptor blockade, using the trypan blue exclusion assay and propidium iodide (PI)-based flow cytometry. The procedure followed, that developed previously (Truong 2016), with slight modifications. Trypan blue reagent (4 %; Amresco, Solon, OH) was sterile-filtered using the 0.2 µm syringe filter (Corning) before use. The A549 and HMVEC-L cells were plated on to the 24 or 48-well plates at a density of 0.15 x 10⁶ cells/well. Cell death was induced with 0.1 mM hydrogen peroxide (H₂O₂; Acros Organics, New Jersey, NJ) or 20 µM SU5416 over 24 h. SalB was added at 1, 10 or 25 µM and co-incubated with H₂O₂ or SU5416 to examine its protective activities against H₂O₂-induced oxidative cell death and SU5416-induced apoptotic cell death (Kasahara et al. 2000). The media were used as the control vehicle. In some experiments, AG490 at

25 μ M or S31-201 at 50 or 100 μ M was co-incubated with SalB at 25 μ M, while cell death was induced with SU5416 for 24 h to examine whether SalB's anti-cell death activities depend on JAK2 and STAT3, respectively. At 24 h, % cell death was determined in each well by the trypan blue exclusion assay or by the PI-based flow cytometry. For the trypan blue exclusion assay, following trypsinization, the cell suspension was centrifuged at 12,000 rpm (Eppendorf centrifuge 5415 C, Hauppauge, NY) for 2 min. The cell pellet was re-suspended and incubated in the 4 % trypan blue solution at room temperature for 3-5 min. The cells were again centrifuged, re-suspended in the fresh medium, plated on to 24 –well plates and allowed to settle for 30 min. In each well, over 300 cells were differentiated and counted as stained dead cells and unstained live cells under the microscope (Omax, Kent, WA), to calculate % dead cells from:

$$\% \text{ dead cells} = \frac{\text{the number of dead cells}}{\text{the total number of live and dead cells}} \times 100$$

For the flow cytometry assay, at 24 h of the H₂O₂ –induced cell death with or without SalB incubation, the cells were trypsinized, re-suspended at 1x10⁶ cells/ml in 100 μ l of media, and incubated with 5 μ l of PI reagent of the FITC Annexin V Apoptosis detection kit I (BD Biosciences, San Diego, CA) at room temperature for 15 min. Following 5-times dilution with the assay buffer of the kit, over 10,000 cells were introduced into the Attune flow cytometer (Thermo Fisher Scientific) and sorted, according to 488 and 617 nm of the excitation and emission wavelengths, respectively. Note that proper performance of the flow cytometer had been ensured before each assay using CytoFLEX Daily QC fluorospheres (Beckman-Coulter, Brea, CA) as a quality

control test. Using the Attune NxT software, cells were gated to exclude the debris and clumps, and then sorted with respect to PI fluorescence signal set at a threshold of 2×10^4 , i.e., the cells exceeding this threshold of the fluorescence intensity were counted as PI-positive dead cells to calculate the % cell death in each well.

4.2.4. Cell proliferation activity assessment

The A549 and HMVEC-L cell proliferation activities were measured by the MTT (3-[4,5-dimethylthiazol-2-yl]-2,5-diphenyltetrazolium bromide) assay (Cayman Chemical Company) and BrdU (5-bromo-2-deoxyuridine) assay (Biovision Milpitas, CA). In 96-well plates, 0.02 or 0.04×10^6 cells were plated and allowed to settle overnight. Subsequently, the A549 cells were treated with SalB at 0, 10 or 25 μM in FBS suppressed (2 %) media for 0-48 h; and the HMVEC-L cells were treated with SalB at 0, 5, 10 or 25 μM in the growth media for 0-48 h. In the MTT assay, the MTT reagent (10 μl of 5 mg/ml) was added to 100 μl of the incubation media at 4 h before the end of treatment. At 48 and 24 h, respectively, the incubation media were removed, and replaced with 0.04 N HCl in isopropanol crystal dissolving solution (prepared in-house), for 15 min. The 570 nm absorbance (Abs_{570}) was then measured using a microplate reader (BioTek, Winooski, VT). In some studies, JAK2, STAT3 and VEGF inhibitors, AG490, S31-201 and SU5416 were co-incubated at 25, 50 or 100, and 5 μM , respectively, with SalB at 25 μM to examine the mechanism of SalB's cell proliferation stimulatory activities. Additionally, in the HMVEC-L cells, the cell proliferation activity of SalB was also measured with the BrdU activity, according to the kit protocol. Following 20 h incubation, the BrdU-labeled proliferative cells were quantified with the 450 nm

absorbance (Abs_{450}) measured using the microplate reader.

4.2.5. Cell migration activity assessment

The cell migration activities were determined using an in vitro scratch wound closure assay established and validated in house according to a method previously described by Liang et al. (2007). The HMVEC-L and A549 cells were seeded at 0.4×10^6 M cells/well on a 6-well plate and grown to confluence. The cell monolayers were scratched using a 200 μ l pipette tip and incubated with SalB (2.5, 5, 10, 25 μ M) or the vehicle for 12 and 48 h, respectively. In the A549 cells, a serum-suppressed medium (2% FBS) was used. Guided by the markings made on the well plate, images of the scratch wound were taken at 3 different points in each well. Pre- and post-incubation scratch wound areas (WA_{pre} and WA_{post}) were measured using ImageJ (NIH). For each treatment group, 3 wells were used. The percent wound closure was calculated using the equation:

$$\% \text{ wound closure} = \frac{WA_{pre} - WA_{post}}{WA_{pre}} \times 100$$

In some experiments, to clarify the mechanism of SalB's activity, AG490 (25 μ M), S31-201 (50 or 100 μ M) or SU5416 (5 μ M) were co-incubated with SalB to examine JAK2-STAT3 and VEGF dependence on the SalB's cell migration promotion activity.

4.2.6. Trans-endothelial migratory stem cell recruitment activity assessment

The MSC recruitment into the lung through the endothelial barrier was modeled using the in vitro trans-endothelial migration assay. The method originated from Muller

and Luscinskas (2008) and modified for use in MSC migratory recruitment. It was established in-house to determine SalB's activity in promoting stem cell recruitment. Human fibronectin (Corning) was prepared as a 1 mg/ml stock solution by reconstitution in distilled water and stored at -20 °C prior to use. This stock solution was diluted 20 times with HEPES buffer (Lonza) from which 50 µl was applied to coat each of the Fluoroblock 8.0 µm transwell[®] filters (Figure 4.1 (A), 0.3 cm² area, Corning), according to the instructions. The HPMVEC-L cell monolayers was grown on the fibronectin-coated filters upon seeding of 30,000 cells on each filter, as shown in Figure 4.1 (B). Upon confluence, typically on day 5, the trans-endothelial electrical resistance (TEER) was measured using the volt-ohmmeter and STX-2 electrodes (EVOM; World Precision Instruments, Sarasota, FL) and ensured to be in a range of 85-90 Ωcm² (ohms cm²), as reported by Sedgwick et al. (2002). DiIC12(3) fluorescent dye (Corning; 100 mg/ml stock solution prepared in degassed DMSO and stored at -20 °C; 549/565 nm, Excitation/Emission) was used at 0.5 µg/ml to stain the MSCs in culture for 2 h, according to the supplier's instructions, and the labeling efficiency and duration were determined prior to the use. Subsequently, the DiIC12-labeled MSCs were trypsinized from which 50,000 cells were added onto the HMVEC-L cell monolayers of the fluoroblock transwell filters. Initial experiments determined the DiIC12-labeled MSC migration over 24 h in the presence or absence of SalB at 25 µM or 30 % FBS in the basolateral side, as shown in Figure 4.1 (C). By contrast, in the subsequent experiments, the HMVEC-L cell monolayers was pre-treated with SU5416 at 5 µM for 2 h followed by addition of MSCs with or without SalB at 25 µM to assess the impaired MSC recruitment due to VEGF receptor blockade and its recovery with SalB. At 24 h of migration, the

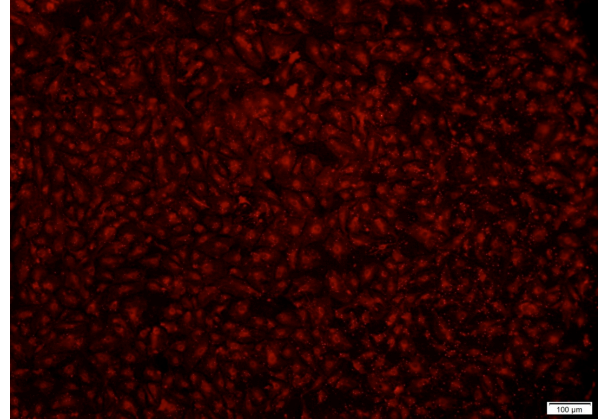
apical side of the transwell was washed 3 times with sterile PBS (Quality biological, Gaithersburg, MD), and the MSC and HMVEC-L cells on the apical side were swabbed using a cotton swab. After the inserts were flipped over, the cells on the basolateral side of the transwell filter were fixed for 15 min with 4 % paraformaldehyde (Sigma-Aldrich) solution in PBS. The filters were carefully cut and mounted on glass slides. The basolateral side of the fluoroblock filters was then observed under the fluorescence microscope (Olympus 1X51, Center Valley, PA). Five 100X images were taken for each filter, accounting for the 20 % of the filter area. DiIC12-labeled MSCs were counted in each image using ImageJ (Appendix 3). The total number of MSCs migrated to the basolateral side were calculated as 5 times the total cells counted by ImageJ from the 5 filter images. Percent cells migrated was calculated by using the equation:

$$\% \text{ migrated} = \frac{\textit{Total number of MSCs migrated to the basolateral side}}{50,000 \textit{ (Number of MSCs added on the apical side)}} \times 100$$

A)



B)



C)

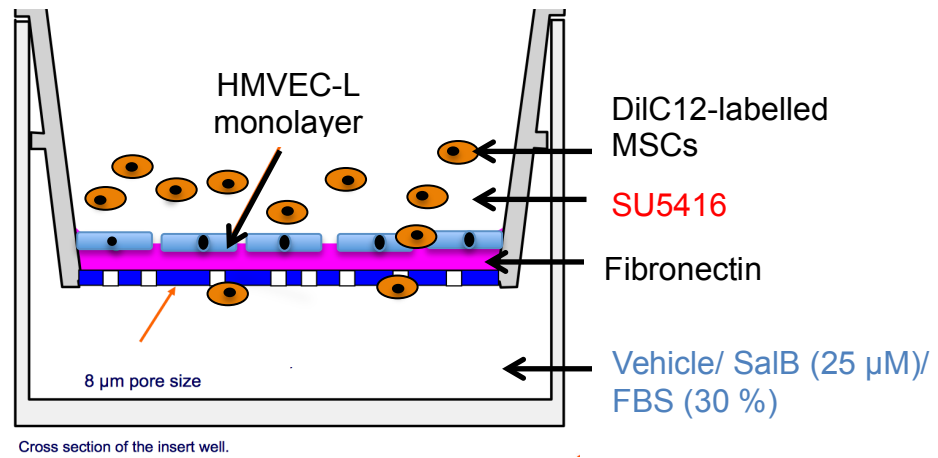


Figure 4.1: (A) Fluoroblock transwell insert (B) Fluorescence microscope image (100X) of DilC12-labelled HMVEC-L monolayer grown on the fibronectin-coated fluoroblock transwell filter (C) Schematic representation of the trans-endothelial migration assay showing cross section of the fluoroblock insert transwell.

4.2.7. Data description and statistical analyses

The results of SalB's in vitro activities were expressed as mean±SD (n=3-9). Statistical analyses for group comparison were carried out using Prism[®] 7 (GraphPad Software, San Diego, CA) or JMP-Pro[®] 12 (SAS Institute, Inc., Cary, NC) by one-way analysis of variance (ANOVA). Post-hoc analysis for multiple comparison testing was performed by the Tukey's or Dunnett's method, the latter being used to compare multiple test groups to the vehicle control group and not among each other. p<0.05 was considered as significant.

4.3. Results

4.3.1. Anti-lung cell death activities of SalB

In vitro inhibitory activities of SalB against alveolar epithelial A549 cell death induced with 0.1 mM H₂O₂, i.e. oxidative stress, were determined using the trypan blue exclusion and PI –based flow cytometry assays, as shown in Figures 4.2 and 4.3, respectively. H₂O₂ -induced A549 cell death by 6.5 –fold ($p < 0.05$), by the trypan blue exclusion assay (Figure 4.2). However, SalB significantly inhibited this induced cell death by 80.1 % with 10 μ M and by 86.0 % with 25 μ M ($p < 0.05$), but not with 1 μ M, while SalB at 25 μ M alone did not induce cell death (Figure 4.2). This concentration-dependent anti-cell death activity of SalB could be reasonably attributed to negated oxidative insult with the SalB’s anti-oxidative activity shown in Chapter 3 ($IC_{50} = 3.7$ μ M, Figure 3.1). Figure 4.3 (A and B) shows the H₂O₂ –induced A549 cell death and its inhibition with SalB at 25 μ M, determined by the PI –based flow cytometry assay. As seen with the trypan blue exclusion assay, H₂O₂ -induced cell death by 5.9 –fold, to which SalB exhibited a significant 59.2 % inhibition ($p < 0.05$).

SalB at 25 μ M was also examined against A549 cell death induced by VEGF-receptor blockade using SU5416. As shown in Figure 4.4 (A), SU5416 at 10 and 20 μ M induced cell death by 1.8 –fold and 3.6 –fold, respectively ($p < 0.05$); and SalB at 25 μ M inhibited SU5416-induced cell death by 121.8 % and 88.4 %, respectively ($p < 0.05$). AG490 and S31-201 were then respectively added as JAK2 and STAT3 inhibitors, to examine their counter effects on the SalB’s anti-cell death activities. As shown in Figure 4.4 (B), AG490 and S31-201 each blocked the SalB’s anti-cell death activities by 96.8 % and 68.2 %, respectively ($p < 0.05$). It should be noted that these inhibitors alone did not

cause cell death in SU5416 –treated A549 cells, as validated in Table 4.1.

Likewise, as shown in Figure 4.5, in the HMVEC-L cells, SU5416 at 20 μM induced cell death by 3.3 –fold and that cell death was inhibited with SalB at 25 μM significantly by 47.7 %. Moreover, AG490 and S31-201 inhibited the SalB’s anti-cell death activity by 85.8 % and 131.2 %, respectively ($p < 0.05$). Therefore, SalB was potently (i.e., at 25 μM) cytoprotective against lung epithelial (A549) and endothelial (HMVEC-L) cell death induced with VEGF receptor blockade (SU5416) in a JAK2 and STAT3 –dependent mechanism.

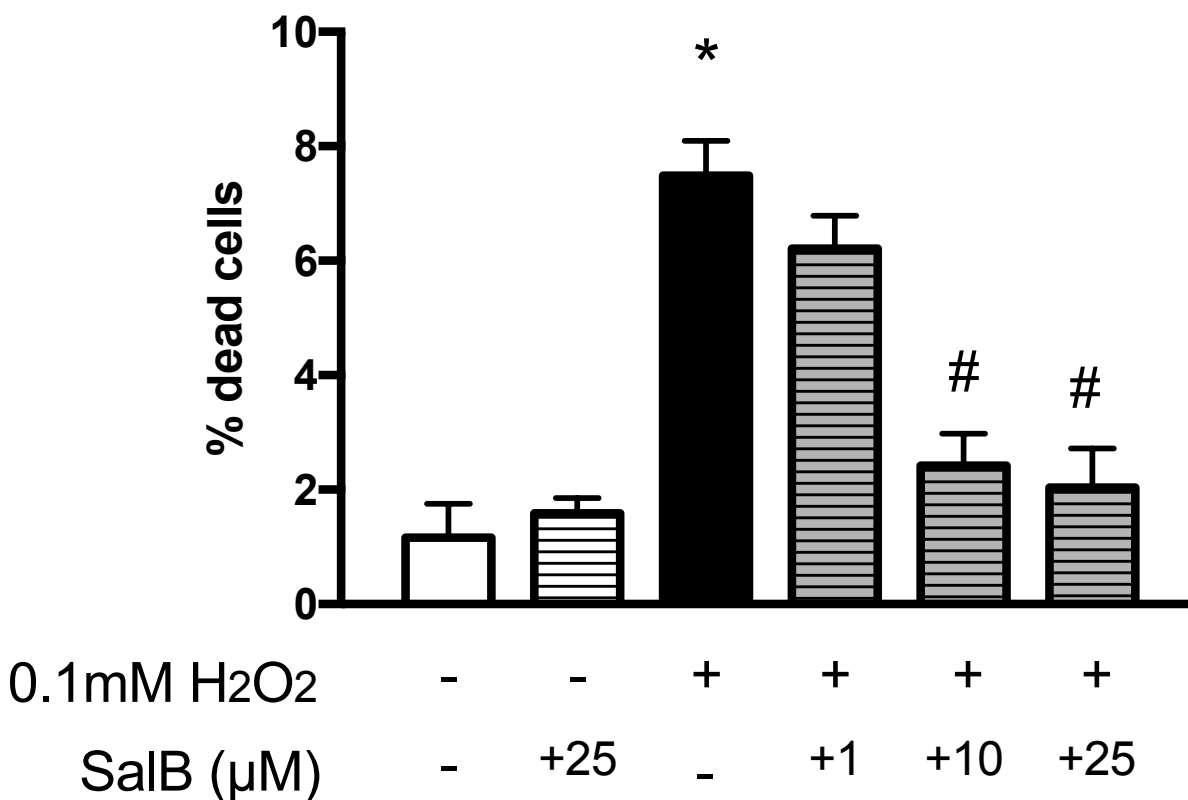


Figure 4.2: In vitro anti-cell death activities of SalB at 1, 10 and 25 μM against H₂O₂-induced cell death in the A549 cells, determined by the trypan blue exclusion assay. Data: mean±SD (n=3 - 6) (+) present; (-) absent *p<0.05, compared to vehicle treated/induced control; #p<0.05, compared to the H₂O₂ -induced and vehicle treated cells, by ANOVA and Tukey's multiple comparison test. SalB at 25 μM alone did not cause significant cell death.

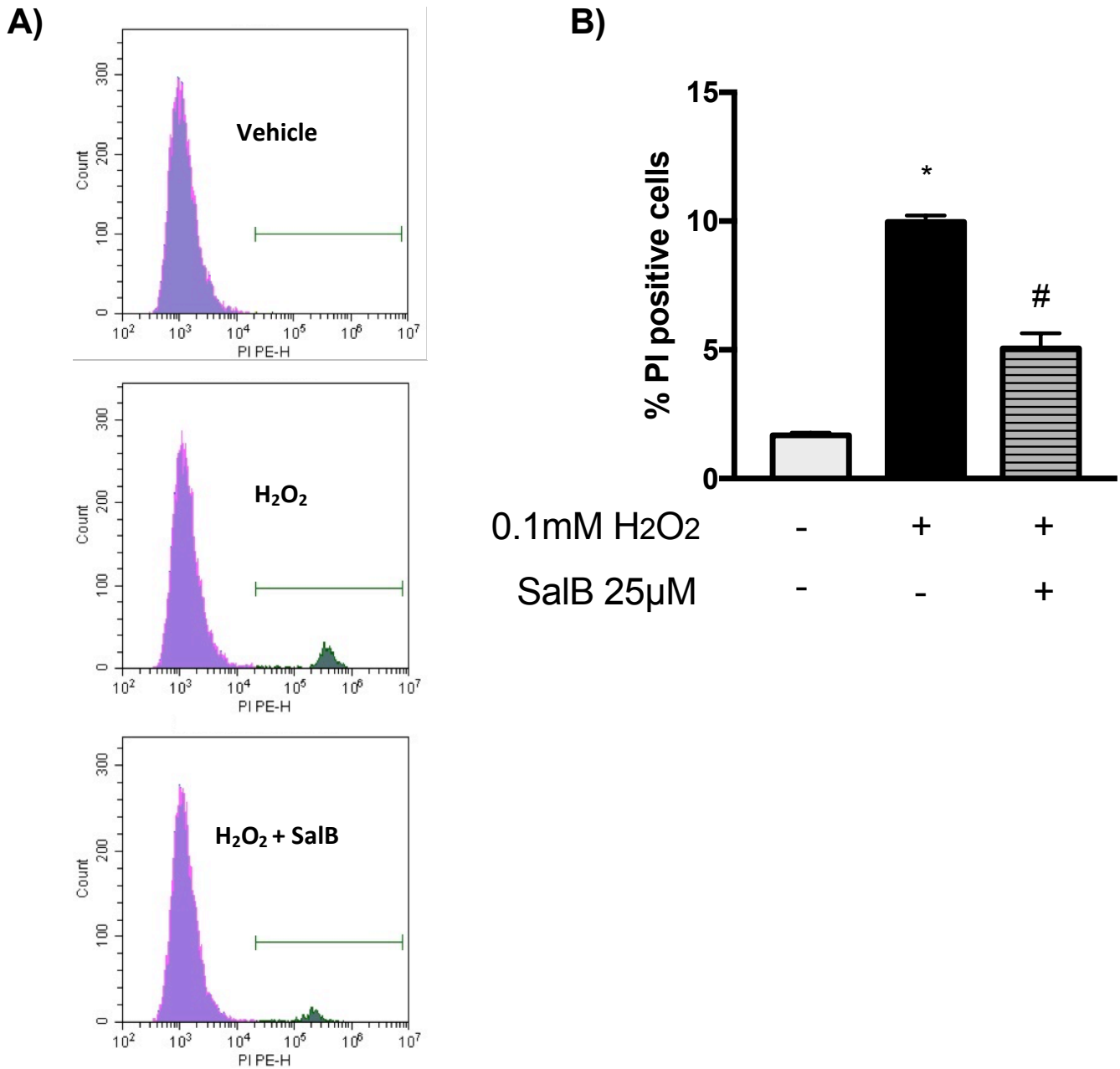


Figure 4.3: In vitro anti-cell death activities of SalB at 25 μ M against H₂O₂-induced cell death in the A549 cells, determined by PI –based fluorescence flow cytometry; **(A)** Representative PI –based cell population histograms. **(B)** % of PI positive cells, following vehicle or H₂O₂–induction and vehicle or SalB treatment. The cells in the horizontal range in Panel A were counted as PI positive dead cells. Panel B: Data: mean \pm SD (n=3) (+) present; (-) absent *p<0.05, compared to the vehicle – treated/induced control; #p<0.05, compared to the H₂O₂ induced and vehicle treated cells, by ANOVA and Tukey’s multiple comparison test.

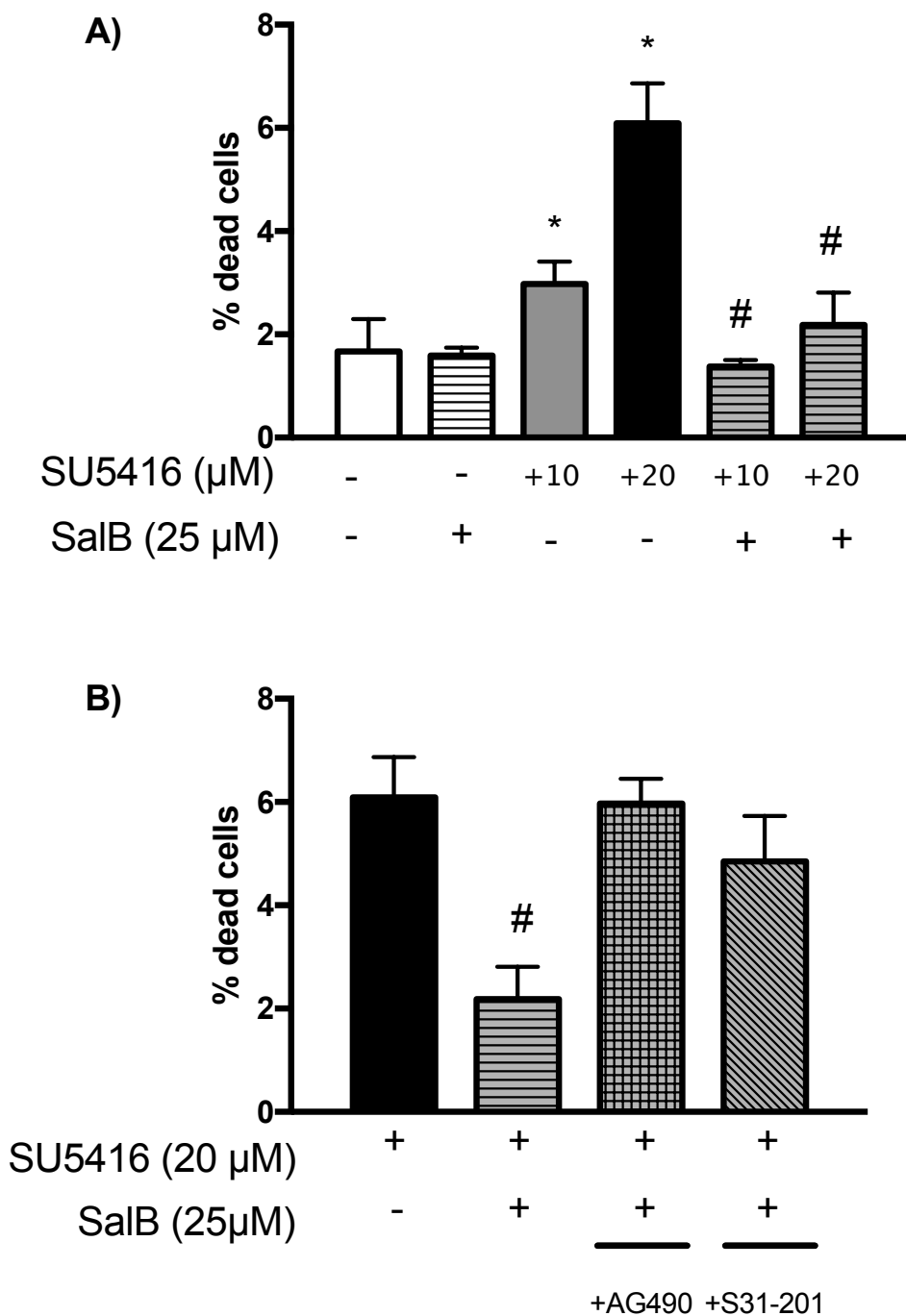


Figure 4.4: (A) In vitro cytoprotective activities of SalB at 25 μM against cell death induced by SU5416 at 10 or 20 μM in the A549 cells with or without AG490 (25 μM) or S31-201 (100 μM), determined by the trypan blue exclusion assay; (B) Effect of AG490 or S31-201 addition on SalB's anti-cell death activity. Data: mean \pm SD (n=3) (+) present; (-) absent *p<0.05, compared to the vehicle-treated/induced control; #p<0.05, compared to SU5416-induced and vehicle treated cells, by ANOVA and Tukey's multiple comparison test. Panel B: no significant difference in the SU5416-induced cells between the vehicle treatment and the SalB treatment co-incubated with AG490 or S31-201.

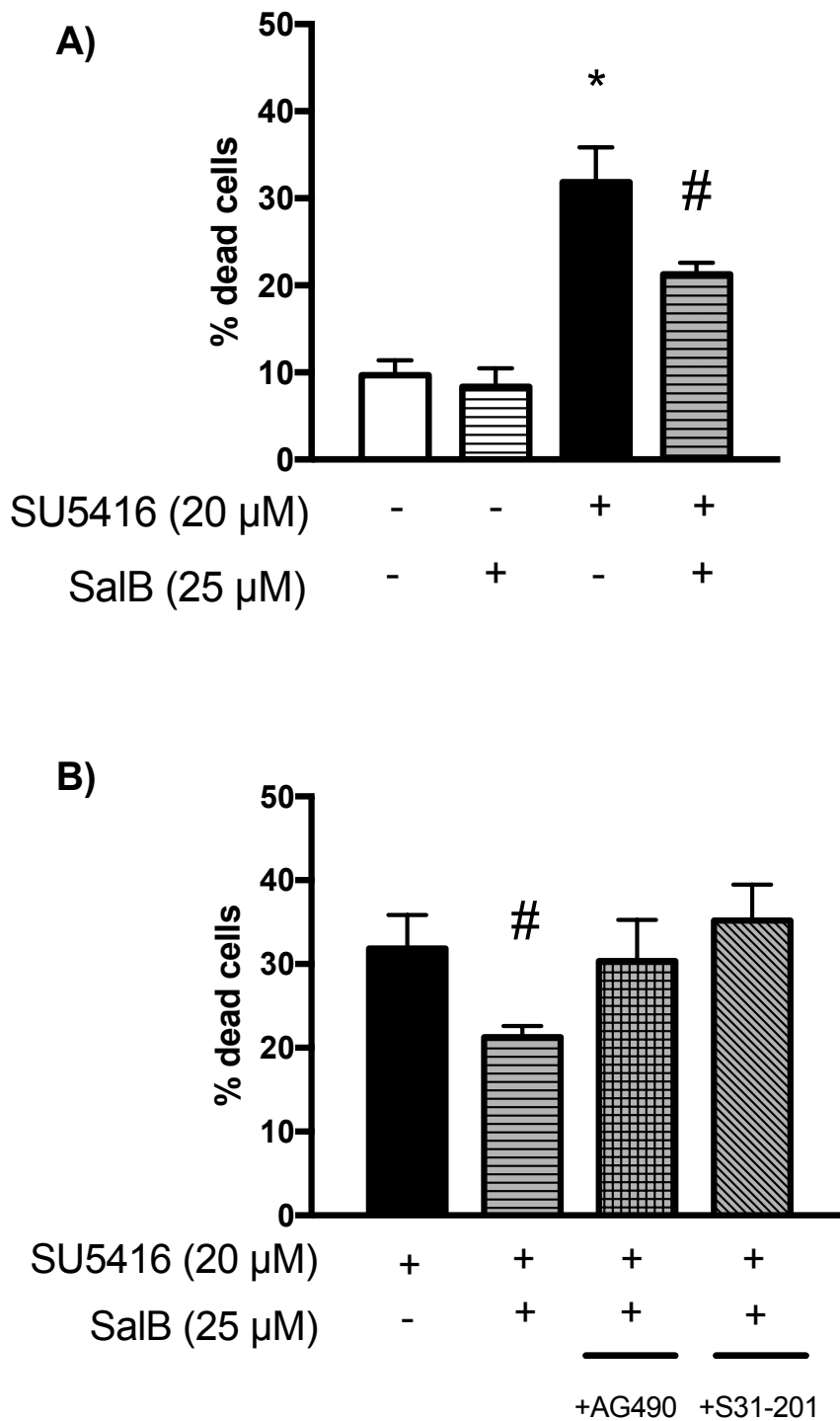


Figure 4.5: In vitro cytoprotective activities of SalB at 25 μ M against cell death induced with SU5416 at 20 μ M in the HMVEC-L cells with or without AG490 (25 μ M) or S31-201 (50 μ M), determined by the trypan blue exclusion assay (**A**) SU5416 induced cell death and its inhibition with SalB; (**B**) Effect of AG490 or S31-201 addition on SalB's anti-cell death activity. Data: mean \pm SD (n=3-5) (+) present; (-) absent *p<0.05, compared to vehicle control; #p<0.05, compared to SU5416 induced cell death, by ANOVA and Tukey's multiple comparison test. Panel B: no significant difference in the SU5416 -induced cells between the vehicle treatment and the SalB treatment co-incubated with AG490 or S31-201.

Table 4.1: Effects of AG490 and S31-201 on the SU5416 –induced A549 cell death.

Cell type	Treatment	Inhibitor	% Cell death
A549	SU5416	-	6.1 ± 0.78
		AG490	5.3 ± 0.94
		S31-201	5.8 ± 0.42

Data: mean±SD (n=3-4). No significant difference in the SU5416 –induced A549 cell death following the vehicle treatment and the AG490 or S31-201 treatment.

4.3.2. Lung cell proliferation stimulatory activities of SalB

Figure 4.6 shows the in vitro A549 cell proliferation activities following 24 or 48 h treatment with SalB at 10 or 25 μM or the vehicle with or without addition of AG490, S31-201 or SU5416, determined by the MTT assay. Upon confirmation of continued cell proliferation over 48 h (as shown in Panel A), SalB was found to stimulate A549 cell proliferation over 48 h in a concentration –related manner and significantly by 3.4 –fold at 25 μM ($p < 0.05$), as shown in Panel B. However, this A549 cell proliferation stimulatory activity was entirely diminished by co-incubation with AG490, S31-201 and SU5416, as shown in Panel C, thereby respectively suggesting its JAK2, STAT3 and VEGF –dependent mechanism. Note that these inhibitors alone had no effect on the A549 cell proliferation activities (Panel C).

Likewise, Figure 4.7 shows the in vitro HMVEC-L cell proliferation activities following 24 or 48 h treatment with SalB at 5-50 μM or the vehicle with or without addition of AG490, S31-201 or SU5416, determined by the MTT assay. Again, upon confirmation of continued cell proliferation over 48 h (as shown in Panel A), SalB was found to stimulate HMVEC-L cell proliferation over 24 h in a concentration –related manner and significantly by 1.8 and 1.9 –fold at 25 and 50 μM ($p < 0.05$), respectively, as shown in Panel B. However, the HMVEC-L cell proliferation stimulatory activity of SalB was also diminished significantly by 62.9, 144.3 and 94.3 % ($p < 0.05$), when AG490, S31-201 and SU5416 were co-incubated with SalB at 25 μM , again suggesting its JAK2, STAT3 and VEGF –dependent mechanism. Note that these inhibitors alone had no effects on HMVEC-L cell proliferation (Panel C).

The cell proliferation stimulatory activities of SalB were further confirmed in the HMVEC-L cells, determined with the 450 nm absorbance (Abs_{450}) by the BrdU assay, as shown in Figure 4.8. SalB at 25 μ M was shown to result in a significantly higher Abs_{450} by 1.4 –fold ($p < 0.05$), compared to the vehicle -treated cells. Taken all together, therefore, SalB was potently (i.e., at 25 μ M) stimulatory to the lung epithelial (A549) and endothelial (HMVEC-L) cell proliferation in a JAK2, STAT3 and VEGF –dependent manner.

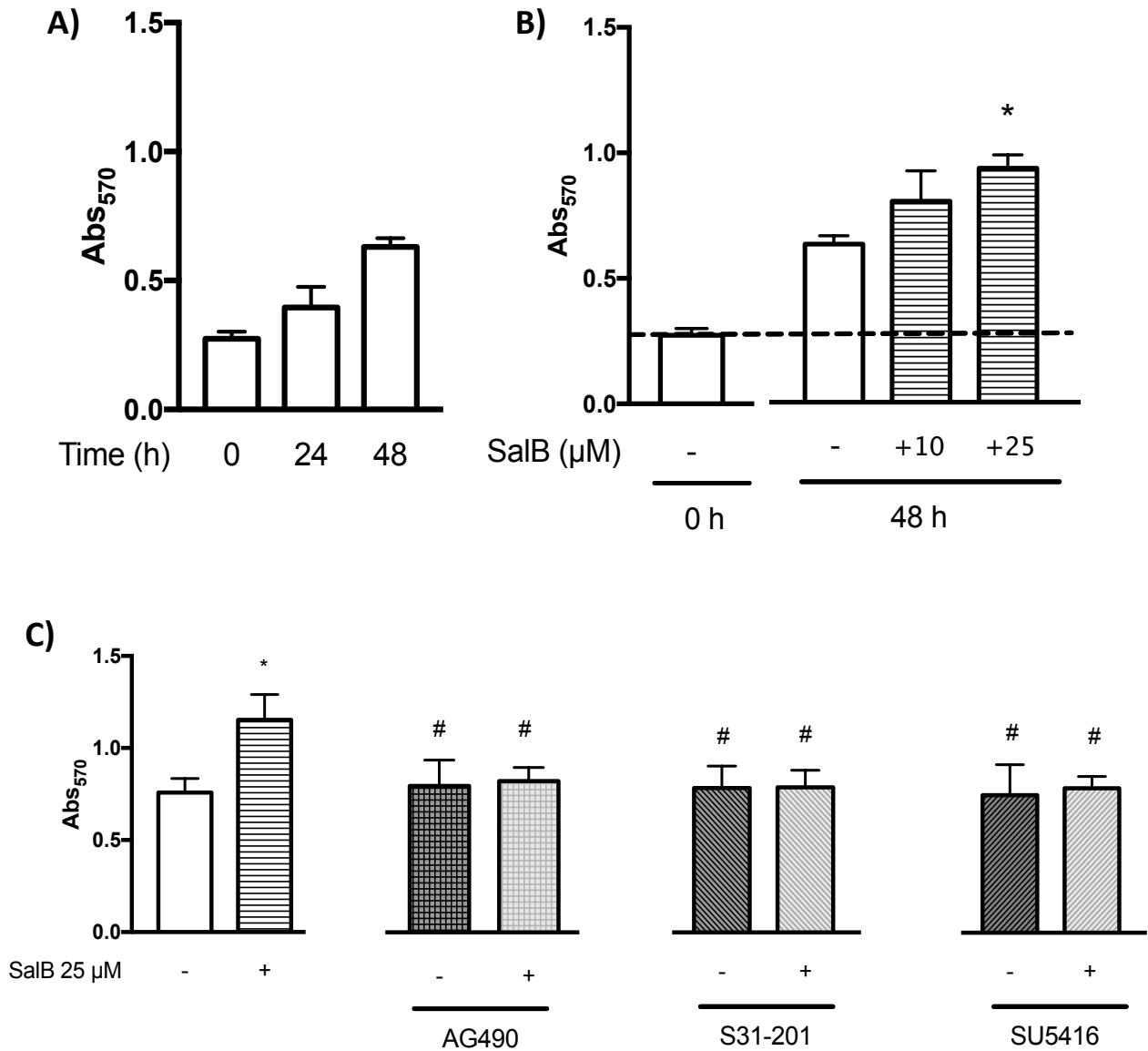


Figure 4.6: In vitro cell proliferation activities in the A549 cells following various treatments determined with the 570 nm absorbance (Abs₅₇₀) by the MTT assay **(A)** following 0, 24 and 48 h incubation; **(B)** following 48 h of treatment with SalB at 10 or 25 µM or the vehicle, relative to at 0 h of plating; **(C)** following 48 h treatment with SalB at 25 µM or the vehicle, co-incubated with or without AG490 (25 µM), S31-201 (100 µM) and SU5416 (5 µM). Data: mean±SD (n=4-7) (+) present; (-) absent *p<0.05, compared to vehicle-treated control; #p<0.05, compared to the 25 µM SalB -treated cells, by ANOVA and Tukey's or Dunnett's multiple comparison test.

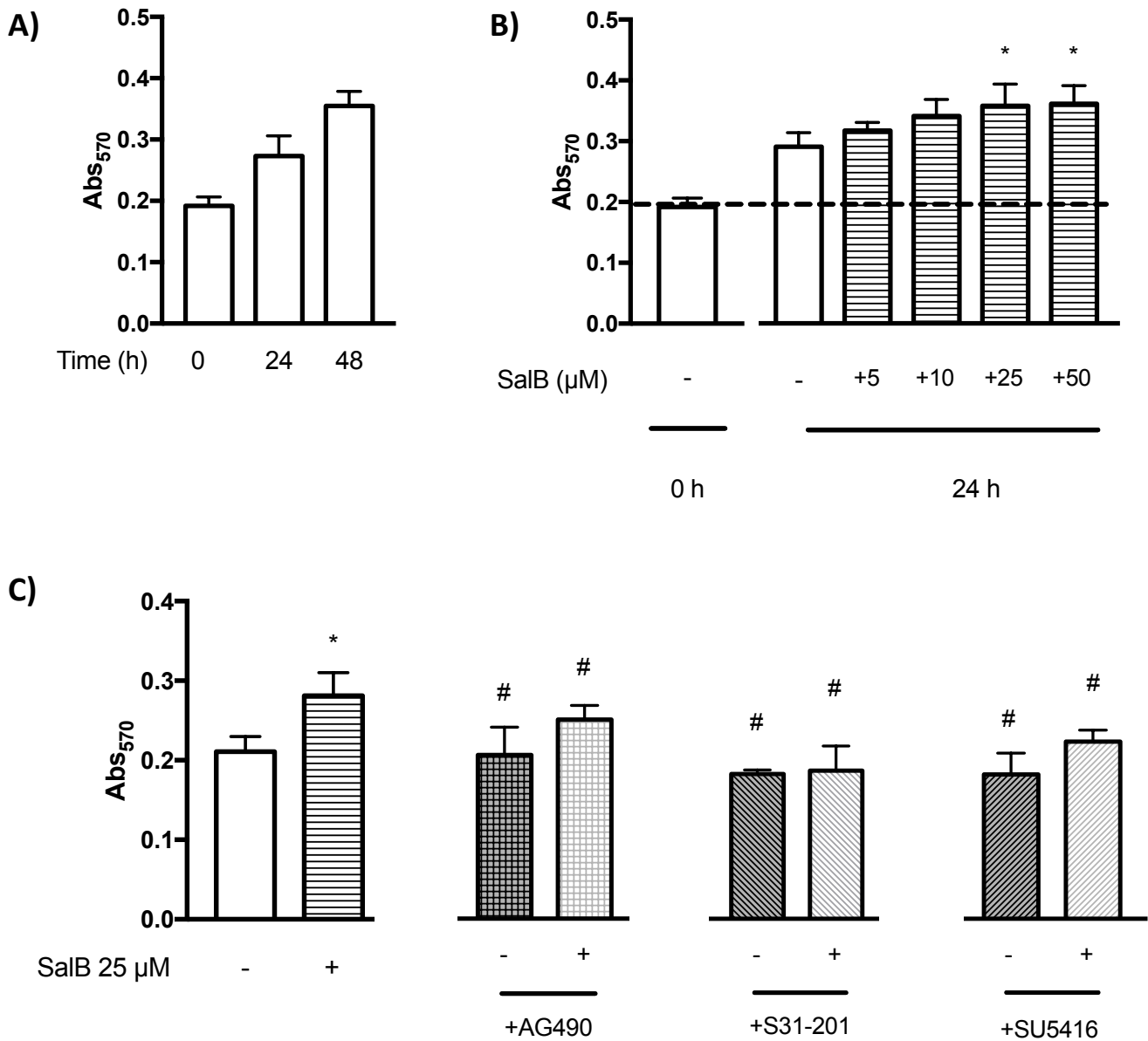


Figure 4.7: In vitro cell proliferation activities in the HMVEC-L cells following various treatments determined with the 570 nm absorbance (Abs_{570}) by the MTT assay **(A)** following 0, 24 and 48 h incubation; **(B)** following 48 h of treatment with SalB at 10 or 25 μ M or the vehicle, relative to at 0 h of plating; **(C)** following 48 h treatment with SalB at 25 μ M or the vehicle, co-incubated with or without AG490 (25 μ M), S31-201 (100 μ M) and SU5416 (5 μ M). Data: mean \pm SD (n=4-11) (+) present; (-) absent *p<0.05, compared to vehicle-treated control; #p<0.05, compared to the 25 μ M SalB -treated cells, by ANOVA and Tukey's or Dunnett's multiple comparison test.

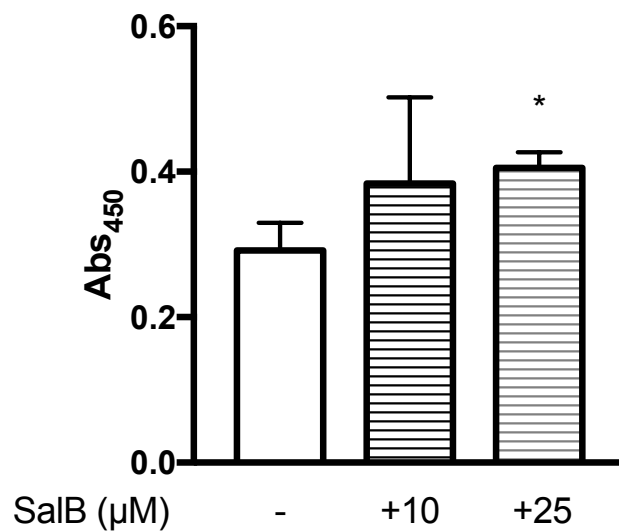


Figure 4.8: In vitro cell proliferation activities in HMVEC-L following 24 h treatment with SalB at 10 or 25 μM or the vehicle, determined with the 450 nm absorbance (Abs_{450}) by the BrdU assay. Data: mean \pm SD (n=4); (-) absent *p<0.05, compared to vehicle control, by ANOVA and Dunnett's multiple comparison test.

4.3.3. Lung cell migration promoting activities of SalB

Figures 4.9 – 4.11 show the result of the *in vitro* scratch wound closure studies in the confluent A549 cells with or without SalB and /or the inhibitors. As shown in Figure 4.9, the cell scratch wounds made at 0 h were gradually closed over 48 h. The wound areas were determined as the areas without cell coverage identified by using Image J to accurately trace the wound boundaries, as shown in Figure 4.10 (A). Thus, Figure 4.10 (B) shows % wound closure at 48 h of different treatments. SalB promoted the wound closure in a concentration-related manner, and significantly by 1.5 -fold at 25 μM ($p < 0.05$). However, this promoted wound closure with SalB at 25 μM was opposed with AG490 (25 μM), S31-201 (100 μM) and SU5416 (5 μM) significantly by 108.8, 47.7 and 85.2 %, respectively ($p < 0.05$; Figure 4.11). Because these inhibitors alone did not affect the wound closure, SalB's wound closure promoting activities were suggested to depend on JAK2, STAT3 and VEGF, like its anti-cell death and cell proliferation stimulatory activities (Figures 4.4-4.7).

Similarly, Figures 4.12-4.15 show the results of the *in vitro* scratch wound closure studies in the confluent HMVEC-L cells with or without SalB and/or the inhibitors. The cell scratch wounds made at 0 h were gradually closed over 18 h, as shown in Figures 4.12 and 4.13. The wound areas were determined at 12 h via the accurate tracing of wound boundaries (Figure 4.13 (A)) to calculate % wound closure following different treatments. Figure 4.13 (B) shows the time course of % wound closure in the HMVEC-L cells treated with the vehicle or SalB at 10 μM . SalB at 10 μM accelerated the wound closure, compared to the vehicle treatment. As shown in Figure 4.14, SalB promoted the wound closure in a concentration-dependent manner and

significantly at $\geq 5 \mu\text{M}$ ($p < 0.05$). At $25 \mu\text{M}$, SalB showed a 1.6 –fold greater % wound closure, relative to the vehicle –treated control ($P < 0.05$). Figure 4.15 shows % wound closure with SalB at $25 \mu\text{M}$ and its significant inhibition with AG490, S31-201 and SU5416 by 75.3, 92.9 and 77.7 %, respectively. It should be noted that, % wound closure appeared to be cell passage dependent as 23.1 % and 42.9 % of wound closure was seen with passage 9 and 6, respectively.

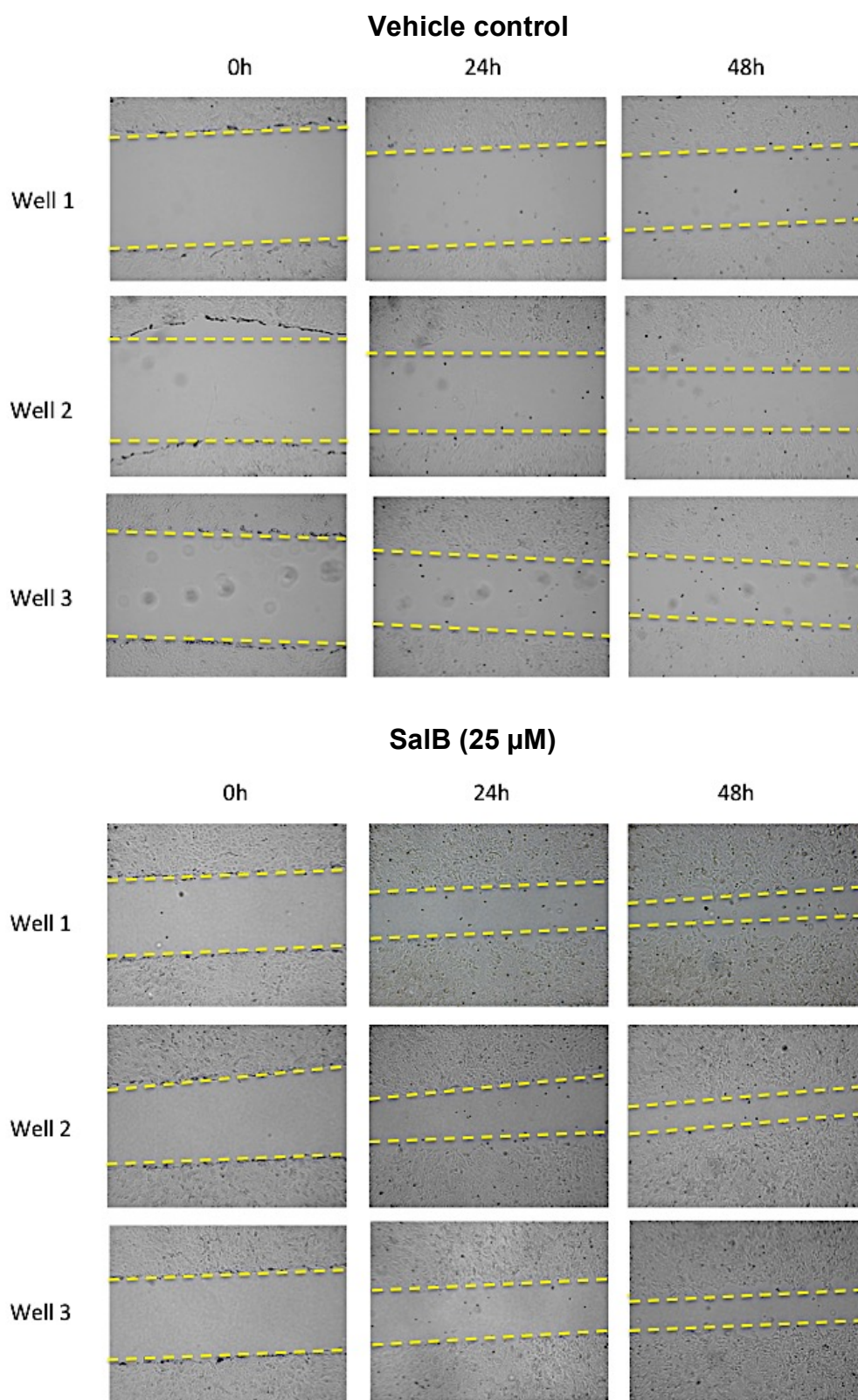


Figure 4.9: Representative images of linear scratch wounds made at 0 h and their closures at 24 and 48 h in the A549 cells in three different wells, treated with the vehicle or SalB at 25 μ M. The linear dotted lines are to demonstrate cell wound closure over 48 h. The wound areas were calculated by tracing wound boundaries like Figure 4.10 (A).

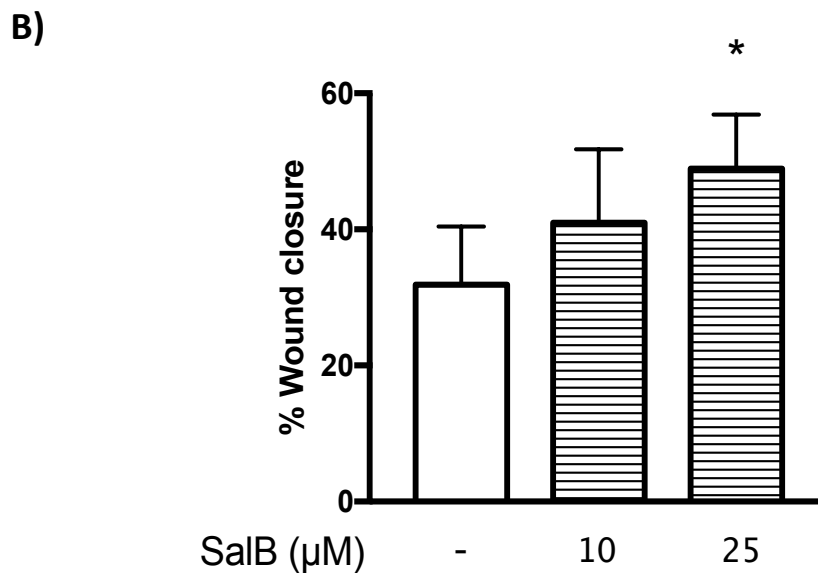
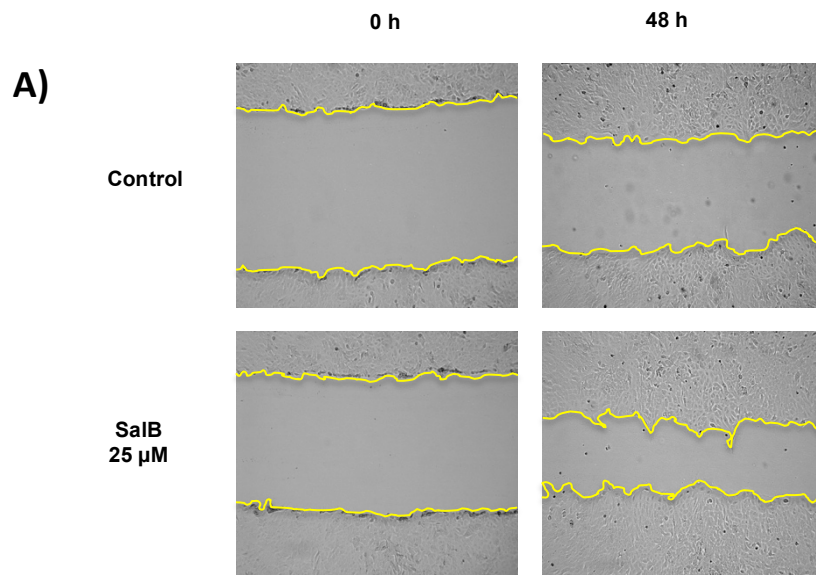


Figure 4.10: (A) Representative images of linear scratch wound at 0 and 48 h of the treatment with the vehicle or SalB at 25 μM in the A549 cells; (B) % wound closure in the A549 cells following 48 h treatment with the vehicle or SalB at 10 and 25 μM. Data: mean±SD (n=7-8) (-) absent *p<0.05, compared to vehicle -treated control, by ANOVA and Dunnett's test.

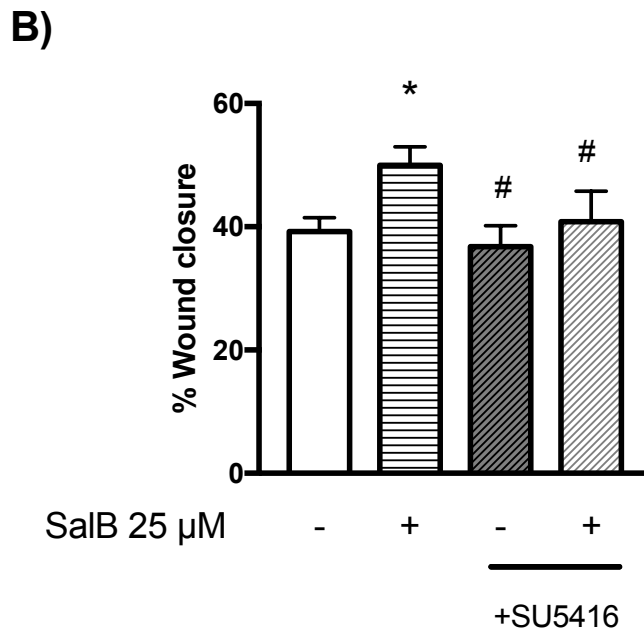
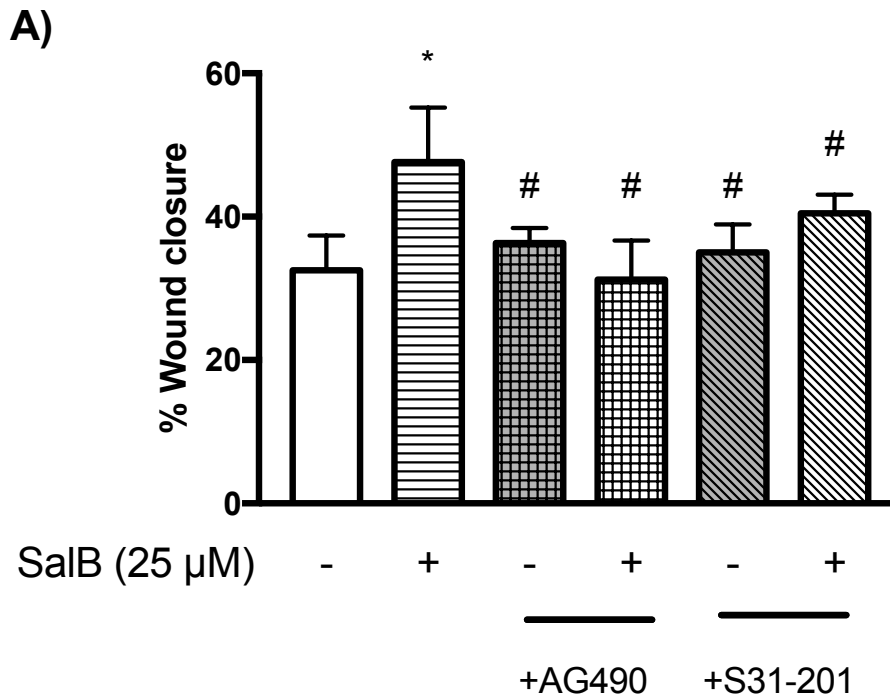


Figure 4.11: In vitro % wound closure at 48 h in the A549 cells with or without SalB at 25 μ M and/or inhibitors: **(A)** Effect of AG490 (25 μ M) or S31-201 (100 μ M); and **(B)** Effect of SU5416 (5 μ M). Data: mean \pm SD (n=3-6) (+) present; (-) absent *p<0.05, compared to vehicle – treated control; #p<0.05, compared to the SalB (25 μ M) –treated cells, by ANOVA and Tukey’s multiple comparison test. Addition of AG490, S31-201 or SU5416 alone did not alter % wound closure, relative to the vehicle –treated control.

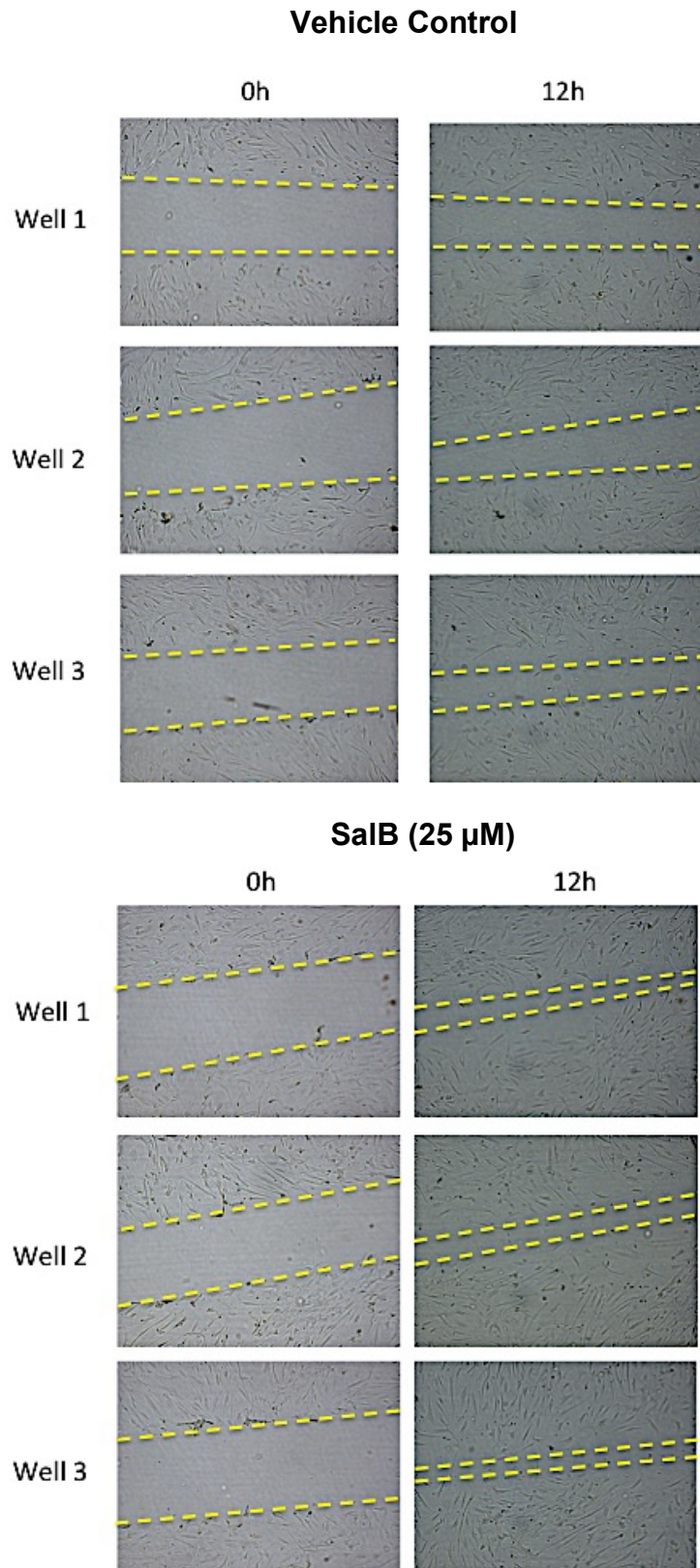


Figure 4.12: Representative images of linear scratch wounds made at 0 h and their closures at 12 h in the HMVEC-L cells in three different wells, treated with the vehicle or SalB at 25 μ M. The linear dotted lines are to demonstrate cell wound closure over 12 h. The wound areas were calculated by tracing wound boundaries like Figure 4.13 (A).

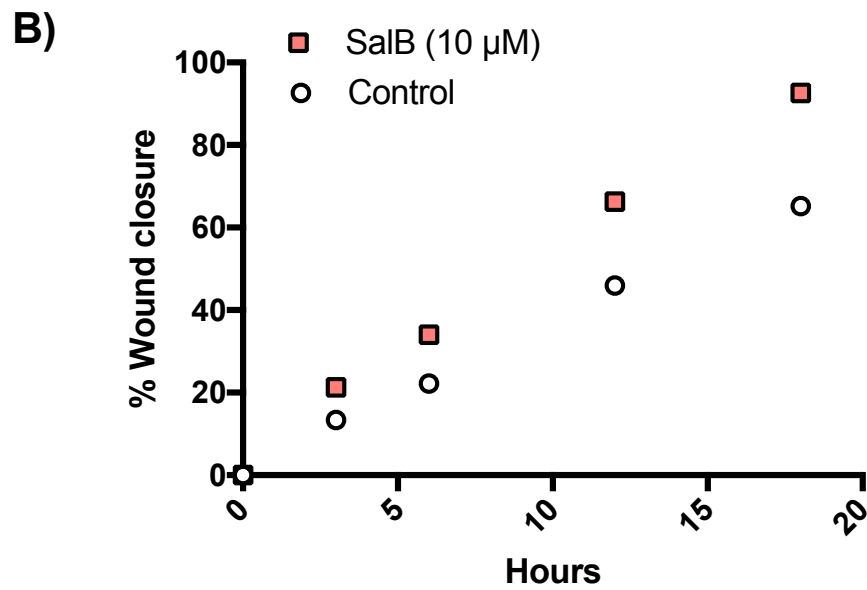
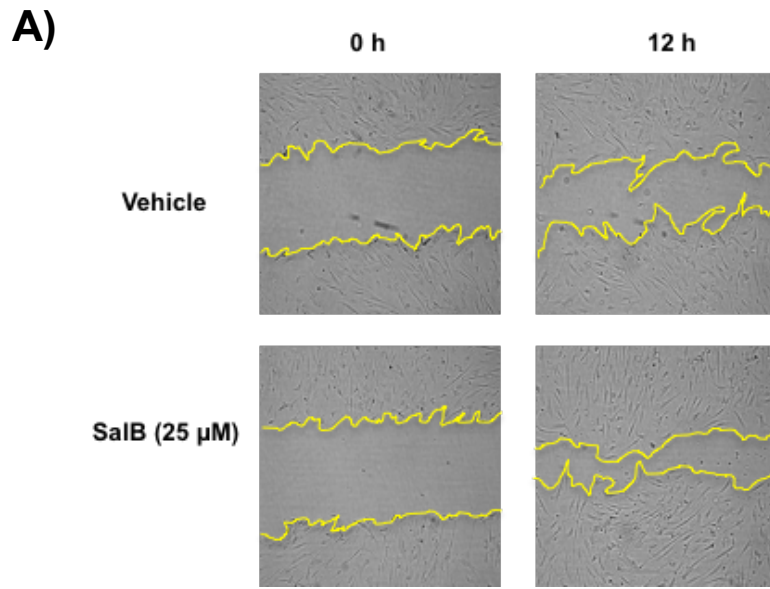


Figure 4.13: (A) Representative images of the linear scratch at 0 and 12 h of the treatment with the vehicle or SalB at 25 μ M in the HMVEC-L cells; (B) Time course changes of the % wound closure over 18 h during the treatment with the vehicle or SalB at 10 μ M in the HMVEC-L cells

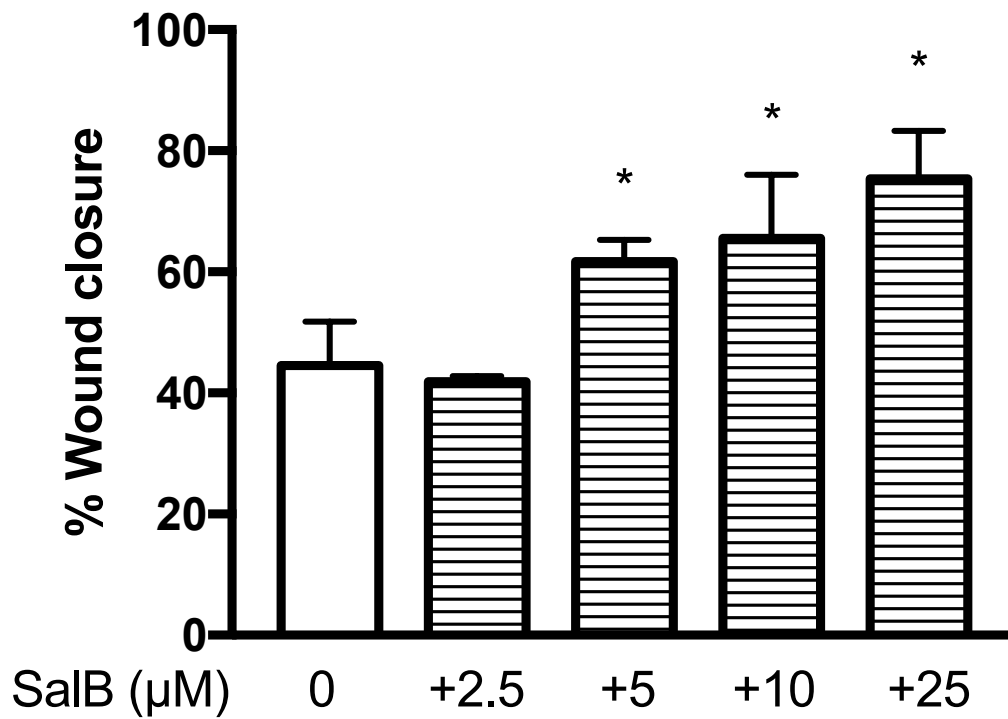


Figure 4.14: In vitro % wound closure in the HMVEC-L cells following 12 h treatment with SalB at 2.5 – 25 μM or the vehicle. Data: mean \pm SD (n=3-10) (+) present * $p < 0.05$, compared to vehicle control, by ANOVA and Dunnett's multiple comparison test.

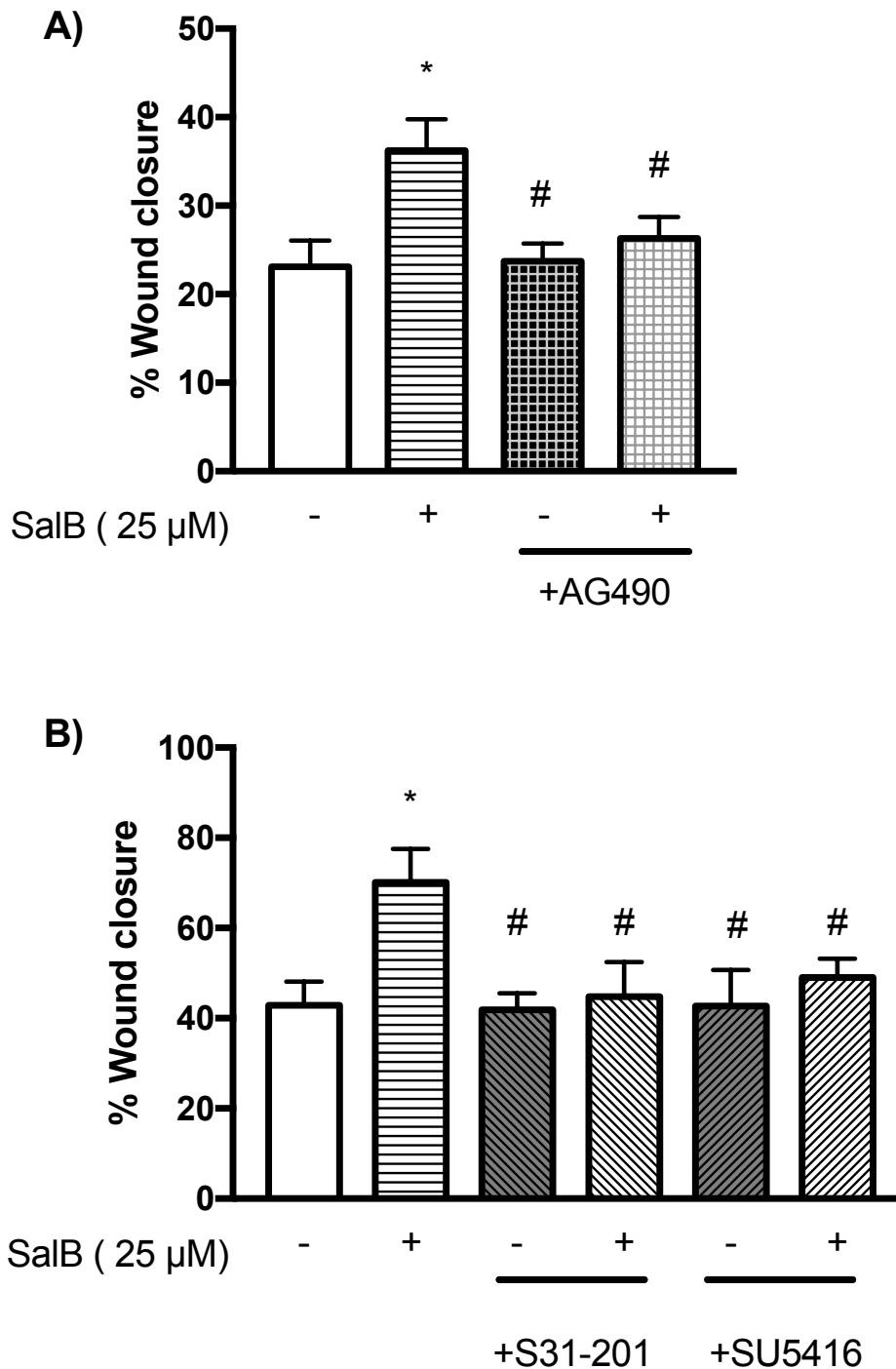


Figure 4.15: In vitro % wound closure in the HMVEC-L cells treated with or without SalB at 25 μM and/or inhibitors: **(A)** Effect of AG490 (25 μM) and **(B)** Effect of S31-201 (100 μM) or SU5416 (5 μM). Data: mean±SD (n=3-9) (+) present; (-) absent *p<0.05, compared to vehicle -treated control; #p<0.05, compared to the SalB (25 μM) -treated cells, by ANOVA and Tukey's multiple comparison test. Addition of AG490, S31-201 and SU5416 alone did not alter the % wound closure, relative to the vehicle -treated control.

4.3.4. Stem cell recruitment promoting activities of SalB

Figure 4.16 shows % of MSCs migrated from the apical side to the basolateral side of the fluoroblock transwell filters with or without the HMVEC-L monolayers over 24 h. Despite physically a barrier, the HMVEC-L monolayers promoted MSC migration significantly by 1.3 –fold ($p < 0.05$), suggesting an active role of the endothelial cells in the MSC migratory recruitment. Figure 4.17 shows the trans-HMVEC-L cell monolayer migratory recruitment of MSCs over 24 h in the absence or presence of 30 % FBS. As similarly shown by Luscinskas (2008), FBS promoted MSC migration significantly by 1.6 –fold ($p < 0.05$), thus successfully validating this newly developed system to assess the trans-endothelial MSC migration. Accordingly, Figure 4.18 shows the results of trans-HMVEC-L cell monolayer migratory recruitment of MSCs with or without SU5416 and/or SalB treatment. The microscopic images of MSCs migrated to the basolateral side of the fluoroblock filters were converted to the dot cell images for counting using ImageJ, as shown in Figure 4.18 (A). Upon SU5416 treatment, MSC migration was decreased significantly by 51.7 % ($p < 0.05$), as shown in Figure 4.18 (B). However, SalB at 25 μM recovered this MSC migration activity by 60.0 % ($p < 0.05$), while it alone did not affect MSC migration. It was clear therefore that SalB potently (i.e., at 25 μM) restored the trans-endothelial MSC recruitment impaired as a result of VEGF receptor blockade.

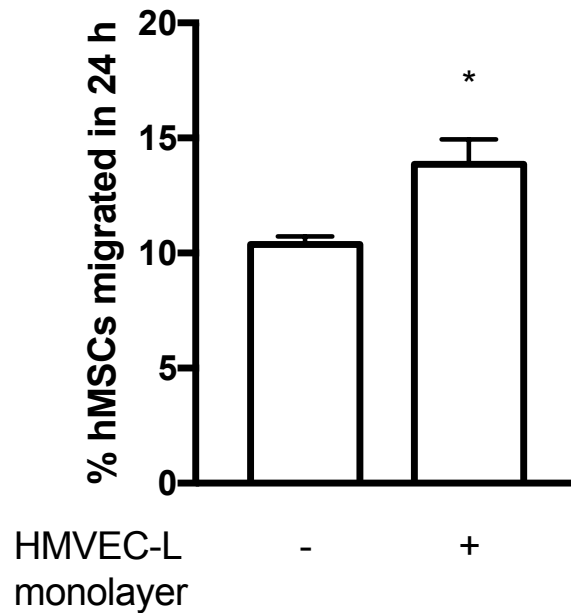


Figure 4.16: % of MSCs migrated through the fluoroblock filters to the basolateral side with or without the HMVEC-L monolayers at 24 h. Data: mean±SD (n=3) (+) present; (-) absent *p<0.05, compared to the MSC migration in the absence of the HMVEC-L cell monolayers, by one -sided *t*-test.

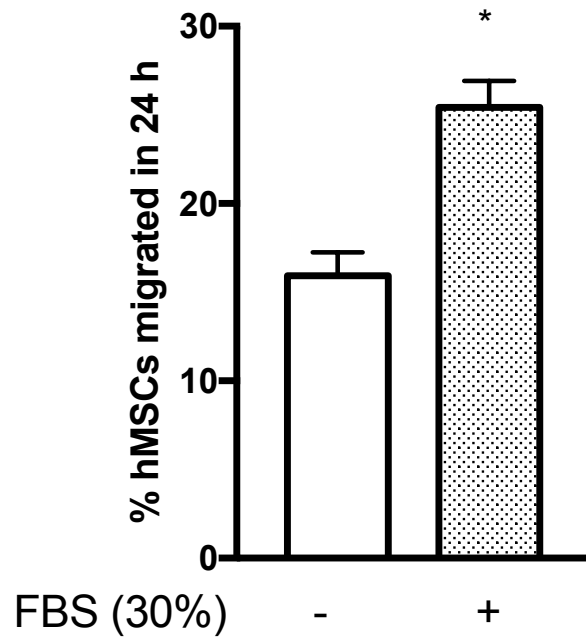


Figure 4.17: Trans-HMVEC-L cell monolayer migration of MSCs in 24 h with or without 30 % FBS. Data: mean±SD (n=3) (+) present; (-) absent *p<0.05, compared to the MSC migration in the absence of FBS, by one -sided *t*-test.

A)

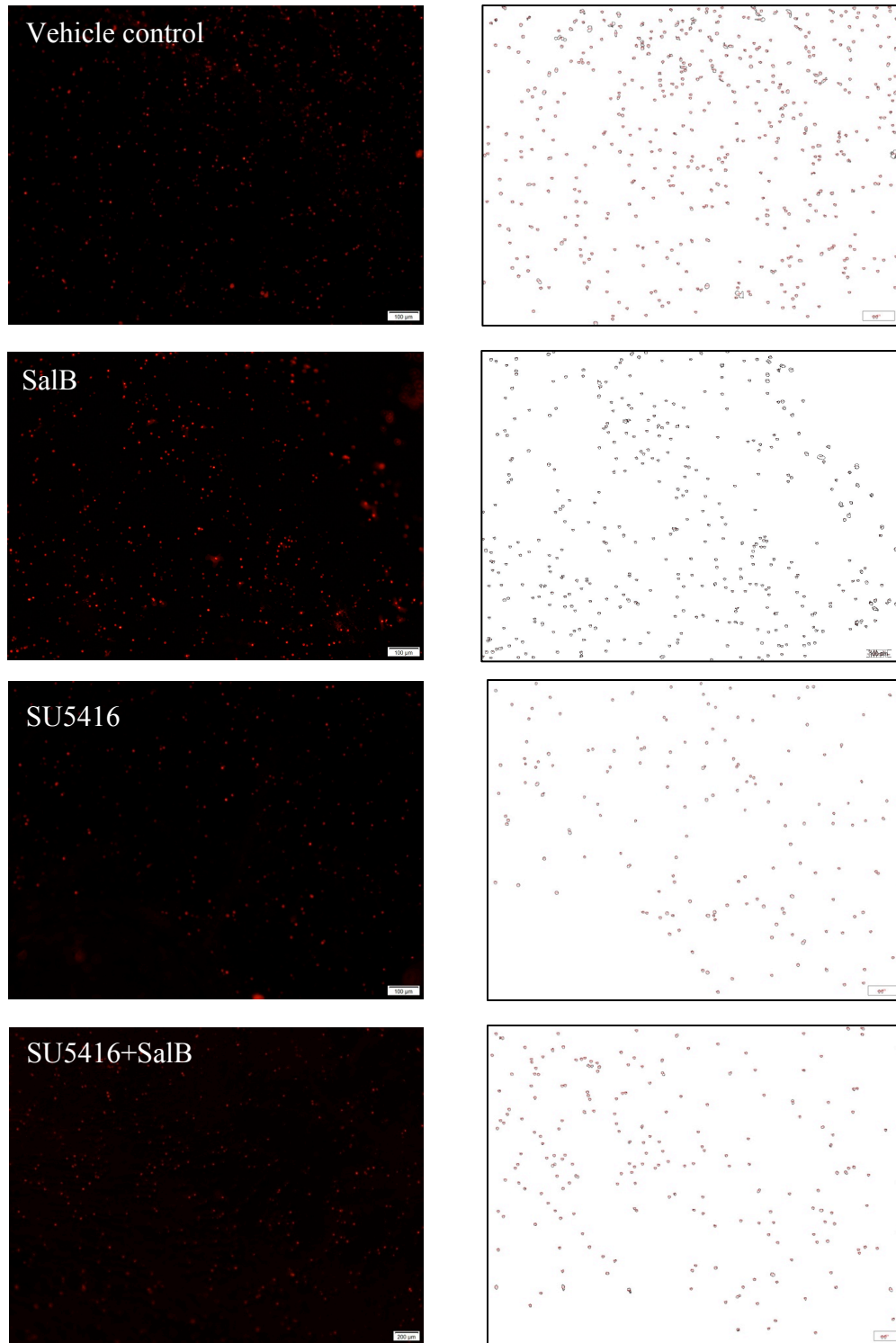


Figure 4.18: (A) Representative images of MSCs migrated to the basolateral side of the Fluoroblock transwell insert under fluorescence microscope (Left panel) and fluorescent cells counted by Image J in each of the microscopic image (Right panel) (100X).

B)

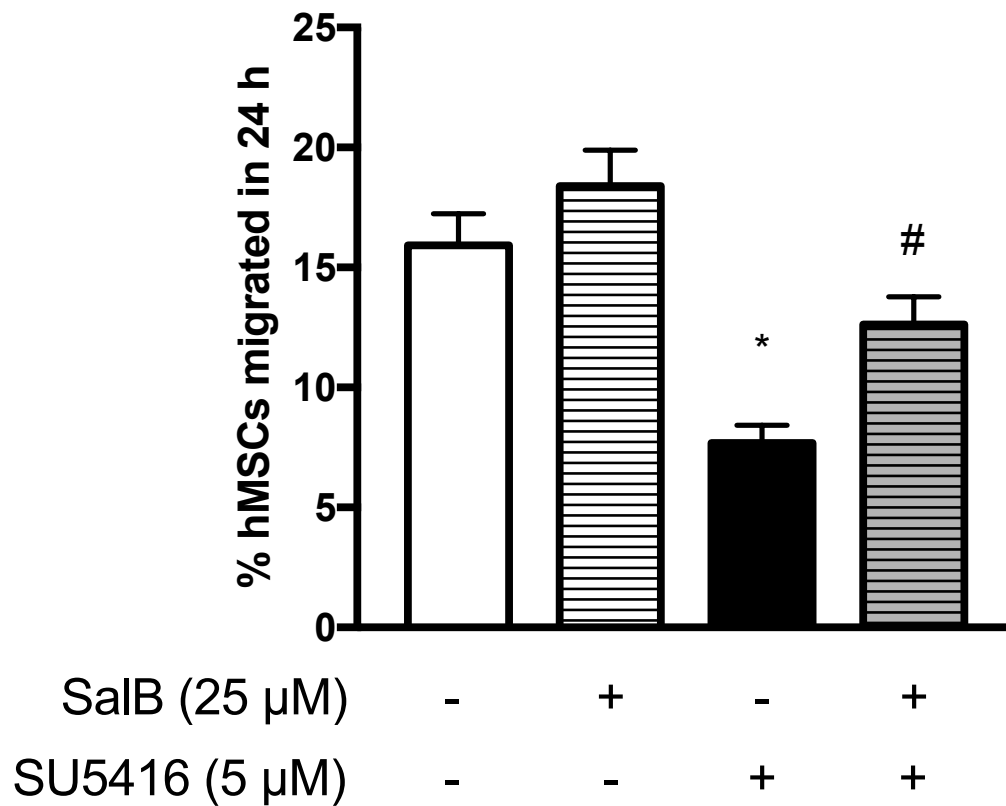


Figure 4.18: (B) Trans-HMVEC-L cell monolayer migration of MSCs in 24 h with or without SalB at 25 μ M and/or SU5416 (5 μ M) pretreatment. Data: mean \pm SD (n=3-6) (+) present; (-) absent *p<0.05, compared to vehicle-treated control; #p<0.05, compared to SU5416 pretreated and vehicle-treated cells, by ANOVA and Tukey's multiple comparison test.

4.4. Discussion

In this chapter, a series of in vitro methods have been used to assess cell-specific VEGF-dependent pharmacological activities of SalB. Lung alveolar epithelial type II A549 cells and endothelial HMVEC-L cells were studied in the trypan blue exclusion and propidium iodide (PI) –based flow cytometry assays to evaluate the anti-cell death activities of SalB against induced oxidative stress and VEGF receptor blockade. Cell proliferation and migration stimulatory activities of SalB were assessed using the MTT or BrdU assay and the in vitro scratch wound closure assay, respectively. SalB showed potent (i.e., at 10-25 μ M) anti-cell death, cell proliferation and migration promoting activities, which appeared to be related to the JAK2-STAT3-VEGF signaling pathway, since the inhibitors to this pathway suppressed SalB's stimulatory effects. Subsequently, a novel trans-endothelial migration assay was developed to study the effect of SalB on the recruitment of MSCs through the lung endothelium. SalB at 25 μ M was able to correct the VEGF receptor blocker -induced impairment in the trans-endothelial migration of MSCs in this assay. This unique ability of SalB is promising in studying lung repair in emphysema, which is characterized by reduced alveolar cell survival, proliferation, migration and recruitment (Song et al. 2010).

4.4.1. SalB protects lung epithelial and endothelial cells from oxidative stress and VEGF-receptor blockade

Cigarette smoke is a major causative factor in COPD and contains oxidants that have the ability to induce lung cell death when accompanied by the depletion of pulmonary antioxidants resulting in an oxidant/antioxidant imbalance and emergence of oxidative stress (Demkow 2009; Li et al. 2013). Thus, protecting lung cells from

oxidative stress and improving their survival are a key to halting the ongoing alveolar destruction. As described in Chapter 3, SalB has a potent anti-oxidant radical scavenging activity with IC_{50} of 3.67 μ M (Figure 3.1). Thus we hypothesized that SalB will have protective effects against oxidative cell death. Accordingly, SalB showed concentration related anti-cell death activity against 0.1 mM H_2O_2 -induced oxidative stress in A549 cells, significantly inhibiting cell death at 25 μ M by 86.0 % and 59.2 % ($p < 0.05$) by the trypan blue exclusion assay and the PI based flow cytometry assay, respectively. While the trypan blue exclusion assay offers the advantages of sensitivity and robustness, the flow cytometry assay has the advantage of a more objective analysis (Vermes et al. 1995). In both these independent studies, SalB at 25 μ M showed significant anti-cell death activities against induced oxidative stress.

Increased apoptosis of alveolar septal cells in emphysema, at least in part, due to the depletion of VEGF -a survival factor for both epithelial and endothelial cells, has been widely reported (Brusselmans et al. 2005; Kanazawa et al. 2003; Imai et al. 2005). Therefore, SalB's cytoprotective activities were studied against emphysematous cell-death induced by SU5416, a competitive inhibitor of VEGF, to mimic the impaired VEGF signaling conditions (Kasahara et al. 2000). SU5416 at 20 μ M (VEGF-receptor inhibition $IC_{50} = 7 \mu$ M) induced 3.6 and 3.3 -fold ($p < 0.05$) cell death in A549 and HMVEC-L cells, respectively by the trypan blue exclusion assay. SalB at 25 μ M inhibited this SU5416 -induced cell death in both A549 and HMVEC-L cells by 88.4 and 47.7 %, respectively ($p < 0.05$). Given SalB's pSTAT3 and VEGF elevating activities (Chapter 3), JAK2-pSTAT3-VEGF signaling pathway was proposed as the mechanism of SalB's anti-cell death activity against SU5416. In order to study the dependence of this

signaling pathway, inhibitors to JAK2 and STAT3, AG490 and S31-201, respectively were co-incubated with SalB at 25 μ M and were shown inhibit SalB's anti-cell death activities by 96.8 and 68.2 % in A549 cells and by 85.8 and 131.2 % in HMVEC-L cells, respectively. Through this study, SalB was clearly shown to have protective effects against two different types of emphysematous cell death induced by oxidative stress and VEGF receptor blockade, resulting in improved cell survival.

4.4.2. SalB stimulates proliferation and migration of lung epithelial and endothelial cells

Cellular proliferation and migration are important components of the repair process, where the former overcomes the cell loss while the later causes spreading of the cells to restore the structure (Wagner 2003). In the adult lung, cell death is balanced with cell proliferation and migration to maintain the alveolar structure such that an imbalance in these processes have been suggested to result in alveolar structural destruction and development of emphysema (Lee et al. 2012). In fact, increased cell death and decreased cell proliferation and migration were found in the COPD/emphysema patient derived lung epithelial cells (Perotin et al. 2014). Therefore, SalB's repair activities in the lung alveolar epithelial and endothelial cells were studied with respect to stimulation of cell proliferation and migration.

SalB potently (i.e., at 10-50 μ M) increased proliferation of A549 and HMVEC-L cells by 3.5 and 1.8 –fold ($p < 0.05$) after 48 and 24 h of treatment, respectively, by the MTT assay. While in the MTT assay SalB at 25 μ M showed a 1.3 –fold increase in HMVEC-L cell proliferation compared to the vehicle control, in the ELISA -based BrdU assay SalB showed a comparable 1.4 –fold increase in proliferation, thus confirming its

proliferation stimulatory activity. SalB was also found to potently (i.e., 5-25 μM) promote A549 and HMVEC-L cell migration by 1.5 and 1.6 –fold ($p < 0.05$), respectively, as compared to the vehicle control in the scratch wound closure assay. Since cell proliferation is a critical part of wound closure, especially in the fast growing A549 cells, SalB’s wound closure promoting activity may be a combined result of its effects on cell proliferation and migration (Kim et al. 2010). Notably, HMVEC-L cell migration activities were found to be passage –dependent, where older passage cells showed slower migratory activity, as similarly shown by Liao et al. (Liao et al. 2014). While SalB was recently shown to induce proliferation in human fibroblast cells at the concentration of 25-100 μM (Chen et al. 2014), to our knowledge, this is the first time that SalB has shown migration promoting activity in vitro.

Inhibitors AG490, S31-201 and SU5416 were used to study the dependence of SalB’s activities on the JAK2-pSTAT3-VEGF signaling pathway. In HMVEC-L cells, the inhibition of STAT3 activation by S31-201 and VEGF signaling by SU5416 were studied by the western blot analysis using primary antibodies to pSTAT3 (1:1000, phosphorylated STAT3-Tyr705, rabbit polyclonal, #9131 Cell Signaling technology) and pVEGFR2 (phosphorylated-VEGF receptor 2; 1:1000 rabbit polyclonal, #07-722 EMD Millipore, Temecula, CA). Figure 4.19 (A and B) shows the reduced expression of pSTAT3 and pVEGFR2 upon treatment with 50 μM S31-201 and 5 μM SU5416, respectively, suggesting impaired STAT3 activation and VEGF signal transduction at the receptor VEGFR2, thus confirming the utility of the inhibitors (Hoeben et al. 2004; Hermann et al. 2009). In the cell proliferation assay, AG490, S31-201 and SU5416 inhibited the A549 proliferation by 84.5, 93.6 and 94.1 % and the HMVEC-L cell

proliferation by 62.9, 144.3 and 94.3 %, respectively, suggesting the dependence of JAK2-pSTAT3-VEGF signaling on SalB's activities. The A549 and HMVEC-L cell migration promotion activities of SalB were also respectively inhibited by 108.8, 47.7 and 85.2 %; and by 75.3, 92.9 and 77.7 % by AG490, S31-201 and SU5416.

In our studies we saw a dependence of SalB's anti-cell death, proliferation and migration activity on JAK2-STAT3-VEGF pathway. Extracellular receptor epidermal growth factor-receptor (EGFR) carries out signal transduction through the JAK2-STAT3-VEGF pathway and has been predicted to be the most probable direct target of SalB by proteomic assay and binding affinity studies in vitro (Feng et al. 2011; Wang et al. 2008). Therefore EGFR could be the upstream, extracellular target for SalB, especially given its low intracellular permeability (Chen et al. 2014). However, further studies are required to conclusively show SalB's binding to EGFR and its effect on signal transduction.

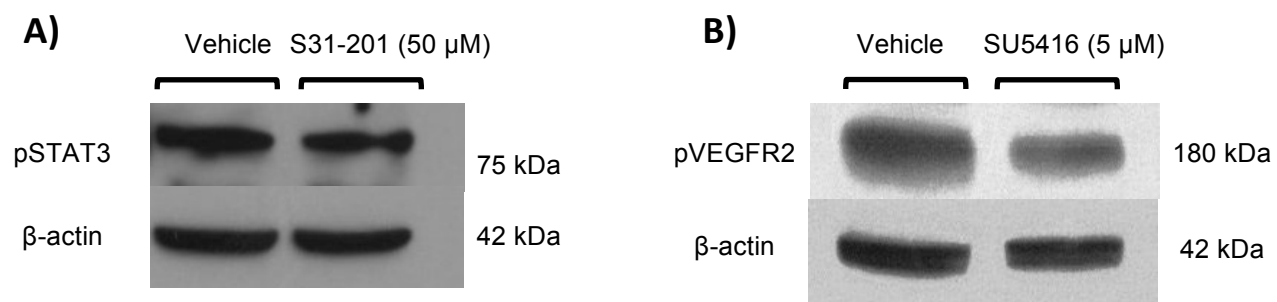


Figure 4.19: HMVEC-L cell (cytoplasmic) expression of pSTAT3 (A) and pVEGFR2 (B) after 24 h treatment with S31-201 at 50 μM or SU5416 at 5 μM, respectively.

4.4.3. SalB restores the impaired recruitment of stem cells

While the *in vivo* models have been used to study bone-marrow derived stem cell recruitment in lung diseases, there are limitations to the available techniques that can assess the stem cell recruitment *in vitro* (Ishizawa et al. 2004). Here, we present an *in vitro* assay that is designed to model recruitment of MSCs through the microvascular lung endothelial barrier using a transwell system. In this assay, we found that the endothelial cells actively promoted migration of the MSCs through the monolayer, which has also been reported previously by Becker et al. (2007). The significantly altered permeability of the MSCs towards the permeability-inducing agent FBS was used to validate this assay (Luscinskas 2008).

VEGF is known to stimulate the expression of stromal derived factor 1 (SDF-1), a potent chemoattractant for stem cells, thus inducing stem cell permeability (Du et al. 2008). VEGF depletion may therefore impair the recruitment of stem cells with important consequences in emphysema (Kurtagic et al. 2015). In our studies, VEGF receptor blockade by SU5416 at 5 μM significantly impaired the trans-endothelial migration of MSCs by 51.7 % ($p < 0.05$). However, SalB at 25 μM restored this impaired migration by 60.0 % ($p < 0.05$). These findings suggest that the VEGF signaling plays an important role in the recruitment of stem cells and SalB corrects the SU5416 -induced impaired stem cell recruitment, presumably because of its VEGF elevating activity. Further studies with JAK2 and STAT3 inhibitors may be important to establish the mechanism of SalB's action in the stem cell recruitment.

4.5. Conclusions

SalB exhibited the anti-cell death activities against emphysematous lung cell death induced by oxidative stress and VEGF receptor blockade. SalB also significantly increased proliferation and migration of lung alveolar epithelial and endothelial cells. Additionally, the inhibitors AG490, S31-201 and SU5416 blocked SalB's in vitro activities. Given the pSTAT3 and VEGF elevating action of SalB shown in Chapter 3, these findings support the hypothesis that the in vitro activities of SalB are dependent on the JAK2-pSTAT3-VEGF signaling pathway. Furthermore, in the newly developed trans-endothelial migration assay, SalB was shown to recover the VEGF receptor blockade-induced impairment in the stem cell recruitment. Therefore, SalB could show the ability to repair alveolar structural destruction and loss by increasing lung resident cell survival, proliferation and migration and circulating stem cell recruitment in vitro. These VEGF – dependent pharmacological repair activities of SalB may be useful in the reversal of emphysema, to be studied in Chapter 5.

CHAPTER 5

SALVIANOLIC ACID B (SalB): IN VIVO REVERSAL OF EMPHYSEMA IN RATS FOLLOWING LUNG DELIVERY

5.1. Introduction

The in vitro lung cell studies described in Chapter 4 have demonstrated that SalB potently exerted the anti-cell death activity, stimulated cell proliferation, and promoted cell migration at 25 μ M, while recovering from impaired stem cell recruitment through the lung endothelia. These activities appeared to be dependent on JAK2, STAT3 and VEGF, and in vivo lung administration of SalB at a dose of 0.2 mg/kg was shown to activate STAT3 and elevate VEGF levels in the lungs of rats, as shown in Chapter 3. Therefore, this chapter was designed to assess the reversal activities of SalB in two differently induced rat models of *established* emphysema. Specifically, emphysema was induced and established with porcine pancreatic elastase (PPE) or cigarette smoke extract (CSE) in rats; and SalB was then spray-instilled at 0.2 mg/kg into the lungs over three weeks period. The reversal activities in functional treadmill exercise endurance, morphological airspace enlargement and destruction, and lung's cell death and proliferation markers as well as pSTAT3 and VEGF expressions were assessed.

5.2. Materials and Methods

5.2.1. Animals

Adult male Sprague-Dawley rats (250–275 g) purchased from Hilltop Lab were used after 3-5 days of acclimatization, according to the animal experimental protocol approved by the VCU’s IACUC. Rats were housed in the AAALAC- accredited animal care facility in the Smith Building basement, maintained at 20-23 °C, 40-70 % of relative humidity and 12-12 h light-dark cycling (the light cycle between 6 am and 6 pm). Food and water were supplied *ad libitum*.

5.2.2 Protocols with PPE- and CSE -induced rat models of *established* emphysema

SalB (Ivy Fine Chemicals) was freshly prepared in saline as dosing solutions on each day. A total of 35 rats were divided into 6 groups and used in two differently induced rat models of *established* emphysema, as shown in Table 5.1. In the PPE-induced model, two dose levels of SalB at 0.1 and 0.2 mg/kg were tested, while in the CSE-induced model, SalB was dosed only at 0.2 mg/kg. The experimental protocols of emphysema induction, SalB administration, animal assessments and tissue harvest in both models are described in Figures 5.1 and 5.2.

Table 5.1: Six experimental groups to examine the reversal activities of SalB in the PPE- and CSE-induced rat models of *established* emphysema

Group	n	Induction	Treatment
1	10	None	Saline
2	6	PPE	Saline
3	3	PPE	SalB (0.1 mg/kg)
4	6	PPE	SalB (0.2 mg/kg)
5	5	CSE	Saline
6	5	CSE	SalB (0.2 mg/kg)

In both models, rats were first trained for 1-2 weeks to run on the AccuPacer rodent treadmill (Accuscan Instruments, Columbus, OH) to assess their exercise endurance, as described in Appendix 2. In the PPE-induced model (Figure 5.1; Group 2-4), emphysema was induced with a single orotracheal (OT) spray-instillation of PPE (80 U/rat) following isoflurane-induced anesthesia using PennCentury's MicroSprayer on day 1. PPE (135 U/mg; 95 % purity) was obtained from Elastin Products Co., as a lyophilized powder, and its instillation solution (6 mg/ml) was also freshly prepared in saline. Animals were left over 21 days only with treadmill training; rats in Group 1 were left as received over 21 days, again only with treadmill training. On day 20 and 21, pre-dose exercise endurance was measured as described below (5.2.3 Treadmill exercise endurance) to confirm the development and establishment of emphysema with impaired running times. Rats were then treated with 0.1 ml OT spray-instillations of saline (Group 1 and 2), SalB at 0.1 mg/kg (Group 3) or SalB at 0.2 mg/kg (Group 4), three times weekly over three weeks period (i.e., total 9 instillations) using the MicroSprayer. On day 40 and 41, post-dose exercise endurance was measured, followed by animal sacrifice, as described below. In the CSE-induced model (Figure 5.2; Group 5-6), emphysema was induced over 21 days with three weekly intraperitoneal (IP) injections of CSE on day 1, 7 and 14. On each day, CSE was freshly prepared by bubbling one research-grade cigarette 3R4F (University of Kentucky, Lexington, KY) into 1 ml saline with a smoking machine. As in the PPE-induced model, pre-dose exercise endurance was measured to confirm the development and establishment of emphysema with impaired running times. Rats were then treated with 0.1 ml OT spray-instillations of saline (Group 5) or SalB at 0.2 mg/kg

(Group 6), three times weekly over three weeks period, followed by post-dose exercise endurance measurement and animal sacrifice, as described below.

On day 42, animals were sacrificed and lungs were harvested. Under the surgical anesthesia with an IP injection of urethane at 1 g/kg, the trachea was cannulated through an incision made on the neck area. The animals were sacrificed by exsanguination, and their lung and heart were carefully removed from the body. The bronchial airway lumens to the right lung lobes were tightly closed with a surgical suture. The left lung lobe was then inflated through the tracheal cannula with 8-10 ml of a warm 0.5 % agarose solution at a hydrostatic pressure of 20 cm. This solution of agarose (Invitrogen, Carlsbad, CA) had been prepared in distilled, deionized water (DDW) at 80 °C and maintained at 50 °C prior to use. Immediately, the lungs were placed in an ice bath for 10 min to solidify the agarose. The right lung lobes were then removed for Western blot and myeloperoxidase (MPO) activity analyses as described below. The inflated left lung lobe was fixed with 10 % buffered formalin (Fisher Scientific) at 4°C for over 24 h. At the VCU Anatomical Pathology Laboratory, the left lungs were embedded in paraffin blocks, from which 4 µm-thick lung histology sections were prepared on slides with hematoxylin and eosin (H&E)-staining. These lung section slides were used to assess the alveolar airspace morphology (i.e., size and destruction) via determination of mean linear intercept (MLI) and destructive index (DI), as described below.

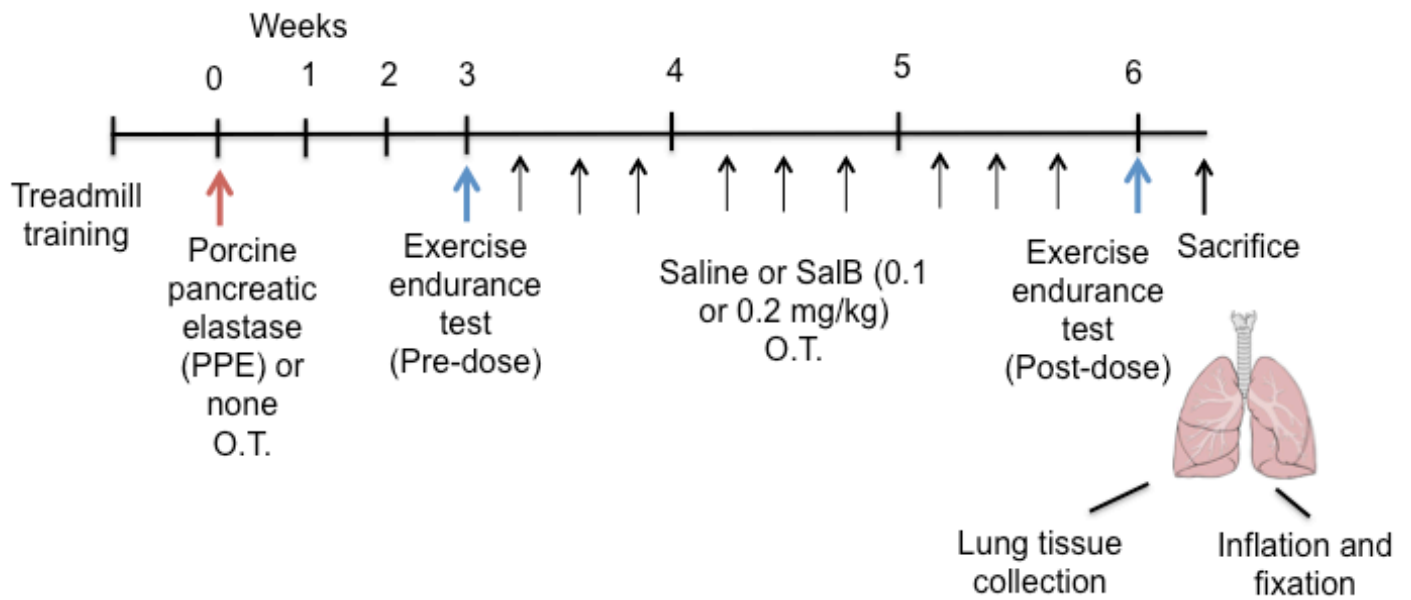


Figure 5.1: Experimental protocol used to assess the reversal activities of SalB in the PPE-induced rat model of *established* emphysema. (OT, orotracheal instillation)

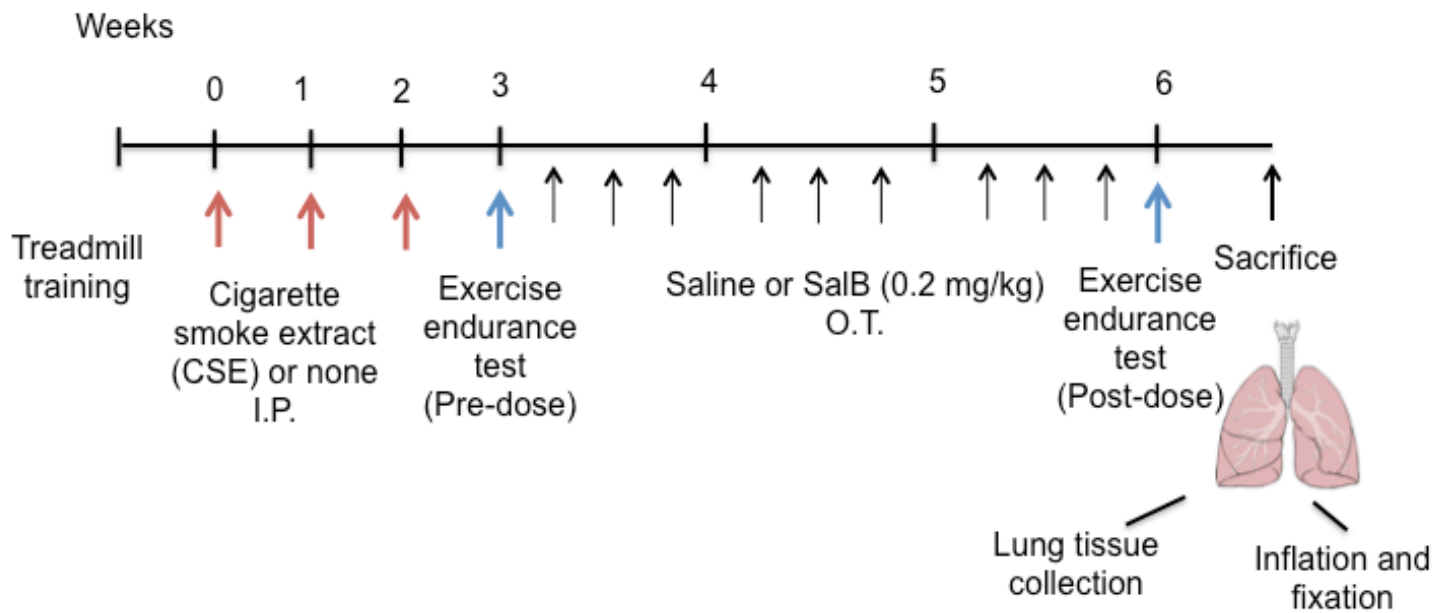


Figure 5.2: Experimental protocol used to assess the reversal activities of SalB in the CSE-induced rat model of *established* emphysema. (IP, intraperitoneal injection)

5.2.3. Treadmill exercise endurance

Running times on the treadmill to exhaustion were used to measure the functional exercise endurance for rats. Following training, as described in Appendix 2, pre-dose and post-dose exercise endurances were measured on day 20 & 21 and 40 & 41, respectively, on the AccuPacer rodent treadmill. Briefly, trained rats were allowed to run against a speed of 10 m/min and an inclination of 5 degrees of the running belt. Exhaustion was judged when the animals received a 5th electrical foot shock from the bar grid or displayed an inability to return to the running belt. In each measurement, the exercise endurance was reported as an average running time for exhaustion.

5.2.4. Alveolar airspace size by mean linear intercept (MLI)

Alveolar airspace size was assessed in each rat using the mean linear intercept (MLI) measured by the method first described by Thurlbeck (Thurlbeck, 1966) and modified in-house. Each H&E-stained alveolar section of the left lung lobe was observed under the microscope (at 25X magnification; Nikon Optishot II equipped with Zeiss Axiocam digital camera), and 5 microscopic images (3450 x 2585 μm) were randomly selected and printed out. In each image, 5 horizontal lines (3450 μm) were drawn with equal (431 μm) vertical intervals, and their intercepts with the alveolar walls were counted to determine the MLI values (3450 mm / the number of the intercepts). Therefore, the MLI value for each animal was calculated as an average of the 25 MLI values (5 horizontal lines per image x 5 images).

5.2.4. Alveolar structural destruction by destructive index (DI)

Alveolar structural destruction was assessed in each rat using the destructive index (DI) determined by a microscopic point count technique, according to a method described by Eidelman (Eidelman, 1991), modified in-house. In each H&E-stained alveolar section of the left lung lobe observed under the microscope (at 100X magnification; Nikon Optishot II and Zeiss Axiocam digital camera), 40-60 non-overlapping fields were randomly selected and printed out. Over each image, a grid of 66 equally spaced dot points was then placed, and the alveolus lying underneath each point was evaluated for the presence of destruction. The destruction was defined based on one of the following criteria:

- a) Two or more alveolar walls nick or defect in a single alveolus or two adjacent alveoli opening into the same duct
- b) Two or more islands of lung parenchyma within an alveolar or ductal space
- c) Cuboidal epithelial lining on alveolar structure with or without nicks or defects

Each point on the alveolus was counted as either normal (N) or destroyed (D) alveolus, based on the above criteria. Only the points falling on the whole alveoli or ducts were counted. Over 20,000 dot points were assessed in each animal to calculate the % DI using the equation:

$$\% DI = 100 \times \frac{D}{D + N}$$

5.2.6. Protein extraction and western blot analysis

After sacrifice on day 42, 300 mg of right lung tissue were minced, homogenized using the hand homogenizer (Pro 200; Pro Scientific, Inc.) in NP-40 lysis buffer with a cOmplete™ protease inhibitor cocktail tablet and a PhosSTOP™ phosphatase inhibitor tablet (Roche Diagnostics) in ice and centrifuged to obtain supernatant. For nuclear extracts, the minced lung tissues were extracted using the Nuclear/Cytosol Fractionation kit (Biovision) according to the manufacturer's protocol. After determining the protein content of the supernatant by the BCA assay, 40 µg of protein was denatured at 100 °C for 10 min, electrophoresed on a 10 % Mini-PROTEAN TGX polyacrylamide gel (Bio-Rad; Hercules, CA), and transferred to nitrocellulose membranes (0.2 mm; Bio-Rad), as described in Appendix 2. After 1 h blocking at room temperature, the membranes were probed via overnight incubation at 4 °C with each of the mouse or rabbit antibodies raised against: 1) cleaved caspase-3 (1:1000, rabbit monoclonal, #9664, Cell Signaling, Danvers, MA), 2) proliferating cell nuclear antigen (PCNA, 1:2000, mouse monoclonal, #2586, Cell Signaling), 3) pSTAT3 (1:1000, phosphorylated STAT3-Tyr705, rabbit polyclonal, #9131, Cell Signaling), 4) VEGF (1:100, mouse monoclonal, sc-7269, Santa Cruz, Dallas, TX.), 5) b-actin (1:5,000; Sigma-Aldrich) and 6) lamin B1 (1:1000, rabbit monoclonal, #12586, Cell Signaling). Subsequently, the membranes were incubated in the horseradish peroxidase-conjugated goat anti-mouse or anti-rabbit antibody (Bio-Rad Laboratories) in the blocking buffer for 80 min at room temperature. The probed protein was detected with the SuperSignal West Pico enhanced chemiluminescent substrate kit (Pierce) in the film processor (X-Omat 2000A; Eastman Kodak, Rochester, NY). Their band signals were quantified with ImageJ (NIH). Each protein signal was normalized

with the corresponding β -actin or lamin B1 signal, and expressed as the value relative to that for the untreated healthy rat lungs.

5.2.7. Lung Myeloperoxidase (MPO) activity

The MPO activity was assessed in the lung tissues as an index of neutrophil accumulation by the method developed by Goldblum et al. (Goldblum, 1985), with in-house modifications. The minced right lung tissues (50 mg) were homogenized in upto 0.5 ml of 0.02 M EDTA solution in water (pH= 4.7) on ice and centrifuged at 12,000 rpm for 15 minutes at 4 °C to separate the pellet from the supernatant. This pellet was re-suspended in 0.5 ml of 0.5 % hexadecyltrimethyl ammonium bromide solution in PBS (pH = 6) and centrifuged (12,000 rpm, 15 min) at 4 °C. In a 96-well plate, 20 μ l of the supernatant was reacted with 180 μ l of 0.17 mg/ml O-dianisidine dihydrochloride and 0.0005 % H₂O₂ solution in PBS. The absorbance increase in 5 min (Δ Abs) was measured at 405 nm using a plate reader (SynergyTM 2), as an indicator of MPO activity. Finally, the BCA assay was used to normalize the MPO activity with the protein concentration and the results were expressed as Δ Abs in 5 min per mg protein.

5.2.7. Data description and statistical analyses

The results of the in vivo assessments were expressed as treatment group mean \pm SE (n=3-10). Statistical analyses for group comparison were carried out using Prism[®] 7 or JMP-Pro[®] 12 by student *t*-test or one-way analysis of variance (ANOVA); p<0.05, 0.01 or 0.001 was considered to be statistically significant. Post-hoc analysis for multiple comparison testing was performed by the Tukey's method.

5.3. Results

5.3.1. SalB reversed impaired exercise endurance in *established* emphysema

Figure 5.3 shows the treadmill exercise endurance of each rat on day 21-22 and 43-44, before and after three weeks pulmonary administration of saline or SalB at 0.1 or 0.2 mg/kg (three times per week) in the rat models of *established* emphysema induced with PPE and CSE, compared to that in healthy rats treated with or without pulmonary administration of SalB at 0.2 mg/kg. Note that the later data with healthy rats were taken during the studies described in Chapter 3. Untreated healthy rats ran for 47.7 ± 3.2 . The SalB treatment slightly shortened the running time to 41.6 ± 1.6 min, but this reduction was not significant. In contrast, the exercise endurance was drastically impaired (i.e., reduced) to 6.7 ± 1.1 min of the across group running time or by average 86.0 % on day 21-22 following PPE instillation. Note, however, that these reduced pre-dose running times were comparable between three different treatment groups of rats. While the saline treatment left the endurance impaired at 5.7 ± 1.6 min, the SalB treatment at 0.1 mg/kg only moderately improved them to 15.1 ± 3.3 min or by 20.5 % ($p < 0.01$). However, SalB at 0.2 mg/ml remarkably improved the running times significantly ($p < 0.01$) to 40.1 ± 2.6 min or by 81.5 % suggesting the functional reversal of *established* emphysema in this PPE –induced rat model.

Likewise, the repeated CSE injections reduced the exercise endurance on day 21-22 to 8.0 ± 0.2 min, of the across group running times or by average 83.3 %. Again, these pre-dose running times were equally impaired between two different treatment groups of rats. While the endurance remained unchanged at 9.0 ± 2.0 min by the saline treatment, SalB at 0.2 mg/kg again improved the endurance time significantly ($p < 0.01$) to 30.7 ± 5.9 or by average 57.2 %. Figure 5.4 shows difference in the exercise endurance (Δ

Endurance) measured on day 20-21 and day 41-42 i.e., before and after three weeks of pulmonary administration of saline or SalB at 0.1 or 0.2 mg/kg in the PPE and CSE – rat models of *established* emphysema. In the PPE –induced emphysema, three weeks pulmonary administration of SalB at 0.1 or 0.2 mg/kg increased the endurance significantly by 10 and 31 –fold ($p<0.05$), respectively, while in the CSE –induced rat model of *established* emphysema, SalB at 0.2 mg/kg increased endurance by 18 –fold ($p<0.05$), as compared to saline treated rats. These results strongly suggested the reversal of functional damages of the emphysematous lungs.

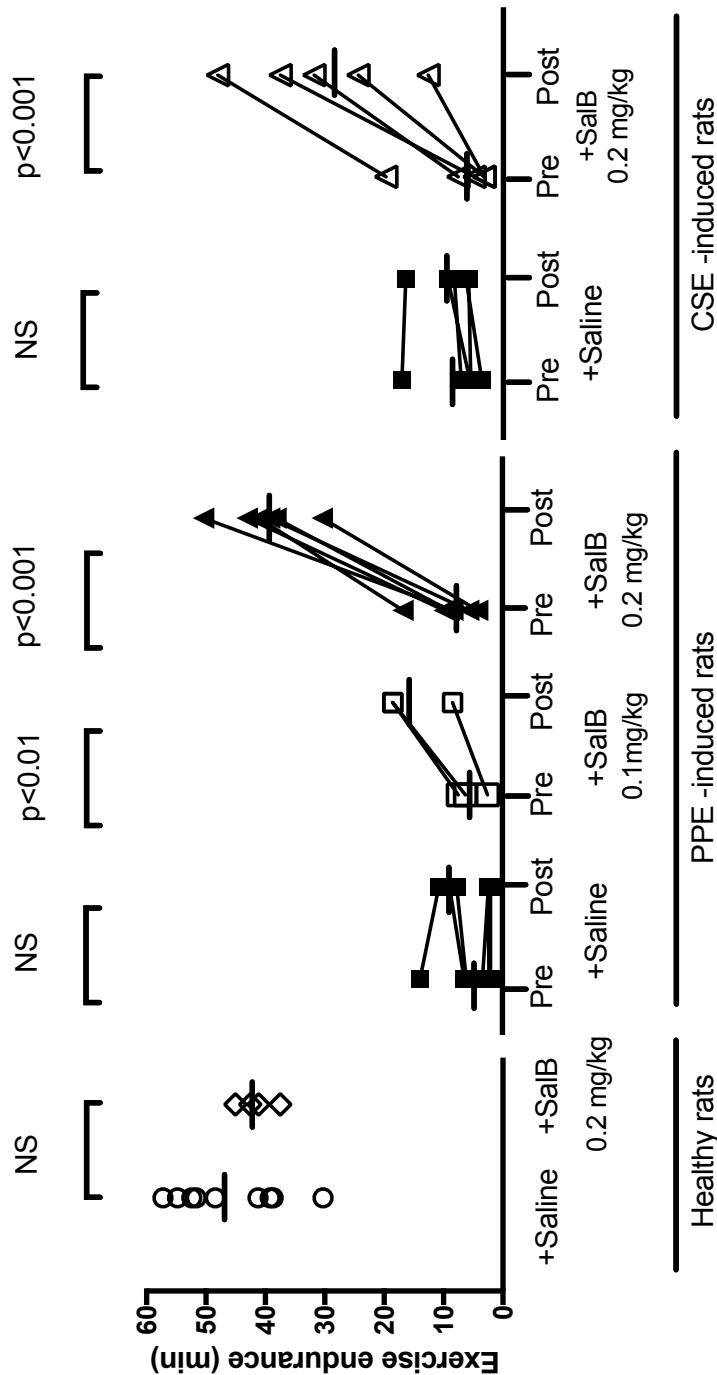


Figure 5.3: Treadmill exercise endurance of each rat measured on day 21-22 and 43-44, respectively, before (Pre) and after (Post) three weeks of pulmonary administration of saline or SalB at 0.1 or 0.2 mg/kg (three times per week) in rat models of *established* emphysema induced with PPC and CSE, compared to that in healthy rats with or without two weeks pulmonary administration of SalB at 0.2 mg/kg (fives times/week). Each treatment group n = 3-10. Horizontal bar represents group mean value. Changes of the pre- vs. post- dose exercise endurance were either significant ($p<0.01$ or $p<0.001$) or not significant (NS), identified by the student's *t*-test comparing with 0. In healthy rats, SalB treatment did not change the treadmill endurance (NS).

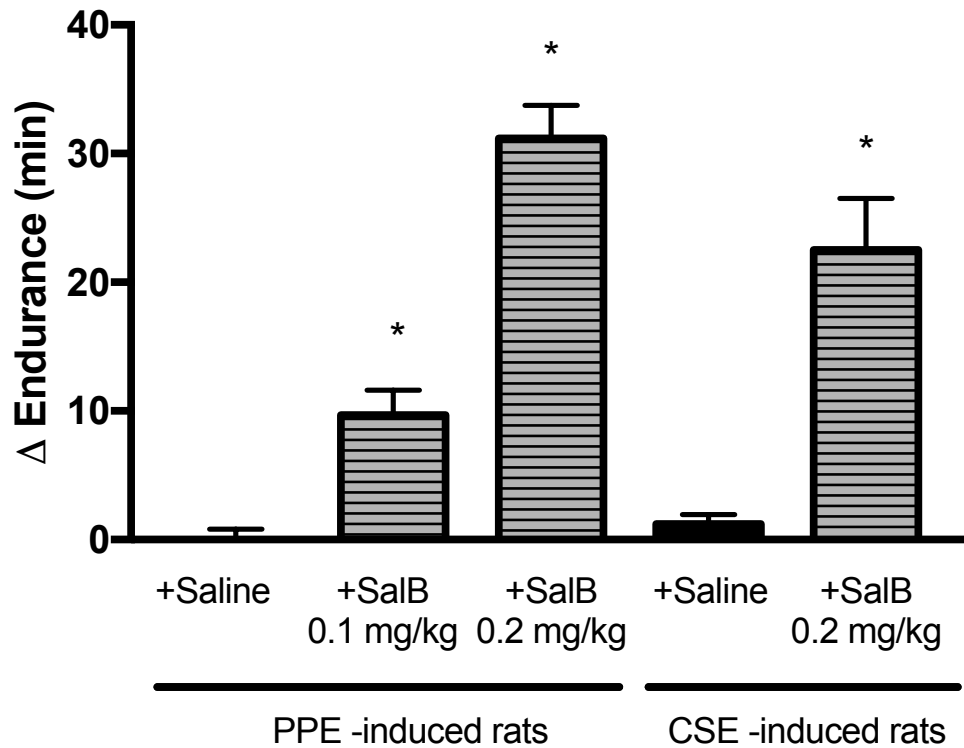


Figure 5.4: Difference in the exercise endurance (Δ Endurance) measured on day 20-21 and day 41-42 i.e. before (Pre) and after (Post) three weeks of pulmonary administration of saline or SalB at 0.1 or 0.2 mg/kg (three times per week) in rat models of *established* emphysema induced with PPE and CSE. Data: mean \pm SE (n=3-10); *p<0.05, compared to the corresponding rats with *established* emphysema treated with saline, by ANOVA followed by Tukey's multiple comparison test.

5.3.2 SalB reversed airspace enlargement and alveolar destruction in *established* emphysema

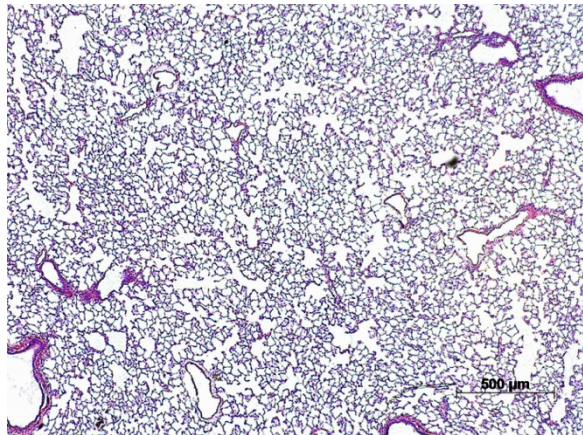
Figure 5.5 shows the representative alveolar airspace images in the rat models of *established* emphysema induced with PPE or CSE on day 43-44 following three weeks pulmonary administration of saline or SalB at 0.2 mg/kg (three times/week), compared to those in healthy rats treated with or without pulmonary administration of SalB at 0.2 mg/kg. While the alveolar airspace morphology remained unchanged and appeared to be normal in healthy rats following SalB administration at 0.2 mg/kg (Figure 5.5 A and B), abnormal airspace enlargement and alveolar destruction were evident in the PPE and CSE –induced emphysematous rats following saline treatment (Figure 5.5 C and E, respectively). However, SalB treatment at 0.2 mg/kg appeared to recover this airspace enlargement and alveolar destruction in these models of *established* emphysema (Figure 5.5 D and F, respectively).

The MLI values and DI% in different treatment groups of rats are thus shown in Figure 5.6 and 5.7, respectively, as group measures of airspace enlargement and alveolar destruction. As predicted from the alveolar airspace images, the SalB treatment alone did not alter the MLI value in healthy rats (58.5 ± 3.3 and 54.7 ± 2.0 μm with and without SalB treatment, respectively), as shown in Figure 5.6. In the PPE -induced emphysematous rats, the MLI value was significantly increased to 97.8 ± 3.2 μm or by 1.8 –fold ($p < 0.05$), compared to that in healthy rats. However SalB treatment enabled a significant 58.6 % ($p < 0.05$) recovery of this airspace enlargement, demonstrating an MLI value of 72.5 ± 1.97 μm . Likewise, as in Figure 5.7, the DI% was significantly elevated to 17.3 ± 1.6 % in the PPE –induced emphysematous rats, compared to 4.3 ± 0.4 % seen in healthy rats

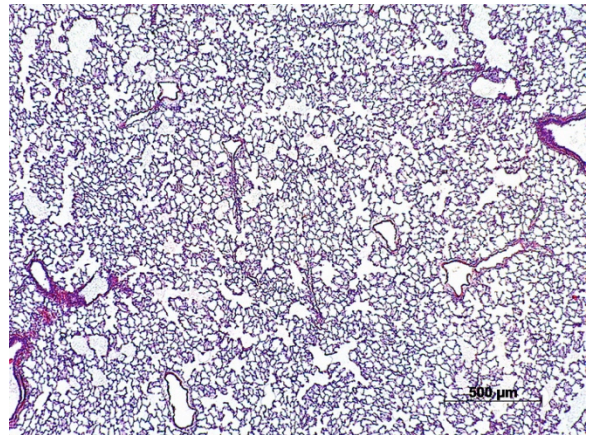
($p < 0.05$). However, SalB at 0.2 mg/kg again significantly recovered the DI% to 9.4 ± 0.3 % or by 61.0 % ($p < 0.05$), which suggested that the SalB treatment reversed the airspace enlargement and alveolar destruction in the PPE -induced model of *established* emphysema. Figure 5.8 shows correlation plot between MLI and DI% values of each rat belonging to the three treatment groups. The MLI and DI% values were highly correlated indicating a close association between these emphysematous abnormalities.

In the CSE -induced model of *established* emphysema, the MLI value was also abnormally higher at 84.6 ± 1.7 μm , a significant 1.6 -fold greater value from 54.7 ± 2.0 μm for healthy rats ($p < 0.05$), as shown in Figure 5.6. However, the SalB treatment at 0.2 mg/kg produced a 74.8 % recovery of the airspace enlargement, as demonstrated by the MLI value of 62.2 ± 3.4 μm ($p < 0.05$).

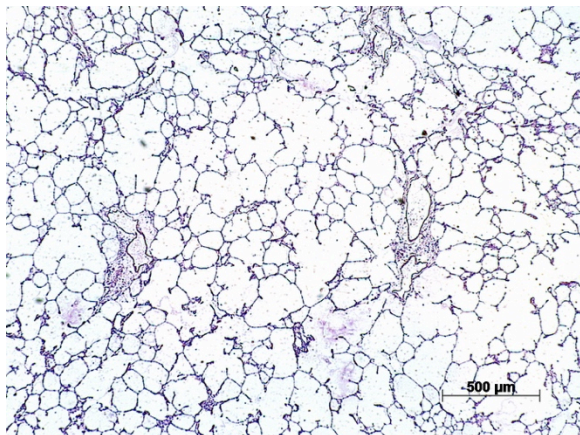
A) Healthy rats treated with saline



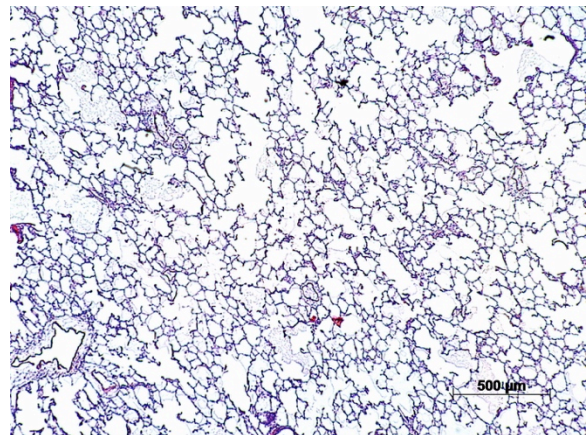
B) Healthy rats treated with SalB (0.2 mg/kg)



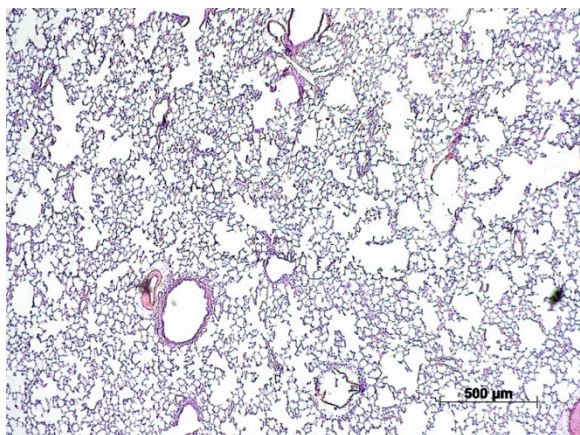
C) PPE -induced rats treated with saline



D) PPE -induced rats treated with SalB (0.2 mg/kg)



E) CSE -induced rats treated with saline



F) CSE -induced rats treated with SalB (0.2 mg/kg)

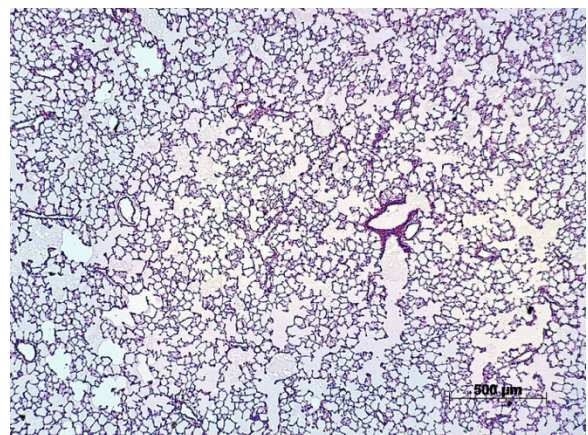


Figure 5.5: The representative H&E stained micrographs of the alveolar airspaces in the left lung lobes in rat models of *established* emphysema induced with PPE or CSE following three weeks pulmonary administration of saline or SalB (0.2 mg/kg, three times/week), compared to those in healthy rats with or without two weeks pulmonary administration of SalB (0.2 mg/kg, five times/week). Magnification = 25X; the scale bars represent 500 μ m.

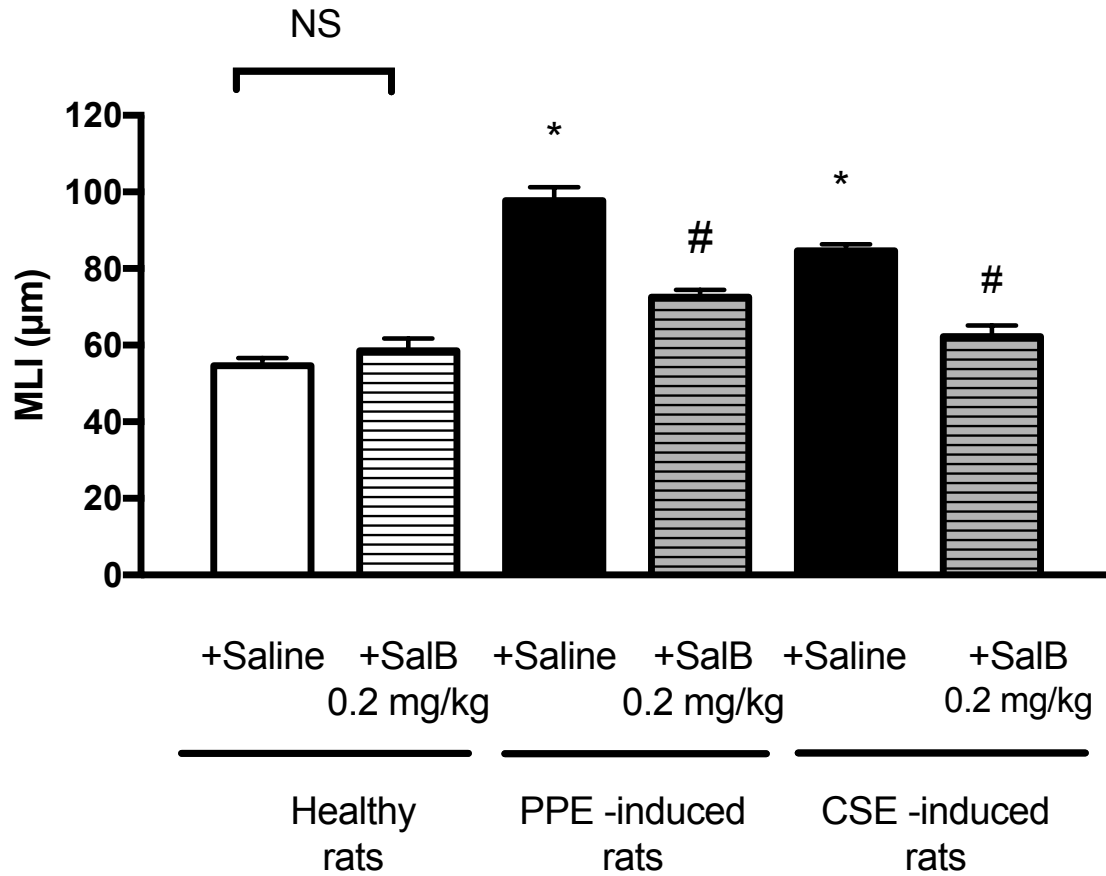


Figure 5.6: Mean linear intercept (MLI) values of the alveolar airspaces in the rat models of *established* emphysema induced with PPE or CSE following three weeks pulmonary administrations of saline or SalB at 0.2 mg/kg (three times/week), compared to those in healthy rats treated with saline or SalB (0.2 mg/kg, five times/week). Data: mean±SE (n=4-6) *p<0.05, compared to healthy saline treated rats; #p<0.05, compared to the corresponding rats models of *established* emphysema treated with saline, by ANOVA and Tukey's multiple comparison test. NS: not significant.

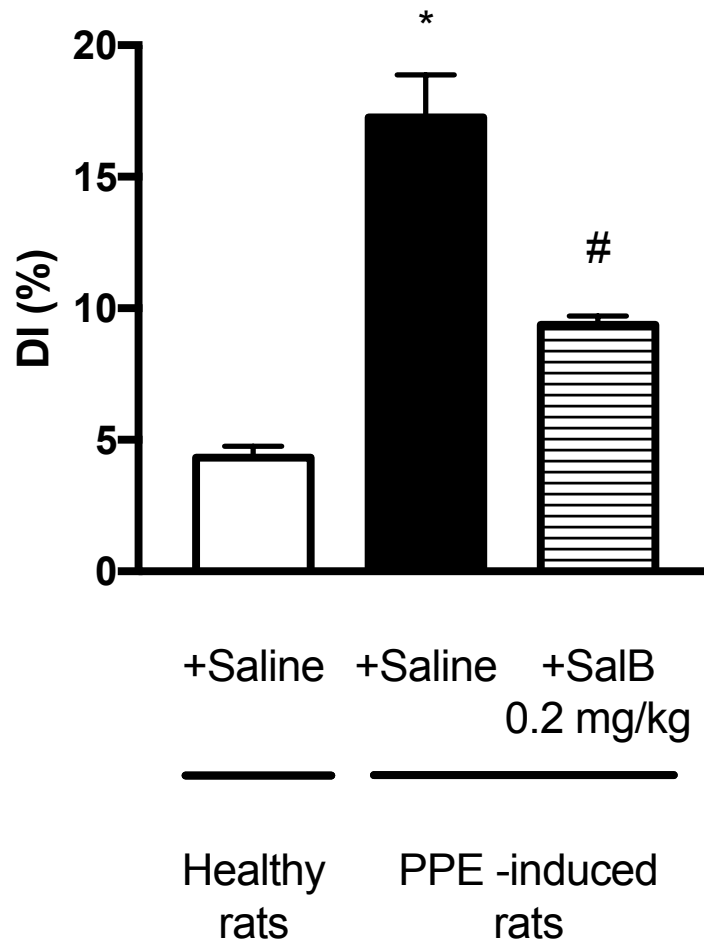


Figure 5.7: Destructive index (DI) measurements obtained from the H&E stained 100X images of healthy or PPE –induced emphysema rats either treated with saline or SalB. Data: mean±SE (n=3) *p<0.05, compared to healthy saline control; #p<0.05, compared to PPE –induced saline treated control, by ANOVA and Tukey’s multiple comparison test.

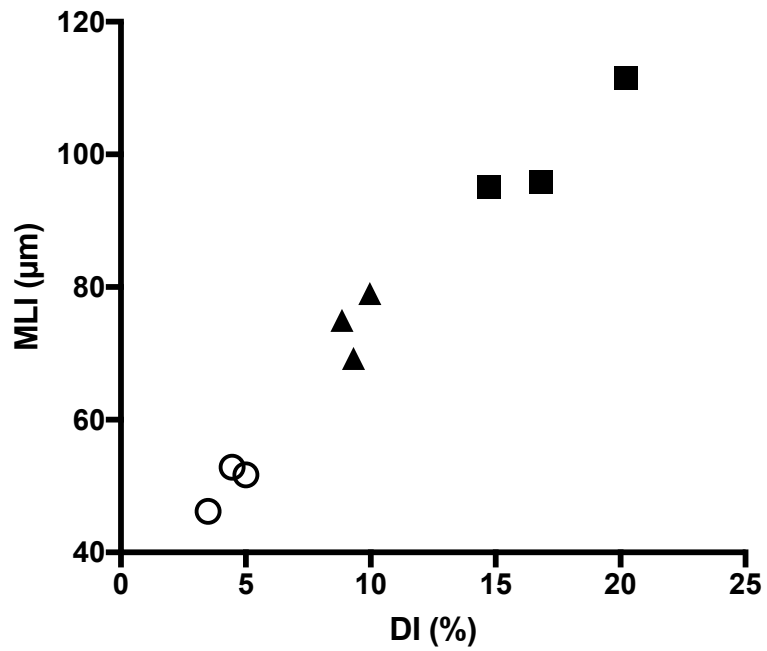


Figure 5.8: Correlation between alveolar airspace enlargement (MLI) and destruction (DI) in \circ = healthy saline treated rats, \blacktriangle = PPE-induced SalB -treated rats and \blacksquare = PPE-induced saline treated rats.

5.3.3. Lung tissue expression of protein markers

To examine if the functional and morphological reversal activities of SalB shown above are associated with the modulations in the cell death and proliferation activities in the lung, cleaved caspase 3 and PCNA, were chosen as biomarkers of apoptotic cell death and proliferation, respectively. Figure 5.9 shows the cleaved caspase 3 expression in the lungs of PPE –induced rats with or without SalB treatment, relative to that of healthy rats. The saline treatment left the cleaved caspase 3 expression elevated by 13 –fold ($p<0.05$), indicating increased lung cell apoptosis and emphysematous damage. However, the SalB treatment enabled significant suppression by 94.3 % ($p<0.05$), suggesting the reversal of the lung’s apoptotic activity. By contrast, as shown in Figure 5.10, the saline treatment resulted in rather stimulated PCNA expression, but insignificantly by 1.6 –fold. However, the SalB treatment significantly increased the PCNA expression further in the PPE – induced animals ($p<0.05$), resulting in a 2.6 –fold greater level, when compared to that in healthy rat lungs ($p<0.05$).

Figures 5.11 show the (A) cytoplasmic and (B) nuclear expressions of pSTAT3 in the lungs of the PPE –induced rats with or without SalB treatment, in comparison with the healthy rats. In the PPE –induced emphysematous rats, both the cytoplasmic and nuclear expression of pSTAT3 appeared to remain lower by 18.4 and 45.0 %, respectively, yet these reductions did not reach statistical differences. By contrast, the SalB treatment seemed to restore or stimulate the pSTAT3 levels, but again, these changes did not reach statistical differences. However, as shown in Figure 5.12, it became clear that the SalB treatment normalized the lung expression of VEGF from a significant 35.6 % reduction ($p<0.05$) seen in the PPE-induced emphysematous rats

following saline treatment.

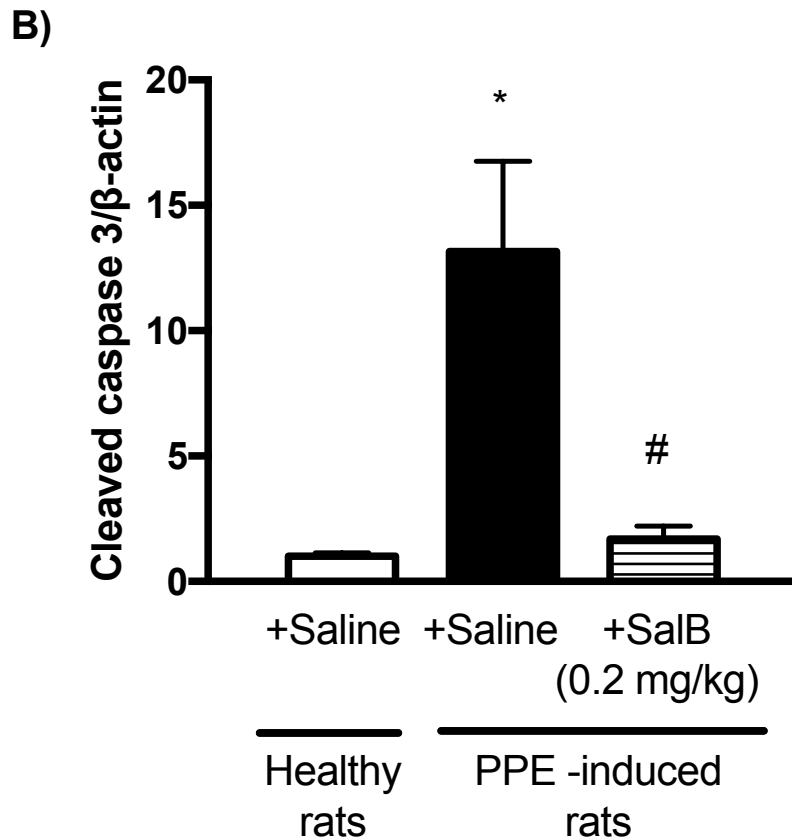
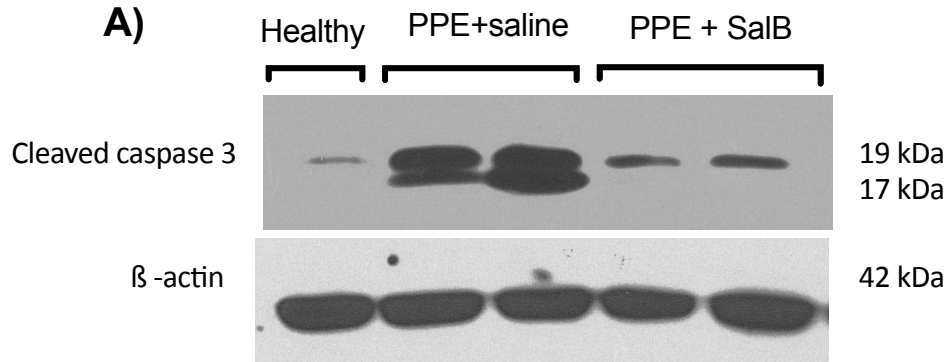


Figure 5.9: Lung tissue (cytosolic) expression of cleaved caspase 3 in the rat model of *established* emphysema induced with PPE following three weeks pulmonary administration of saline or SalB (0.2 mg/kg, three times/week), relative to that in healthy rats. **(A)** Representative western blots of cleaved caspase 3 at 17 and 19 kDa and β -actin at 42 kDa. **(B)** Signal band ratios of cleaved caspase 3 to β -actin relative to that for the healthy rat lungs. Data represent mean \pm SE, from n=3-6, *p<0.05, compared to the healthy rats; #p<0.05, compared to the PPE-induced saline treated rats, by ANOVA and Tukey's multiple comparison test.

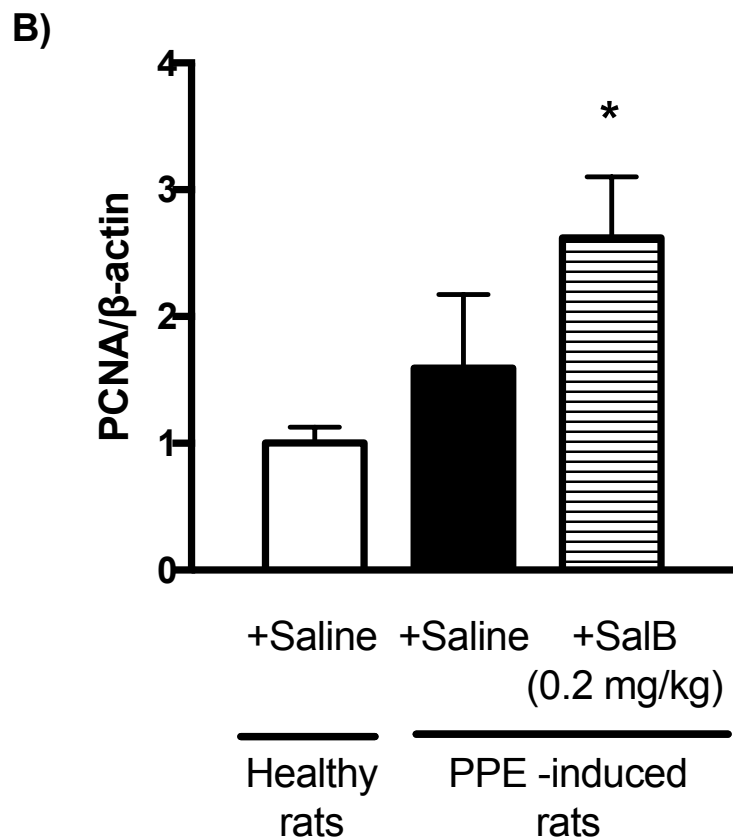
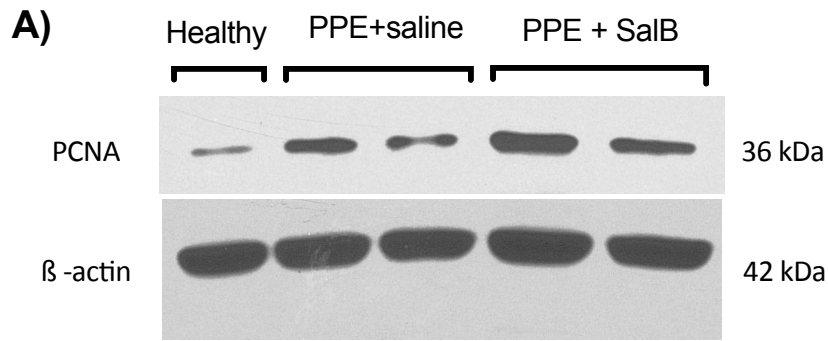


Figure 5.10: Lung tissue (cytosolic) expression of proliferating cell nuclear antigen (PCNA) in the rat model of *established* emphysema induced with PPE following three weeks pulmonary administration of saline or SalB (0.2 mg/kg, three times/week), relative to that in healthy rats. **(A)** Representative western blots of PCNA at 36 kDa and β -actin at 42 kDa. **(B)** Signal band ratios of PCNA to β -actin relative to that for the healthy rat lungs. Data represent mean \pm SE, from n=3-6, *p<0.05, compared to the healthy rats, by ANOVA and Tukey's multiple comparison test.

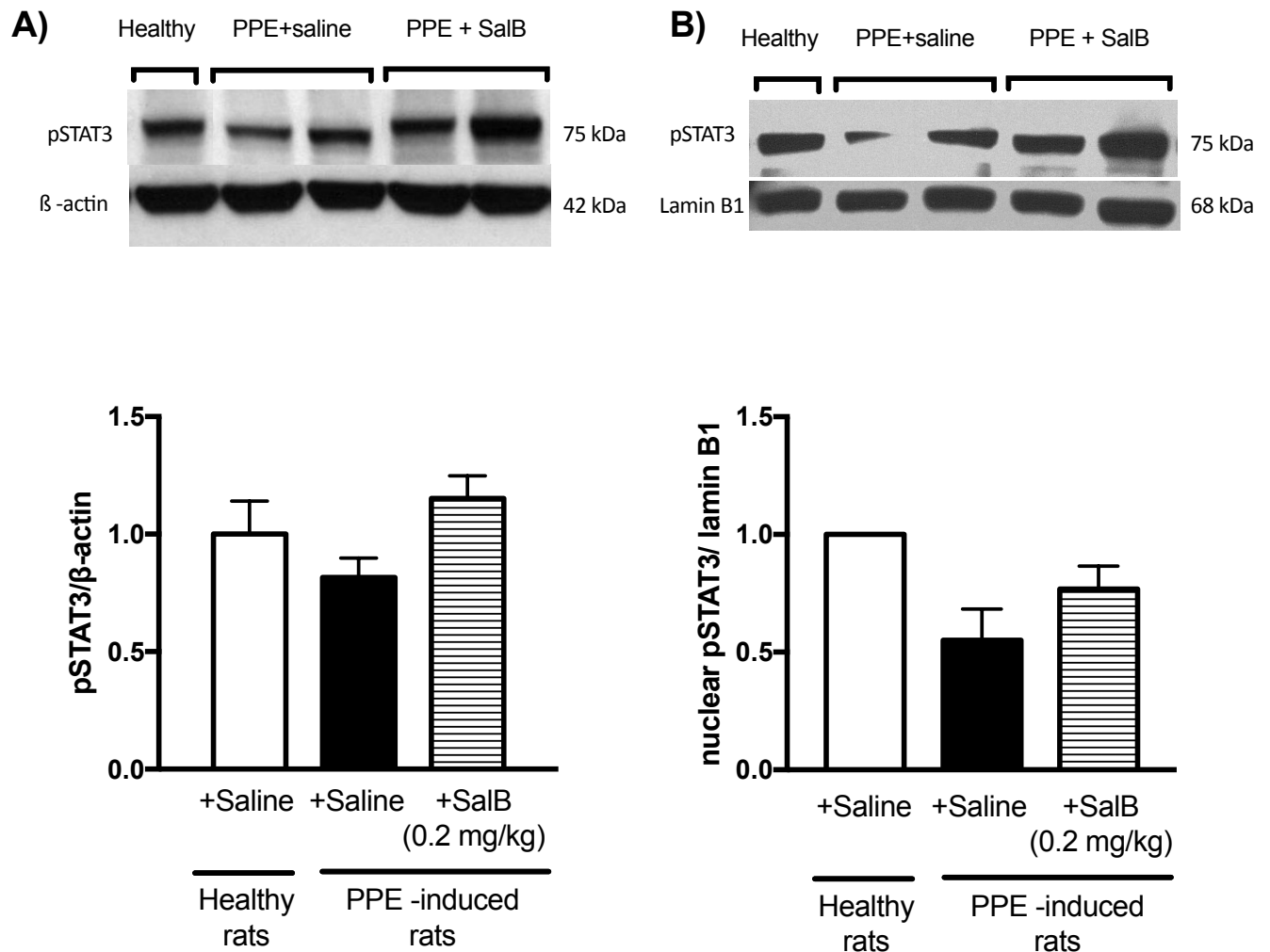


Figure 5.11: Lung tissue cytosolic and nuclear expression of pSTAT3 in the rat model of *established* emphysema induced with PPE following three weeks pulmonary administration of saline or SalB (0.2 mg/kg, three times/week), relative to that in healthy rats. **(A)** Representative western blots of cytosolic pSTAT3 at 75 kDa, β -actin at 42 kDa and their signal band ratios of pSTAT3 to β -actin relative to that for the healthy rat lungs. **(B)** Representative western blots of nuclear pSTAT3 at 75 kDa, lamin B1 at 68 kDa and their signal band ratios of pSTAT3 to lamin B1 relative to that for the healthy rat lungs. Data represent mean \pm SE, from n=2-7.

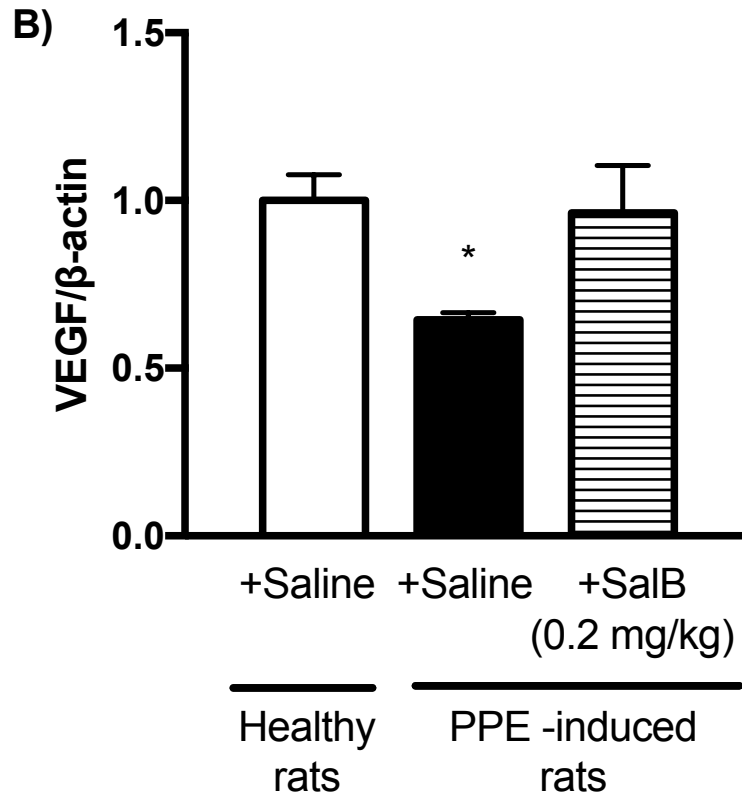
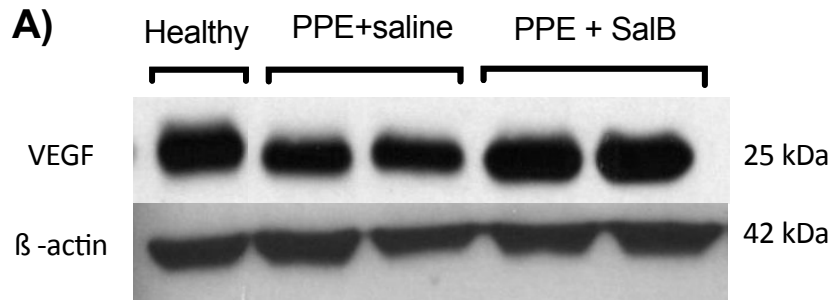


Figure 5.12: Lung tissue (cytosolic) expression of VEGF in the rat model of *established* emphysema induced with PPE following three weeks pulmonary administration of saline or SalB (0.2 mg/kg, three times/week), relative to that in healthy rats. **(A)** Representative western blots of VEGF at 25 kDa and β -actin at 42 kDa. **(B)** Signal band ratios of VEGF to β -actin relative to that for the healthy rat lungs. Data represent mean \pm SE, from n=3-6, *p<0.05, compared to the healthy rats, by ANOVA and Tukey's multiple comparison test.

5.3.4. Lung MPO activity

Because PPE –induced emphysema and its alveolar destruction are associated with neutrophil infiltration into the lungs (Antunes & Rocco 2011), the MPO activity was assessed as a biomarker for neutrophilic lung damage. Figure 5.13 shows the MPO activities measured with Δ Abs in 5 min normalized by the protein content. In the PPE – induced emphysematous rats (following saline treatment), the lungs MPO activity was significantly higher by 4 –fold ($p < 0.05$), compared to that of healthy lungs, indicating elevated neutrophil infiltration as a result of elastolytic insult. Following SalB treatment, the MPO activity still remained equally elevated, which suggested lack of SalB’s effect on neutrophil infiltration.

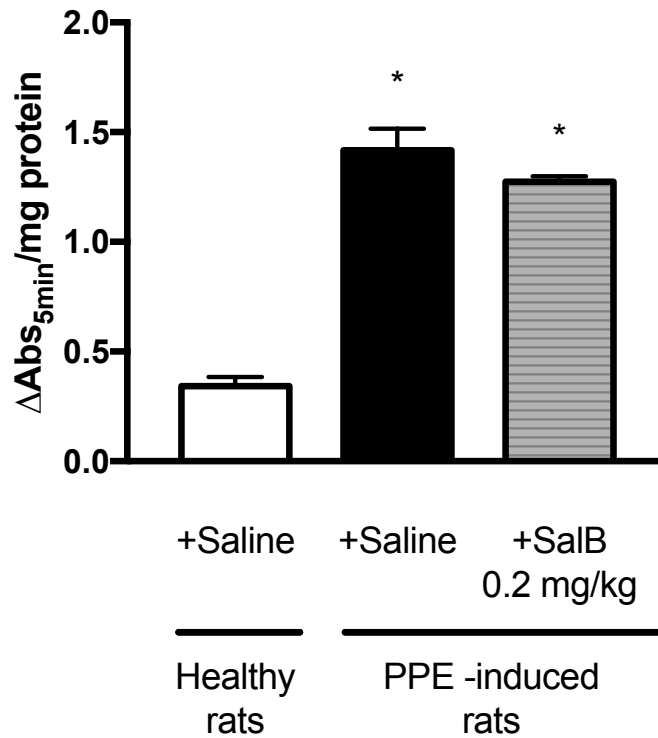


Figure 5.13: Lung MPO activity in the rat model of *established* emphysema induced with PPE following three weeks pulmonary administration of saline or SalB (0.2 mg/kg three times/week), compared to that in healthy rats. The MPO activities were described as the 405 nm absorbance change in 5 min ($\Delta\text{Abs}_{5\text{min}}$) normalized with the sample protein content. Data: mean \pm SE, from n=5-8, *p<0.05, compared to the healthy rats, by ANOVA and Tukey's multiple comparison test. SalB did not change the MPO activity in the PPE – induced rats.

5.4. Discussion

In this chapter, PPE and CSE rat models of *established* emphysema were used to determine if pulmonary administration of SalB results in the reversal of emphysematous lung damages. Initiation of SalB treatment following PPE or CSE –induced functional impairment enabled a more clinically realistic assessment of its application in the treatment of emphysema. SalB treatment at 0.2 mg/kg enabled recovery of impaired functional endurance and morphology in PPE and CSE –induced emphysema. This recovery was associated with normalization of the lung expressions of cell death marker cleaved caspase 3 and VEGF along with an increase in proliferative marker PCNA. All the evidence taken together suggests reversal of *established* emphysema by pulmonary administration of SalB.

5.4.1. SalB recovered functional impairment in PPE and CSE –induced *established* emphysema

Single orotracheal (OT) instillation of 80 U of PPE induces emphysema in rats by triggering elastolysis and inflammation, resulting in alveolar structural destruction that is a characteristic of the disease (Inoue, 2010). Due to its faster onset, progressive and largely irreversible nature, the elastase model is ideal for testing new therapeutic approaches for reversing emphysematous damage to the lung (Stevenson & Birrell 2011). In this study, PPE significantly reduced the exercise endurance in rats by 7.2 –fold (47.7 min → 6.7 min, $p < 0.05$), a clinically relevant observation seen in emphysema patients (Yao et al. 2012). While treatment with SalB at 0.1 mg/kg only marginally improved the endurance by 20.5 % (6.7 min → 15.1 min, $p < 0.05$), SalB at 0.2 mg/kg recovered this

impaired endurance by 81.5 % (6.7 min → 40.1 min, $p < 0.05$).

None of the animal models can reproduce all the features of emphysema as it occurs in humans since the natural history and the comorbidities that are often observed in humans are absent in animals (Oliveira et al. 2016). Although widely used, the PPE experimental model has several limitations because the emphysema is induced by instillation of a single high dose of a protease rather than a continuous low-grade inflammation believed to be present in chronic cigarette smokers (Flo et al. 2006). To address some of these limitations, the CSE –induced emphysema model, first described by Taraseviciene-Stewart and coworkers, was used in addition to PPE for studying SalB's emphysema reversal activities (Taraseviciene-Stewart et al. 2007). In this study, three IP injections of CSE for 3 weeks significantly reduced exercise endurance of the rats by 6.0 –fold (47.7 min → 8.0 min, $p < 0.05$), thus suggesting functional impairment as similarly reported by Zhang et al. (Zhang et al. 2013). However, SalB at 0.2 mg/kg significantly recovered the impaired exercise endurance by 57.2% (8.0 min → 30.7 min, $p < 0.05$). Thus, SalB substantially reversed the lung's functional impairment of treadmill exercise endurance in both PPE and CSE –induced *established* emphysema.

5.4.2. SalB reversed morphological impairment in PPE and CSE –induced *established* emphysema

Single instillation of PPE increased MLI by 1.8 –fold (54.6 μm → 97.8 μm) and DI by 4.0 –fold (4.3 % → 17.3 %) ($p < 0.05$), causing significant airspace enlargement and destruction. Pulmonary administration of SalB showed recovery of the MLI by 58.6 % (97.8 μm → 72.5 μm) and DI by 61.0 % (17.3 % → 9.4%) ($p < 0.05$). IP injections of

CSE also caused significant airspace enlargement resulting in a 1.5 –fold (54.6 μm \rightarrow 84.6 μm) ($p < 0.05$) increase in MLI as compared to healthy, which showed recovery upon administration of SalB (0.2 mg/kg) by 74.8 % (84.6 μm \rightarrow 62.2 μm) ($p < 0.05$). These findings suggest reversal of abnormal airspace enlargement and destruction by SalB in the PPE and CSE –induced emphysema.

5.4.3. SalB normalized the lung tissue expression of cleaved caspase-3 and VEGF but showed no effect on the MPO activity

Cell apoptosis marker, cleaved caspase 3 expression was substantially increased in PPE –induced emphysema rat lungs by 13 –fold ($p < 0.05$) compared to healthy, indicating elevated cell death in the lungs of these rats. On the other hand, cleaved caspase 3 expression was significantly reduced in PPE –induced SalB treated rats by 94.3 % ($p < 0.05$), suggesting inhibition of induced cell death by SalB. PPE –induced emphysema rats showed higher lung tissue expression of proliferative biomarker PCNA, which was not significant as compared to healthy rats. Imai et al. also reported increased PCNA expression in lung tissues of emphysema patients attributing this to the lung repair response following the elevated cell death (Imai et al. 2005). Since there is persistent airspace enlargement and destruction in PPE –induced rats, the substantial increase in cell death may overwhelm the marginally increased cell proliferation. However, treatment with SalB further significantly increased the lung tissue expression of PCNA by 2.6 –fold ($p < 0.05$), thus showing SalB’s ability to induce proliferation. These results are consistent with the previously demonstrated activities of SalB in elevating lung VEGF expression (Chapter 3) and stimulating pharmacological repair in lung cells by reducing cell death

and increasing proliferation (Chapter 4).

Both cytoplasmic and nuclear pSTAT3 expressions appeared to be lower in the PPE –induced emphysema rats and SalB treatment increased these expressions, but insignificantly. In contrast, the VEGF expression was significantly reduced in PPE –induced emphysema rats by 35.6 % ($p < 0.05$), similar to the clinically observed epigenetic VEGF deficiency in emphysema patients (Yasuo et al. 2011). SalB treatment successfully recovered the reduced VEGF expression, which is consistent with the original hypothesis. The 4 –fold ($p < 0.05$) increase in MPO activity (Δ Abs: 0.34 \rightarrow 1.42) in PPE –induced rat lungs was unaffected by administration of SalB at 0.2 mg/kg (Δ Abs: 1.42 \rightarrow 1.27), implying that SalB’s mechanism of action may not involve direct inhibition of neutrophil infiltration. To further clarify SalB’s direct target and mechanism of action, in vivo emphysema studies using inhibitors to the JAK2-STAT3-VEGF signaling pathway may be important.

5.5 Conclusions

The emphysema study in rats successfully assessed the potential use of pulmonary administration of SalB at 0.2 mg/kg to normalize the clinically relevant emphysematous characteristics of impaired functional endurance, airspace enlargement and destruction in addition to the pathobiological features of induced cleaved caspase 3 and reduced VEGF expression. SalB at 0.2 mg/kg showed significant improvements in functional endurance by 81.5 % and 57.2 %, and airspace morphology by 58.6 % and 74.8 % in differently induced emphysema by PPE and CSE, respectively ($p < 0.05$). These improvements were accompanied by normalization of the reduced expression of cleaved caspase 3 and VEGF along with significantly increased expression of PCNA. These results clearly suggested that pulmonary administration of SalB at 0.2 mg/kg reversed *established* emphysema in vivo. Although pSTAT3 expression in cytoplasm and nucleus appeared to increase with SalB treatment, further studies are required to clearly demonstrate SalB's STAT3-VEGF-dependent mechanism of action.

CHAPTER 6

SUMMARY AND GENERAL CONCLUSIONS

In this dissertation, SalB was examined *in vitro* and *in vivo* as a novel therapeutic molecule for pulmonary delivery in the treatment of emphysema. SalB's anti-oxidation and anti-elastase activities were first assessed *in vitro* by the chromogenic ABTS•⁺ radical scavenging assay and the chromogenic HSE substrate hydrolysis assay, respectively. SalB showed potent anti-oxidation activity ($IC_{50} = 3.7 \mu\text{M}$), but was devoid of the anti-elastase activity. Pulmonary administration of SalB at 0.2 mg/kg in normal healthy rats over two weeks was shown to increase the lung tissue expression of pSTAT3 and VEGF, while causing no abnormalities in functional treadmill exercise endurance and airspace morphology.

With this encouraging pSTAT3 and VEGF protein data in rats, the *in vitro* lung cell studies were carried out, which spanned 1) the anti-cell death activities; 2) the cell proliferation stimulatory activities; 3) the cell migration stimulatory activities; and 4) the promoting activities of trans-endothelial MSC recruitment. Both lung epithelial (A549) and endothelial (HMVEC-L) cells were used, and JAK2, STAT3 and VEGF-dependence on these SalB's activities were explored with respective pharmacologic inhibitors. The anti-cell death activities were measured with the trypan blue exclusion assay and the propidium iodide-based flow cytometry assay, and SalB at 25 μM inhibited H_2O_2 (0.1 mM)-induced A549 cell death by 86.0 % and 59.2 %, respectively. SU5416 (VEGF receptor antagonist; 20 μM) also induced A549 and HMVEC-L cell death by 3.6 and 3.3-

fold, respectively, but again, SalB at 25 μ M inhibited this induced cell death by 88.4 % and 47.7 %. In the cell proliferation and cell scratch wound closure-based migration assays, SalB at 25 μ M stimulated A549 and HMVEC-L cell proliferation by 1.3 and 1.5-fold, and cell migration by 1.5 and 1.7-fold, respectively, as compared to vehicle control. Notably, pharmacological JAK2, STAT3 and VEGF inhibitions significantly inhibited the anti-cell death and cell proliferation and migration stimulatory activities of SalB, which supported the JAK2-STAT3-VEGF –dependent mechanisms. In a trans-endothelial MSC migration assay, SU5416 (5 μ M) reduced MSC migration by 51.7 %, but SalB at 25 μ M restored this impaired migration by 60.0 %.

SalB was then examined for the reversal activities in the rat models of *established* emphysema induced with porcine pancreatic elastase (PPE) and cigarette smoke extract (CSE). In both models, exercise endurance was reduced on day 21 by 86.0 and 83.3 %, respectively, indicating the development of emphysema. SalB was then administered to the lung at 0.2 mg/kg, three times weekly for three weeks, which found significant 81.5 and 57.2 % improvement of the impaired endurance, suggesting functionality recovery. The airspace enlargement of these animals was assessed with the mean linear intercept (MLI), where PPE and CSE-induced animals (with saline treatment) showed 1.8 and 1.6-fold increased MLI values, relative to those in the healthy animals. In contrast, the SalB treatment at 0.2 mg/kg recovered this MLI values by 58.6 and 74.8 %, respectively. In the PPE-induced model, alveolar structural destruction was also assessed with the destructive index (DI%). The model resulted in a 4-fold greater DI% than the health animals, which was recovered by 61.0 % for emphysematous rats treated with SalB. These results clearly demonstrated the recovery of impaired functional endurance and abnormal airspace

morphology as a result of SalB treatment.

PPE instillation increased the lung expression of cleaved caspase-3 by about 13-fold and reduced the expression of VEGF by 1.6-fold, suggesting induced cell death and reduced cell proliferation/migration in the lungs of *established* emphysema. Pulmonary treatment of SalB at 0.2 mg/kg significantly normalized both proteins. In contrast, the lung's PCNA expression in the lungs appeared to be elevated in the PPE-induced rats, yet SalB treatment still further significantly increased the PCNA expression by 2.6-fold. Paradoxically, the pSTAT3 expression in both cytoplasmic and nuclear fractions of the rat lungs seemed to reduce by 1.2 and 1.8-fold in PPE-induced rats. However, SalB treatment appeared to still increase lung expression of cytoplasmic and nuclear pSTAT3. This suggested SalB's mechanism of STAT3-VEGF recovery. However, further investigation of the lung expression of upstream factors in the STAT3-VEGF signaling pathway may be necessary to delineate SalB's mechanism of action. SalB treatment did not alter the increased neutrophil recruitment in the lungs as a result of PPE instillation, indicated by the lung MPO activity assay. Therefore, SalB mediated reversal of emphysema maybe a result of lung VEGF recovery, but may not involve direct neutrophil recruitment inhibition.

APPENDIX

APPENDIX 1

WESTERN BLOT ANALYSIS

Western blot analysis was performed to assess protein levels in lung cells and tissues in Chapter 3 and 5. A549 or HMVEC-L cells were plated in 10 cm dishes (1×10^6 cells/dish) and grown to confluence. Upon confluence, treatments were added in 2% FBS containing medium for A549 cells and complete medium for HMVEC-L cells. Subsequently, the cells were washed with ice-cold PBS, scrapped with cell scraper (Corning) and cell suspension in 1 ml PBS was collected in the 1.5 ml centrifuge tubes. After centrifugation at 12000 rpm for 2 min (Eppendorf centrifuge 5415 C), cell pellet was collected and extracted in 100 μ l NP-40 lysis buffer using hand homogenizer (Pro 200; Pro Scientific, Inc.) in ice. NP-40 lysis buffer was freshly prepared from 150 mM NaCl, (Fisher Scientific), 50 mM Tris pH 8.0 (Bio-Rad Laboratories) and 1% NP-40 (Fisher Scientific) and one tablet of cOmpleteTM protease inhibitor cocktail tablet and one tablet of PhosSTOP phosphatase inhibitor tablet (Roche diagnostics, Indianapolis, IN) was dissolved in 10 ml of NP-40 buffer. After 1 min of homogenization, the cell extract was centrifuged at 12,000 rpm for 2 min. Supernatant was collected and 5 μ l aliquot was used for bicinchoninic acid assay (BCA, Pierce, Rockford, IL) to determine total protein content. The western blot samples were prepared at a protein concentration of 1.5 μ g/ μ l in loading buffer and denatured at 100 °C for 10 min.

For determining the lung tissue protein expression, 300 mg of right lung tissue

was homogenized with 1 ml of ice-cold NP-40 lysis buffer with protease and phosphatase inhibitors using a hand homogenizer. After 1 min of homogenization in ice, the tissue extract allowed to rest for 15 min, vortexed for 10 seconds and centrifuged at 16,000 g in 4°C (Aventi JE Centrifuge; Beckman Coulter). The supernatant was collected and 2 µl aliquot was used for the BCA assay to determine total protein content and the rest was stored at -70°C. Western blot samples of 2 µg/µl protein concentration were prepared in Laemmli sample buffer (Bio-Rad laboratories, Hercules, CA) and β-mercaptoethanol (1:20) by denaturing the proteins at 100 °C for 10 min.

Approximately 40 µg protein was loaded on each well of the 10 % Mini- Protean Precast Gels (Bio-Rad Laboratories) from the western blot samples and tris/glycine/sodium dodecylsulfate (SDS)-polyacrylamide gel electrophoresis (PAGE) was carried out at 100 V for about 80 minutes. The proteins from the gel were transferred on to a nitrocellulose or PVDF membrane at 100 V for about 90 min in ice. The membranes were washed with tris buffered saline (TBS, prepared in-house, pH 7.5) or phosphate buffered saline (PBS, prepared in house, pH 7.5) containing 0.1 % Tween 20 for 5 minutes and then subjected to 1 h of blocking in the blocking buffers 5% bovine serum albumin (BSA) in TBS or non fat dry milk (Kroger) in PBS, as recommended for each antibody by its suppliers, at room temperature on slow shaker. The nitrocellulose membranes were then incubated with the primary antibodies to protein of interest overnight at 4 °C on slow shaker. Following day, the membranes were washed with TBS/PBS and then incubated for 80 min in appropriate secondary antibodies conjugated with HRP (Bio-Rad Laboratories) on the slow shaker at room temperature. The membranes washed again with TBS/PBS. Subsequently, membranes were incubated in

the chemiluminescent substrate (SuperSignal West Pico, Thermo Scientific) for 1 min to develop luminescence and then exposed to autoradiographic films. The image of the bands were analyzed by densitometry using Image J. Each protein signal was normalized with the corresponding β -actin or lamin B1 signal.

APPENDIX 2

TREADMILL EXERCISE ENDURANCE TRAINING AND TESTING

All the rats were trained to run on the AccuPacer rodent treadmill (Accuscan Instruments, Columbus, OH). The training protocol is described below.

Day 1: Place the rat in the treadmill and close the cover. Turn on the electric shock and watch the rat's movements for 5 minutes. After 5 minutes, start the treadmill at the speed of 2.0 m/min and slowly increase the speed by 1.0-m/m increments when rat learns to avoid the electric shock area. When the speed reaches 5.0 m/min, set the timer to 5 minutes. After 5 minutes, stop the treadmill, and place the rat back into its cage. Repeat the procedure after 3 hours.

Day 2: Place the rat in the treadmill and close the cover. Turn on the electric shock and start the treadmill at the speed of 3.0 m/min. Slowly increase the speed by 1.0- m/min increments when the rat learns to run on the treadmill without touching the shock bar. When the speed reaches 7.0 m/min, set the timer for 10 minutes. After 10 minutes, stop the treadmill, and place the rat back into its cage. Repeat the procedure after 3 hours.

Day 3: Repeat the Day 2 procedure. Slowly increase the speed by 1.0 m/min increments until the speed reaches 10 m/min and set the timer for 10 minutes. After 10 minutes, stop the treadmill and place the rat back into its cage. Repeat the procedure after 3 hours.

Day 4: Place the rat in the treadmill and close the cover. Turn on the electric shock and start the treadmill at the speed of 10 m/m. Set the timer for 15 minutes. After 15 minutes,

stop the treadmill and place the rat back into its cage. Repeat the procedure after 3 hours.

Days 5-10: Place the rat in the treadmill and close the cover. Turn on the electric shock and start the treadmill at the speed of 10 m/min. Set the timer for 30 minutes. After 30 minutes, stop the treadmill and place the rat back into its cage.

Criteria for a well-trained rat: running on the treadmill without touching the electric shock for at least 3 minutes. After PPE or CSE induction, training schedule was limited to Monday, Wednesday, and Friday, twice a day, each time for 5 minutes.

Exercise endurance test:

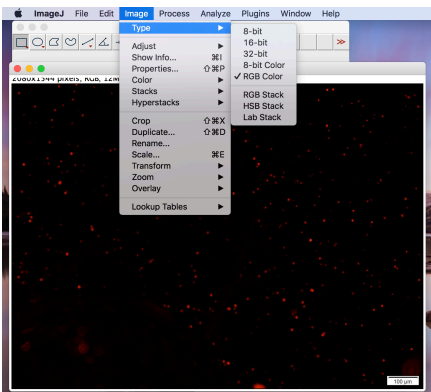
1. Turn on the treadmill and the electric foot shock.
2. Raise the height of the treadmill to a 5 degree angle
3. Place the rat on the treadmill and start at a speed of 10 m/min. Start the timer
4. Carefully watch the rat's running and record how many times it touches the electric foot shock in the first 2 minutes.
5. After 2 minutes, record the time of each shock for 5 shocks total.
6. When the rat runs for over 30 minutes, raise the treadmill angle to 10 degrees
7. When the rat runs for over 40 minutes, raise the angle to 15 degrees

APPENDIX 3

COUNTING OF MIGRATED DILC12-LABELED MSCs USING IMAGE J

ImageJ (NIH) software was used to count the MSCs migrated to the basolateral side of the fluoroblock transwell filters in 24 h. The following procedure was used for cell counting using ImageJ:

1. Convert the image into 8-bit by going to Image-type- 8-bit

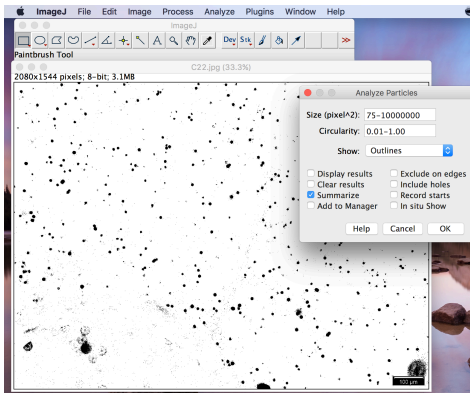


2. Subtract background by going to Process-Subtract background and setting the rolling ball radius to 12.0 pixels
3. Sharpen the image by going to Process-Sharpen
4. Adjust the threshold by going to Image-Adjust-Threshold. Most common adjustment for threshold is between 8-15, such that most cells are defined as black dots against white background. Keep the threshold constant for all the images analyzed.
5. For counting the cells go to Analyze-Particles and setting the parameters to:

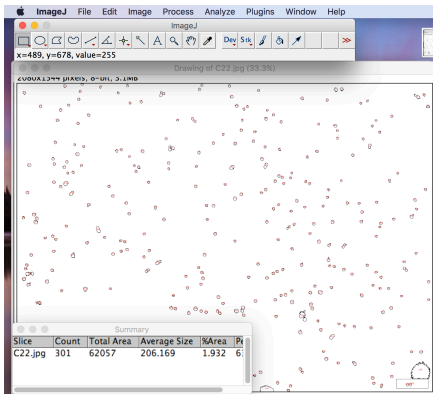
Size: 75-1000000

Circularity: 0.1-1.0

Show: Outlines



6. The image obtained will show the cells counted and the results give the number of cells.



REFERENCES

- van Agteren, J. et al., 2006. Lung volume reduction surgery for diffuse emphysema. *Cochrane Database of Systematic Reviews*, (10), p.N.PAG-N.PAG 1p. Available at: <http://search.ebscohost.com/login.aspx?direct=true&db=ccm&AN=105836577&site=ehost-live>.
- Akinbami, L.J., Liu, X. & American Lung Association, 2013. *Trends in COPD (Chronic Bronchitis and Emphysema): Morbidity and Mortality*, Available at: <http://www.lung.org/assets/documents/research/estimated-prevalence.pdf> <http://www.ncbi.nlm.nih.gov/pubmed/22142836>.
- Anon, 2004. *The global burden of disease 2004 update*, World health Organization (WHO), pp.11–33.
- Antunes, M. a. & Rocco, P.R.M., 2011. Elastase-induced pulmonary emphysema: Insights from experimental models. *Anais da Academia Brasileira de Ciencias*, 83(4), pp.1385–1395.
- ATCC Product Information Sheet: A549 (ATCC CCL-185), American Type Culture Collection. Available online at: <http://www.atcc.org/products/all/CCL-185.aspx#documentation>
- ATCC Product Information Sheet: NR8383 (ATCC CRL-2192), American Type Culture Collection. Available online at: <http://www.atcc.org/products/all/CRL-2192.aspx#documentation>
- Bakakos, P., Patentlakis, G. & Papi, A., 2015. Vascular biomarkers in asthma and COPD. *Current topics in medicinal chemistry*, pp.1–11. Available at: <http://www.ncbi.nlm.nih.gov/pubmed/26420364>.
- Barnes, P.J. & Stockley, R.A., 2005. COPD: Current therapeutic interventions and future approaches. *European Respiratory Journal*, 25(6), pp.1084–1106.
- Becker, A. De et al., 2007. Migration of culture-expanded human mesenchymal stem cells through bone marrow endothelium is regulated by matrix metalloproteinase-2 and tissue inhibitor of metalloproteinase-3. *haematologica*, 92(4), pp.440–449. Available at: <http://haematologica.com/content/92/4/440.short>.
- Bieth, J. & Wermuth, C.G., 1973. The action of elastase on p-nitroanilide substrates. *Biochemical and Biophysical Research Communications*, 53(2), pp.1340–1346.
- Brusselmans, Bono & D, C., 2005. A novel role for vascular endothelial growth factor as an autocrine survival factor for embryonic stem cells during hypoxia. *J Biol Chem*, 280, pp.2493–9.
- Caiado, F. & Dias, S., 2012. Endothelial progenitor cells and integrins: adhesive needs.

Fibrogenesis & Tissue Repair, 5, p.4.

- Chen, Y.S. et al., 2014. Effects of Danshensu and Salvianolic Acid B from *Salvia miltiorrhiza* Bunge (Lamiaceae) on Cell Proliferation and Collagen and Melanin Production. *Molecules*, 19(2), pp.2029–2041.
- Chen, Z. & Zhong, C.H., 2008. STAT3: A critical transcription activator in angiogenesis. *Medicinal Research Reviews*, 28(2), pp.185–200.
- Conese, M. et al., 2014. Hematopoietic and mesenchymal stem cells for the treatment of chronic respiratory diseases: role of plasticity and heterogeneity. *The Scientific World ...*, 2014, p.859817. Available at: <http://www.pubmedcentral.nih.gov/articlerender.fcgi?artid=3916026&tool=pmcentrez&rendertype=abstract%5Cnhttp://www.hindawi.com/journals/tswj/2014/859817/abs/>.
- Demkow, U., 2009. The oxidative stress in emphysema and Chronic Obstructive Pulmonary Disease (COPD). *Central European Journal of Immunology*, 34(2), pp.143–146.
- Diette, G.B. et al., 2015. Treatment patterns of chronic obstructive pulmonary disease in employed adults in the United States. *International Journal of COPD*, 10, pp.415–422.
- Dong, Y. et al., 2010. Cucurbitacin E, a tetracyclic triterpenes compound from Chinese medicine, inhibits tumor angiogenesis through VEGFR2-mediated Jak2-STAT3 signaling pathway. *Carcinogenesis*, 31(12), pp.2097–2104.
- Du, R. et al., 2008. HIF1 α induces the recruitment of bone marrow-derived vascular modulatory cells to regulate tumor angiogenesis and invasion. *Cancer cell*, 13(3), pp.206–220.
- van Eerd, E. et al., 2016. Smoking cessation for people with chronic obstructive pulmonary disease. *Cochrane Database of Systematic Reviews*, 8.
- Eidelman, D.H. et al., 1991. The destructive index and early lung destruction in smokers. *The American review of respiratory disease*, 144(1), pp.156–9. Available at: <http://www.ncbi.nlm.nih.gov/pubmed/2064122>.
- Feng, L.X. et al., 2011. Clarifying the signal network of salvianolic acid B using proteomic assay and bioinformatic analysis. *Proteomics*, 11(8), pp.1473–1485.
- Fischer, B.M., Pavlisko, E. & Voynow, J.A., 2011. Pathogenic triad in COPD: Oxidative stress, protease-antiprotease imbalance, and inflammation. *International Journal of COPD*, 6(1), pp.413–421.

- Fletcher, C. & Peto, R., 1977. The natural history of chronic airflow obstruction. *British Medical Journal*, 1(June), pp.1645–1648.
- Flo, C. et al., 2006. Effects of exercise training on papain-induced pulmonary emphysema in Wistar rats. *J. Appl. Physiol.*, 100(1), pp.281–285.
- Geraghty, P. et al., 2013. STAT3 modulates cigarette smoke-induced inflammation and protease expression. *Frontiers in Physiology*, 4 OCT(October), pp.1–10.
- GOLD, 2017. *Global Initiative for Chronic Obstructive Lung Disease*. Available from: [http://www.goldcopd.org/uploads/users/files/WatermarkedGlobal%20Strategy%202016\(1\).pdf](http://www.goldcopd.org/uploads/users/files/WatermarkedGlobal%20Strategy%202016(1).pdf).
- Goldblum, S.E., Wu, K.M. & Jay, M., 1985. Lung myeloperoxidase as a measure of pulmonary leukostasis in rabbits. *Journal of Applied Physiology*, 59(6), pp.1978–1985.
- Hermann et al., 2009. Rostro-caudal gradual loss of cellular diversity within the periventricular regions of the ventricular system. *Stem Cells*, 27(4), pp.928–941.
- Ho, J.H.-C. & Hong, C.-Y., 2011. Salvianolic acids: small compounds with multiple mechanisms for cardiovascular protection. *Journal of biomedical science*, 18(1), p.30. Available at: <http://www.jbiomedsci.com/content/18/1/30>.
- Hoeben, A. et al., 2004. Vascular endothelial growth factor and angiogenesis. *Pharmacological reviews*, 56(4), pp.549–580.
- Huang, H. et al., 2014. Optimization of liquid chromatographic method for the separation of nine hydrophilic and hydrophobic components in *Salviae miltiorrhizae Radix et Rhizoma* (Danshen) using microemulsion as eluent. *Journal of Chromatography B: Analytical Technologies in the Biomedical and Life Sciences*, 955–956(1), pp.124–133. Available at: <http://dx.doi.org/10.1016/j.jchromb.2014.02.027>.
- Hueper, K. et al., 2015. Pulmonary microvascular blood flow in mild chronic obstructive pulmonary disease and emphysema: The MESA COPD study. *American Journal of Respiratory and Critical Care Medicine*, 192(5), pp.570–580.
- Imai, K. et al., 2005. Correlation of lung surface area to apoptosis and proliferation in human emphysema. *European Respiratory Journal*, 25(2), pp.250–258.
- Inoue, K.-I. et al., 2010. Extensive Analysis of Elastase-Induced Pulmonary Emphysema in Rats: ALP in the Lung, a New Biomarker for Disease Progression? *Journal of clinical biochemistry and nutrition*, 46(2), pp.168–176.
- Ishizawa, K. et al., 2004. Bone marrow-derived cells contribute to lung regeneration after elastase-induced pulmonary emphysema. *FEBS Letters*, 556(1–3), pp.249–252.

- Ito, K. et al., 2005. Decreased histone deacetylase activity in chronic obstructive pulmonary disease. *The New England journal of medicine*, 352(19), pp.1967–1976. Available at: [papers3://publication/doi/10.1056/NEJMoa041892](https://doi.org/10.1056/NEJMoa041892).
- Kanazawa, H. et al., 2003. Possible effects of vascular endothelial growth factor in the pathogenesis of chronic obstructive pulmonary disease. *The American journal of medicine*, 114(5), pp.354–358.
- Kasahara, Y. et al., 2001. Endothelial cell death and decreased expression of vascular endothelial growth factor and vascular endothelial growth factor receptor 2 in emphysema. *American journal of respiratory and critical care medicine*, 163(3 Pt 1), pp.737–744.
- Kasahara, Y. et al., 2000. Inhibition of VEGF receptors causes lung cell apoptosis and emphysema. *Journal of Clinical Investigation*, 106(11), pp.1311–1319.
- Kim, S.H.J. et al., 2010. Simulation of lung alveolar epithelial wound healing in vitro. *Journal of The Royal Society Interface*, 7(49), pp.1157–1170. Available at: <http://rsif.royalsocietypublishing.org/content/7/49/1157><http://rsif.royalsocietypublishing.org/content/royinterface/7/49/1157.full.pdf><http://www.ncbi.nlm.nih.gov/pubmed/20236957>.
- Kurtagic, E. et al., 2015. Neutrophil elastase-generated fragment of vascular endothelial growth factor-A stimulates macrophage and endothelial progenitor cell migration. *PLoS ONE*, 10(12), pp.1–17. Available at: <http://dx.doi.org/10.1371/journal.pone.0145115>.
- Lay et al., 2003. Crude extract of *Salvia miltiorrhiza* and salvianolic acid B enhance in vitro angiogenesis in murine SVR endothelial cell line. *Planta medica*, 69(1), pp.26–32.
- Lay, I.S. et al., 2003. Salvianolic acid B enhances in vitro angiogenesis and improves skin flap survival in Sprague-Dawley rats. *Journal of Surgical Research*, 115(2), pp.279–285.
- Lee, J.H. et al., 2012. Imbalance of apoptosis and cell proliferation contributes to the development and persistence of emphysema. *Lung*, 190(1), pp.69–82.
- Li, Y. et al., 2013. Andrographolide antagonizes cigarette smoke extract-induced inflammatory response and oxidative stress in human alveolar epithelial A549 cells through induction of microRNA-218. *Experimental lung research*, 39(10), pp.463–471.
- Liang C-C, Park AY, Guan J-L. In vitro scratch assay: a convenient and inexpensive method for analysis of cell migration in vitro. *Nat Protoc*. 2007;2(2):329-333.

<http://dx.doi.org/10.1038/nprot.2007.30>.

- Liao, H. et al., 2014. Effects of long-term serial cell passaging on cell spreading, migration, and cell-surface ultrastructures of cultured vascular endothelial cells. *Cytotechnology*, 66(2), pp.229–238.
- Liebow, 1959. Pulmonary Emphysema with Special Reference to Vascular Changes. *American Review of Respiratory Disease*, 80(1P2), pp.67–93.
- Liu, C.H. et al., 2014. Salvianolic acid B maintained stem cell pluripotency and increased proliferation rate by activating Jak2-Stat3 combined with EGFR-Erk1/2 pathways. *Cell Transplantation*, 23(4–5), pp.657–668.
- Liu, X., Fang, Q. & Kim, H., 2016. Preclinical studies of mesenchymal stem cell (MSC) administration in chronic obstructive pulmonary disease (COPD): A systematic review and meta-analysis. *PLoS ONE*, 11(6), pp.1–17. Available at: <http://dx.doi.org/10.1371/journal.pone.0157099>.
- Lonza Product Information Sheet: Clonetics Endothelial Cell System, Lonza Walkersville, Inc. Available online at: http://bio.lonza.com/uploads/tx_mwaxmarketingmaterial/Lonza_ManualsProductInstructions_Instructions__Technical_Info_-_Endothelial_Cell_Systems.pdf
- Luscinskas, F.W., 2008. Assays of Transendothelial Migration in vitro. *Methods Enzymology*, 6879(8), pp.155–176.
- Marcelino, M.Y. et al., 2014. Animal models in chronic obstructive pulmonary disease—an overview. *Experimental Lung Research*, 40(6), pp.259–271. Available at: <http://informahealthcare.com/doi/abs/10.3109/01902148.2014.908250>.
- Marchetti, N. & Criner, G.J., 2016. Update in Chronic Obstructive Pulmonary Disease 2015. *American Journal of Respiratory and Critical Care Medicine*, 193(10), pp.1092–1100. Available at: <http://www.atsjournals.org/doi/10.1164/rccm.201602-0213UP>.
- Medford, a R.L. & Millar, a B., 2006. Vascular endothelial growth factor (VEGF) in acute lung injury (ALI) and acute respiratory distress syndrome (ARDS): paradox or paradigm? *Thorax*, 61(7), pp.621–626.
- Messer, K. et al., 2008. Smoking cessation rates in the United States: A comparison of young adult and older smokers. *American Journal of Public Health*, 98(2), pp.317–322.
- Mizuno, S. et al., 2011. Inhibition of histone deacetylase causes emphysema. *American journal of physiology. Lung cellular and molecular physiology*, 300(December

2010), pp.L402–L413.

Morissette, M.C., Parent, J. & Milot, J., 2009. Alveolar epithelial and endothelial cell apoptosis in emphysema: what we know and what we need to know. *International journal of chronic obstructive pulmonary disease*, 4, pp.19–31. Available at: <http://eutils.ncbi.nlm.nih.gov/entrez/eutils/elink.fcgi?dbfrom=pubmed&id=19436685&retmode=ref&cmd=prlinks%5Cnpapers3://publication/uuid/F5D15642-D31D-47A8-B831-1513228EA325>.

Morissette, M.C., Parent, J. & Milot, J., 2011. The emphysematous lung is abnormally sensitive to TRAIL-mediated apoptosis. *Respiratory research*, 12(1), p.105. Available at: <http://respiratory-research.com/content/12/1/105>.

Oliveira, M. V. et al., 2016. Characterization of a mouse model of emphysema induced by multiple instillations of low-dose elastase. *Frontiers in Physiology*, 7(OCT), pp.1–12.

Park, J.-S., Bang, O.-S. & Kim, J., 2014. Screening of Stat3 inhibitory effects of Korean herbal medicines in the A549 human lung cancer cell line. *Integrative Medicine Research*, 3(2), pp.67–73. Available at: <http://linkinghub.elsevier.com/retrieve/pii/S2213422013000760>.

Perotin, J.-M. et al., 2014. Delay of airway epithelial wound repair in COPD is associated with airflow obstruction severity. *Respiratory Research*, 15(1), pp.1–9. Available at: <http://respiratory-research.com/content/15/1/151>.

Punturieri, A. et al., 2008. Chronic obstructive pulmonary disease: a view from the NHLBI. *Am J Respir Crit Care Med*, 178, pp.441–443.

Rabe, K. et al., 2007. Global strategy for the diagnosis, management, and prevention of chronic obstructive pulmonary disease: GOLD executive summary. *Am J Respir Crit Care Med*, 176, pp.532–555.

Rice-Evans, C., Miller, N. & Paganga, G., 1996. Structure-antioxidation activity relationships of flavonoids and phenolic acids. *Free Radical Biology and Medicine*, 20(7), pp.933–956.

Saluja, B. et al., 2013. Novel low molecular weight lignins as potential anti-emphysema agents: In vitro triple inhibitory activity against elastase, oxidation and inflammation. *Pulmonary Pharmacology and Therapeutics*, 26(2), pp.296–304. Available at: <http://dx.doi.org/10.1016/j.pupt.2012.12.009>.

Saluja B, Li H, Desai UR, Voelkel NF, Sakagami M. Sulfated Caffeic Acid Dehydropolymer Attenuates Elastase and Cigarette Smoke Extract-induced Emphysema in Rats: Sustained Activity and a Need of Pulmonary Delivery. *Lung*.

2014;192(4):481-492. doi:10.1007/s00408-014-9597-2.

Savukinas, U.B. et al., 2016. Concise Review: The Bystander Effect: Mesenchymal Stem Cell-Mediated Lung Repair. *Stem Cells*, 34(6), pp.1437–1444.

Schamberger, A.C. et al., 2014. Epigenetic mechanisms in COPD: implications for pathogenesis and drug discovery. *Expert opinion on drug discovery*, 9(6), pp.609–28. Available at: <http://www.ncbi.nlm.nih.gov/pubmed/24850530>.

Sedgwick, J.B. et al., 2002. Effects of inflammatory cytokines on the permeability of human lung microvascular endothelial cell monolayers and differential eosinophil transmigration. *Journal of Allergy and Clinical Immunology*, 110(5), pp.752–756.

Shaw, T.J. & Martin, P., 2016. Wound repair: A showcase for cell plasticity and migration. *Current Opinion in Cell Biology*, 42, pp.29–37. Available at: <http://dx.doi.org/10.1016/j.ceb.2016.04.001>.

Siniscalco, D. et al., 2008. Stem cell therapy: the great promise in lung disease. *Therapeutic advances in respiratory disease*, 2, pp.173–177.

Sirianni, F.E., Chu, F.S.F. & Walker, D.C., 2003. Human Alveolar Wall Fibroblasts Directly Link Epithelial Type 2 Cells to Capillary Endothelium. *American Journal of Respiratory and Critical Care Medicine*, 168(12), pp.1532–1537.

Snider, G. et al., 1985. The Definition of Emphysema. *The American Review of Respiratory Disease*, 132, pp.182–185.

Snider, G.L., 1981. The pathogenesis of emphysema—twenty years of progress. *American Review of Respiratory Disease*, 124(3), pp.321–324.

Song, S.-Y., Chung, H.-M. & Sung, J.-H., 2010. The pivotal role of VEGF in adipose-derived-stem-cell-mediated regeneration. *Expert Opinion on Biological Therapy*, 10(11), pp.1529–1537.

Stevenson, C.S. & Birrell, M. a, 2011. Moving towards a new generation of animal models for asthma and COPD with improved clinical relevance. *Pharmacology & therapeutics*, 130(2), pp.93–105. Available at: <http://dx.doi.org/10.1016/j.pharmthera.2010.10.008>.

Stockley, R. et al., 2008. *Chronic Obstructive Pulmonary Disease: A Practical Guide to Management*,

Sugahara, K. et al., 2006. Alveolar epithelial cells: differentiation and lung injury. *Respirology (Carlton, Vic.)*, 11 Suppl, pp.S28–S31.

Takahashi, H. et al., 2005. The vascular endothelial growth factor (VEGF)/VEGF receptor system and its role under physiological and pathological conditions.

Clinical science (London, England : 1979), 109(3), pp.227–41. Available at: <http://www.ncbi.nlm.nih.gov/pubmed/16104843>.

Taraseviciene-Stewart et al., 2007. Cigarette smoke extract (CSE)-induced emphysema in mice [abstract]. *Am J Respir Crit Care Med*, 175, p.A529.

Taraseviciene-stewart, L. & Voelkel, N.F., 2008. Molecular pathogenesis of emphysema. *The Journal of clinical investigation*, 118(2), pp.394–402.

Thurlbeck, W., 1966. Measurement of pulmonar emphysema. *Am J Resp Dis*, 94, pp.752–764.

Vermes, I. et al., 1995. A novel assay for apoptosis. Flow cytometric detection of phosphatidylserine expression on early apoptotic cells using fluorescein labelled Annexin V. *Journal of Immunological Methods*, 184(1), pp.39–51. Available at: <http://www.ncbi.nlm.nih.gov/pubmed/7622868>.

Voelkel, N.F. et al., 2006. Vascular endothelial growth factor in the lung. , (25).

Wagner, K.-U. et al., 2004. Impaired alveologenesis and maintenance of secretory mammary epithelial cells in Jak2 conditional knockout mice. *Molecular and cellular biology*, 24(12), pp.5510–5520.

Wagner, P.D., 2003. Vascular endothelial growth factor and the pathogenesis of emphysema. *The American journal of medicine*, 114(5), pp.413–414.

Wang, G. et al., 2008. Sequential activation of JAKs, STATs and xanthine dehydrogenase/oxidase by hypoxia in lung microvascular endothelial cells. *International Journal of Biochemistry and Cell Biology*, 40(3), pp.461–470.

Wang, J., Xiong, X. & Feng, B., 2013. Cardiovascular effects of salvianolic Acid B. *Evidence-based complementary and alternative medicine : eCAM*, 2013, p.247948. Available at: <http://www.ncbi.nlm.nih.gov/pubmed/24174423>.

Warburton, D. et al., 2008. Stem/progenitor cells in lung development, injury repair, and regeneration. *Proceedings of the American Thoracic Society*, 5(6), pp.703–706.

Wu, Y.-T. et al., 2006. Bioavailability of salvianolic acid B in conscious and freely moving rats. *International journal of pharmaceuticals*, 326(1–2), pp.25–31. Available at: <http://www.sciencedirect.com/science/article/pii/S0378517306005527>.

Xu, Q. et al., 2005. Targeting Stat3 blocks both HIF-1 and VEGF expression induced by multiple oncogenic growth signaling pathways. *Oncogene*, 24(36), pp.5552–5560.

Yao, H. et al., 2012. SIRT1 protects against emphysema via FOXO3-mediated reduction of premature senescence in mice. *Journal of Clinical Investigation*, 122(6),

pp.2032–2045.

Yasuo, M. et al., 2011. Hypoxia inducible factor-1a in human emphysema lung tissue. *European Respiratory Journal*, 37(4), pp.775–783.

Yokohori, N., Aoshiba, K. & Nagai, A., 2004. Increased levels of cell death and proliferation in alveolar wall cells in patients with pulmonary emphysema. *Chest*, 125, pp.626–632.

Zhang, B. et al., 2015. Duration of nicotine replacement therapy use and smoking cessation: A population-based longitudinal study. *American Journal of Epidemiology*, 181(7), pp.513–520.

Zhang, Y. et al., 2013. Intraperitoneal injection of cigarette smoke extract induced emphysema, and injury of cardiac and skeletal muscles in BALB/C mice. *Experimental lung research*, 39(1), pp.18–31. Available at: <http://www.ncbi.nlm.nih.gov/pubmed/23216006>.

Zhao, G.R. et al., 2008. Characterization of the radical scavenging and antioxidant activities of danshensu and salvianolic acid B. *Food and Chemical Toxicology*, 46(1), pp.73–81.

Zhao, Y., Guo, Y. & Gu, X., 2011. Salvianolic Acid B, a potential chemopreventive agent, for head and neck squamous cell cancer. *Journal of oncology*, 2011, p.534548.

Zhou, L., Chow, M.S.S. & Zuo, Z., 2009. Effect of sodium caprate on the oral absorptions of danshensu and salvianolic acid B. *International Journal of Pharmaceutics*, 379(1–2), pp.109–118.

VITA

Sneha Dhapare was born on November 2, 1989, in Mumbai, India. She received her Bachelor of Pharmacy degree at the University of Mumbai, in 2011. Following that she came to the US to pursue her Master in Science degree from the Creighton University, Omaha, Nebraska. In Fall 2013, she was admitted to the Doctor of Philosophy (Ph.D.) program at Virginia Commonwealth University (VCU) School of Pharmacy (SOP), Richmond, Virginia with graduate assistantship in the Department of Pharmaceutics, with Dr. Masahiro Sakagami as her advisor. During the graduate program, Sneha has accomplished six research presentations (in an oral or a poster format) in the past 3+ years at scientific meetings and VCU graduate research conferences, Drug Discovery & Therapy World Congress (2015), Respiratory Drug Delivery (2016), American Association of Pharmaceutical Scientists (AAPS; 2016); VCU 3D Summit (2016), and VCU-SOP Research and Career Day (2014 & 2015), and currently, three research papers are in preparation. In 2015 at the VCU-SOP Research and Career Day, Sneha received the Best Poster Award and the PCEU Schwartz Graduate Travel Award; she was also a recipient of the PCEU's Graduate Student Association GSA-AAPS Travel Award. In 2016, she was awarded VCU's Graduate Dissertation Assistantship.

DATA SHEETS

Anti-oxidative activity assessment-ABTS radical scavenging assay

Concentration	n=1	n=2	n=3
0	0.186	0.189	0.198
0.01	0.18	0.192	0.193
0.1	0.159	0.193	0.193
0.5	0.198	0.188	0.192
1	0.177	0.19	0.188
2.5	0.148	0.148	0.148
5	0.058	0.052	0.045
7.5	0.001	0.001	0
10	0	-0.001	0
25	0	0	-0.001
50	0	0	0
100	0	0.001	0

Anti-oxidative activity assessment-HSE hydrolysis assay

Concentration	n=1	n=2	n=3
0	0.974	1.016	1.01
0.1	0.975	1.04	0.988
1	0.975	0.98	1.043
10	0.967	1.036	0.996
25	0.954	0.969	1.018
50	0.95	0.967	1.009
100	0.952	0.971	1.007
200	0.962	1.001	0.988

Western blot-pSTAT3 expression in lung tissues

Treatment	Animal	pSTAT3/b-actin	Average	SE
Healthy	H 15	0.973	1.00	0.15
Healthy	H5	1.276		
Healthy	H10	0.751		
SalB 0.2 mg/kg	TR 178	1.784	1.76	0.20
SalB 0.2 mg/kg	TR 169	1.840		
SalB 0.2 mg/kg	TR 177	2.390		
SalB 0.2 mg/kg	TR 165	1.627		
SalB 0.2 mg/kg	TR 166	1.157		

Western blot-VEGF expression in lung tissues

Treatment	Animal	VEGF/b-actin	Average	SE
Healthy	H 5	0.82	1.00	0.10
Healthy	H 15	1.18		
Healthy	H10	1.00		
SalB 0.2 mg/kg	TR 165	1.79	1.44	0.13
SalB 0.2 mg/kg	TR 166	1.15		
SalB 0.2 mg/kg	TR 169	1.44		
SalB 0.2 mg/kg	TR 177	1.68		
SalB 0.2 mg/kg	TR 178	1.13		

% Stained A549 cells- trypan blue exclusion assay-H₂O₂ –induced cell death

Treatment	n=1	n=2	n=3	n=4	n=5	n=6	Average	SD
Vehicle control	0.75	1.09	0.40	2.10	1.53	1.07	1.16	0.597
SalB 25 μ M	1.86	1.33	1.59				1.59	0.265
0.1 mM H ₂ O ₂	7.59	6.63	7.98	7.27	7.14	8.32	7.49	0.608
+ 1 μ M SalB	6.72	5.58	6.32				6.21	0.578
+ 10 μ M SalB	3.10	1.81	2.60	2.16			2.42	0.558
+ 25 μ M SalB	2.65	1.80	1.19	2.53			2.04	0.681

% Propidium iodide stained A549 cells- Flow cytometry H₂O₂ –induced cell death

Treatment	n=1	n=2	n=3	Average	SD
Vehicle control	1.6	1.8	1.65	1.68	0.10
H ₂ O ₂ 0.1 mM	10.25	9.85	9.79	9.96	0.25
+SalB 25 μ M	5.72	4.63	4.825	5.06	0.58

% Stained A549 cells- trypan blue exclusion assay- SU5416 –induced cell death with inhibitors

Treatment	n=1	n=2	n=3	Average	SD
SU5416 10 μ M	3.63	3.16	2.16	2.98	0.75
+SalB 25 μ M	1.29	1.52	1.34	1.41	0.16
SU5416 20 μ M	5.41	5.51	6.42	6.09	0.560
+SalB 25 μ M	2.50	1.46	2.59	2.18	0.63
SU5416 20 μ M+AG490 25 μ M	6.03	5.57	4.22	5.28	0.94
SU5416 20 μ M+AG490+SalB 25 μ M	5.49	5.48	6.92	5.97	0.83
SU5416 20 μ M+S31-201 100 μ M	5.84	5.39	6.23	5.82	0.42
SU 20 μ M+S31-201+SalB 25 μ M	5.21	6.16	3.17	4.85	1.53

% Stained HMVEC-L cells- trypan blue exclusion assay- SU5416 –induced cell death with inhibitors

Treatment	n=1	n=2	n=3	n=4	n=5	Average	SE
Vehicle control	11.83	10.47	10.28	7.63	8.19	9.68	0.78
SalB 25 μ M	6.20	7.19	11.04	8.97		8.35	0.95
SU5416 20 μ M	31.80	27.91	35.91			31.87	2.31
+SalB 25 μ M	21.30	22.61	19.95			21.29	1.39
+S31-201 50 μ M	33.23	40.10	32.21			35.18	2.48
+AG490 25 μ M	28.54	35.92	26.65			30.37	2.83

A549 cells- MTT assay –Absorbance at 570 nm

Treatment	n=1	n=2	n=3	n=4	n=5	n=6	n=7	Average	SD
Vehicle control (0 h)	0.307	0.279	0.241	0.266				0.273	0.027
Vehicle control (24 h)	0.426	0.314	0.492	0.351				0.396	0.079
Vehicle control (48 h)	0.665	0.675	0.615	0.661	0.471	0.751	0.574	0.630	0.089
SalB 10 μ M	0.978	0.627	0.562	1.038				0.801	0.241
SalB 25 μ M	1.075	0.943	0.888	0.823				0.932	0.107

A549 cells-MTT assay-Absorbance at 570 nm with inhibitors

	n=1	n=2	n=3	n=4	n=5	n=6	n=7	Average	SD
Control	0.806	0.672	0.798					0.759	0.075
SalB 25 μ M	1.103	1.577	1.103	1.007	0.960	1.130	1.191	1.153	0.274
AG 490 25 μ M	0.884	0.631	0.863					0.793	0.140
+SalB 25 μ M	0.893	0.820	0.746	0.676				0.784	0.074
S31-201 100 μ M	0.859	0.838	0.644					0.780	0.119
+SalB 25 μ M	0.893	0.820	0.746	0.676				0.784	0.074
SU5416 5 μ M	0.744	0.627	0.860					0.744	0.116
+SalB 25 μ M	0.801	0.835	0.711					0.782	0.064

HMVEC-L –MTT assay- Absorbance at 570 nm

Treatment	n=1	n=2	n=3	n=4	n=5	n=6	n=7	Average	SD
Vehicle control (0 h)	0.142	0.184	0.19	0.25				0.192	0.026
Vehicle control (24 h)	0.23	0.306	0.307	0.25				0.273	0.039
Vehicle control (48 h)	0.398	0.34	0.348					0.362	0.041
Vehicle control (24 h)	0.23	0.306	0.307	0.25				0.273	0.044
SalB 5 μ M	0.33	0.306	0.307					0.314	0.014
SalB 10 μ M	0.363	0.342	0.31					0.338	0.027
SalB 25 μ M	0.366	0.324	0.374					0.355	0.027
SalB 50 μ M	0.33	0.355	0.389					0.358	0.030

HMVEC-L –MTT assay- Absorbance at 570 nm with inhibitors

Treatment	n=1	n=2	n=3	n=4	n=5	n=6	n=7	n=8	n=9	n=10	n=11	Average	SD
Control	0.242	0.22	0.212	0.181	0.182	0.206	0.192	0.198	0.237	0.203	0.217	0.211	0.021
SalB 25 μ M	0.271	0.307	0.297	0.255	0.241	0.245	0.271	0.323	0.307	0.297		0.281	0.029
AG 490 25 μ M	0.165	0.186	0.156	0.235	0.231	0.195						0.195	0.015
+SalB 25 μ M	0.216	0.24	0.236	0.262	0.232							0.237	0.013
S31-201 100 μ M	0.171	0.18	0.177									0.176	0.005
+SalB 25 μ M	0.192	0.201	0.146									0.180	0.030
SU5416 5 μ M	0.212	0.177	0.155	0.156								0.175	0.029
+SalB 25 μ M	0.2	0.228	0.216									0.215	0.014

HMVEC-L –BrdU assay- Absorbance at 450 nm

Treatment	n=1	n=2	n=3	n=4	Average	SD
Vehicle control	0.272	0.269	0.279	0.348	0.292	0.038
SalB 10 μ M	0.249	0.373	0.537	0.377	0.384	0.118
SalB 25 μ M	0.437	0.398	0.398	0.389	0.4055	0.021

% A549 cell scratch wound closure

Treatment	n=1	n=2	n=3	n=4	n=5	n=6	n=7	n=8	Average	SD
Vehicle control	32.45	33.62	49.46	29.47	35.00	19.97	29.37	25.59	31.87	8.58
SalB 10 μ M	27.52	34.91	39.01	46.88	52.18	30.53	55.58		40.95	10.84
SalB 25 μ M	49.55	60.41	56.11	48.56	36.50	53.78	40.57	46.02	48.94	7.93

% A549 cell scratch wound closure with inhibitors

	n=1	n=2	n=3	Average	SD
Vehicle control	36.23	32.92	28.51	32.55	3.87
SalB 25 μ M	46.68	48.19	47.94	47.60	0.81
S31-201	36.99	37.68	30.44	35.04	4.00
+SalB 25 μ M	37.90	40.50	43.02	40.47	2.56
AG490	35.51	38.02	36.79	36.78	1.26
+SalB 25 μ M	24.26	32.04	33.50	29.93	4.97

% A549 cell scratch wound closure with inhibitors

	n=1	n=2	n=3	n=4	n=5	n=6	Average	SD
Vehicle control	38.80	38.80	41.59	37.12			39.08	1.85
SalB 25 μ M	47.67	54.20	45.62	48.06	50.02		49.11	3.25
SU5416 5 μ M	37.12	35.54	41.17	33.89	36.50	32.24	36.08	3.07
+SalB 25 μ M	33.81	40.73	45.02	43.61			40.79	4.99

% HMVEC-L cell scratch wound closure time study

Hours	Control	SalB 10 μ M
0	0	0
3	13.4	21.33
6	22.18	34.04
12	45.94	66.28
18	65.21	92.6

% HMVEC-L cell scratch wound closure

Treatment	n=1	n=2	n=3	n=4	n=5	n=6	n=7	n=8	n=9	n=10	Average	SD
Vehicle control	49.31	39.92	39.71	38.84	49.89	39.48	51.40	35.17	57.36	39.83	44.09	7.25
SalB 2.5 μ M	42.35	42.46	40.90								41.90	0.87
SalB 5 μ M	57.50	63.73	63.79								61.67	3.61
SalB 10 μ M	66.72	77.10	66.28	48.29	69.03						65.49	10.55
SalB 25 μ M	79.74	78.90	79.52	63.60							75.44	7.90

% HMVEC-L cell scratch wound closure with AG490

Treatment	n=1	n=2	n=3	n=4	n=5	n=6	n=7	n=8	n=9	Average	SD
Vehicle control	21.78	18.54	26.79	22.68	22.95	25.82				23.09	2.96
SalB 25 μ M	32.66	41.14	33.95	32.77	37.77	38.97				36.21	3.58
AG490 25 μ M	25.09	23.79	20.05	23.08	23.92	26.54	22.49	26.07	22.53	23.73	2.01
+SalB 25 μ M	24.87	25.87	29.52	25.69	25.75	23.82	29.66	23.24	28.58	26.33	2.38

% HMVEC-L cell scratch wound closure with inhibitors

Treatment	n=1	n=2	n=3	n=4	n=5	n=6	Average	SD
Vehicle control	49.31	39.92	39.71	38.84	49.89	39.48	42.86	5.24
SalB 25 μ M	66.82	63.95	79.70				70.16	8.39
SU5416 5 μ M	41.3	38.2	48.4				42.65	5.20
+SalB 25 μ M	48.5	47.7	50.8				49.02	1.59
S31-201 50 μ M	50.84	40.42	34.42				41.89	8.31
+SalB 25 μ M	45.61	46.33	42.34				44.76	2.12

% MSCs migrated in 24 h

	n=1	n=2	n=3	Average	SD
No HPMVEC	9.96	10.53	10.61	10.37	0.36
HPMVEC	12.60	14.38	14.58	13.85	1.09
FBS 30%	23.76	25.18	26.76	25.23	1.50

% MSCs migrated in 24 h upon SU5416 pretreatment with SalB

Treatment	n=1	n=2	n=3	n=4	n=5	n=6	Average	SD
Vehicle control	16.94	14.42	16.41				15.92	1.33
SalB 25 μ M	16.85	18.50	19.84				18.40	1.50
SU5416 5 μ M	7.94	7.51	8.58	7.86	6.58		7.69	0.73
+SalB 25 μ M	14.77	12.75	11.74	11.9	12.81	11.82	12.63	1.15

Pre and post dose exercise of rats

											Average	SD
Healthy	48.46	54.84	57.3	52.41	51.67	39.23	30.32	38.7	41.25	62.8	47.70	10.03
SalB (0.2 mg/kg)	41.16	42.59	37.5	45.08							41.58	3.17
PPE (Pre)	6.43	3.35	2	2.28	6.1	13.81					5.66	4.41
PPE (Post)	8.86	2.35	2	2.43	7.68	10.69					5.67	3.86
PPE+SalB 0.1 mg/kg (Pre)	6.2	7.4	2.55								5.38	2.53
PPE+SalB 0.1 mg/kg (Post)	18.39	18.39	8.38								15.05	5.78
PPE+SalB 0.2 mg/kg (Pre)	16.67	9.75	8.35	5.68	4.17	8.99					8.94	4.34
PPE+SalB 0.2 mg/kg (Post)	40.8	42.72	50	38.98	30.18	37.94					40.10	6.48
CSE (Pre)	5.48	7.066	5.63	16.99	3.64						7.76	5.30
CSE (Post)	5.85	8.23	9.33	16.3	6.27						9.20	4.22
CSE+SalB 0.2 mg/kg (Pre)	19.63	7.55	3.22	4.89	3.22						7.70	6.90
CSE+SalB 0.2 mg/kg (Post)	47.73	31.64	24.29	37.28	12.6						30.71	13.26

Mean linear intercept values for each rat

Group	n=1	n=2	n=3	n=4	n=5	n=6	Average	SD
Healthy	62.8	54.84	57.3	52.41	51.67	48.86	54.65	4.92
SalB 0.2 mg/kg	63.37	59.90	52.30				58.52	5.66
PPE	111.5	93.7	92.75	95.06	95.91		97.78	7.76
PPE+SalB	79.02	74.99	69.27	70.80	68.51		72.52	4.41
CSE	80.49	83.17	86.44	88.35			84.61	3.48
CSE+SalB	59.16	61.14	57.75	70.80			62.21	5.89

Destructive index measurements for each rat

	n=1	n=2	n=3	Average	SD
Healthy	4.46	5.00	3.49	4.32	0.76
PPE	20.24	14.72	16.81	17.26	2.79
PPE+SalB	9.97	8.85	9.32	9.38	0.56

MLI and DI correlation

Healthy	62.8	4.46
Healthy	54.84	5.00
Healthy	57.3	3.49
TR 202	111.5	20.24
TR 228	95.06	14.72
TR 230	95.91	16.81
TR 199	79.02	9.97
TR 200	74.99	8.85
TR 201	69.27	9.32

Protein expressions in rat lungs

Cleaved caspase3/b-actin relative to healthy			Average	SD	SE
Healthy	TR 227	1.052	1.000	0.133	0.077
	TR 236	0.849			
	H 22	1.099			
PPE PC	TR 228	13.069	13.15	6.26	3.61
	TR 231	19.453			
	TR 230	6.933			
PPE SalB	TR 226	2.900	1.69	1.27	0.52
	TR 229	3.678			
	TR 232	1.137			
	TR 199	0.787			
	TR 200	0.672			
	TR 201	0.970			

PCNA/b-actin relative to healthy			Average	SD	SE
Healthy	TR 227	1.225	1	0.213	0.123
	TR 236	0.974			
	H 22	0.801			
PPE PC	TR 228	3.063	1.59	1.29	0.65
	TR 231	2.130			
	TR 230	1.125			
	TR 202	0.058			
PPE SalB	TR 226	4.171	2.62	1.14	0.46
	TR 229	3.361			
	TR 232	1.425			
	TR 199	2.509			
	TR 200	3.027			
	TR 201	1.241			

nuclear pSTAT3/lamin B1 relative to healthy			Average	SD	SE
Healthy	TR 227	0.912	1.000	0.084	0.05
	TR 219	1.008			
	TR 236	1.080	0.516	0.229	0.11
PPE PC	TR 228	0.642			
	TR 231	0.176			
	TR 221	0.580			
	TR 213	0.665			
PPE SalB	TR 226	0.513	0.759	0.220	0.08
	TR 229	0.550			
	TR 232	0.729			
	TR 218	0.703			
	TR 225	1.073			
	TR 221	1.043			

cytoplasmic pSTAT3/b-actin relative to healthy			Average	SD	SE
Healthy	TR 227	1.223	1.000	0.243	0.141
	TR 236	0.740			
	TR 222	1.037			
PPE PC	TR 228	1.087	0.816	0.183	0.082
	TR 231	0.658			
	TR 230	0.922			
	TR 213	0.700			
	TR 202	0.712			
PPE SalB	TR 226	1.145	1.152	0.236	0.089
	TR 229	1.396			
	TR 232	0.922			
	TR 199	1.036			
	TR 200	1.479			
	TR 201	0.936			
	TR 214	0.773			

VEGF/b-actin relative to healthy			Average	SD	SE
Healthy	TR 227	1.05	1.00	0.13	0.08
	TR 222	0.85			
	TR 236	1.10			
PPE PC					
	TR 228	0.68	0.64	0.05	0.02
	TR 231	0.68			
	TR 202	0.59			
	TR 230	0.62			
PPE SalB	TR 226	0.86	0.96	0.35	0.15
	TR 229	1.56			
	TR 199	0.90			
	TR 200	0.83			
	TR 201	0.66			

MPO activity assay

	Healthy			PPE			PPE+SalB	
	TR 227	0.355		TR 228	1.26		TR 226	1.208
	H 10	0.32		TR 230	1.25		TR 229	1.248
	H11	0.365		TR 231	1.086		TR 232	1.140
	H12	0.206		TR 213	1.321		TR 199	1.387
	H20	0.468		TR 216	1.795		TR 200	1.321
				TR 220	1.696		TR 201	1.322
				TR 221	1.515		TR 214	1.308
							TR 225	1.258
Average	0.343				1.418			1.274
SD	0.094				0.259			0.072
SE	0.042				0.098			0.026